

# UNIVERSITÄTSKLINIKUM HAMBURG-EPPENDORF

III. Medizinische Klinik und Poliklinik  
(Nephrologie/Rheumatologie/Endokrinologie)

Prof. Dr. med. Tobias B. Huber

**Functional role of T-bet-dependent Th17 to Th1 cell plasticity in immune-mediated diseases**

## **Dissertation**

zur Erlangung des Grades eines Doktors der Medizin  
an der Medizinischen Fakultät der Universität Hamburg.

vorgelegt von:

Jens Christian Kleiner  
aus Pforzheim

Hamburg 2024

Angenommen von der Medizinischen Fakultät der Universität Hamburg am: 11.12.2024

Veröffentlicht mit Genehmigung der Medizinischen Fakultät der Universität Hamburg.

Prüfungsausschuss, der/die Vorsitzende: Prof. Dr. Eva Tolosa

Prüfungsausschuss, zweite/r Gutachter/in: Prof. Dr. Christian Krebs

# Table of Contents

<b>1. Introduction</b>	<b>5</b>
1.1 The immune system	5
1.1.1 The innate immune system	5
1.1.2 The adaptive immune system	6
1.2 CD4+ T cell subsets	7
1.2.1 Th1 cells	7
1.2.1.1 T-Bet / Tbx21	8
1.2.2 Th2 cells	8
1.2.3 Th17 cells	8
1.2.3.1 Th17-Th1 transdifferentiation	9
1.2.4 Regulatory T cells	10
1.2.5 Th22 cells	10
1.2.6 Th9 cells	10
1.3 Autoimmunity	11
1.4 The kidneys	11
1.4.1 Anatomy and function of the kidneys	11
1.4.2 Immune mediated crescentic glomerulonephritis	13
1.4.2.1 Immune-complex glomerulonephritis	14
1.4.2.2 Anti-glomerular basement membrane glomerulonephritis	14
1.4.2.3 Pauci-immune glomerulonephritis	14
1.4.2.4 Diagnosis and course of crescentic glomerulonephritis	15
1.4.2.5 Treatment of crescentic glomerulonephritis	16
1.4.2.6 Th17 cells in crescentic glomerulonephritis	17
1.5 The gastrointestinal tract	18
1.5.1 Anatomy and function of the gastrointestinal tract	18
1.5.2 Inflammatory bowel disease	18
1.5.2.1 Treatment of inflammatory bowel disease	21
1.5.2.2 Th17 cells in inflammatory bowel disease	22
1.6 Hypothesis and research goals	23
<b>2 Material and Methods</b>	<b>24</b>
2.1 Material	24
2.1.1 Mice	24
2.1.2 Primers	24
2.1.3 ELISA-Antibodies	25
2.1.4 FACS Antibodies	25
2.1.5 Buffers, solutions and media	26
2.1.6 Chemicals and consumables	28
2.1.7 Plasticware	29

2.1.8 Kits	30
2.1.9 Equipment	30
2.1.10 Software	32
2.1.11 R and python packages	32
2.2 Methods	33
2.2.1 Ethics statement and handling of laboratory animals	33
2.2.2 Genotyping of transgenic mice	33
2.2.3 Conditional Tbx21 KO in IL-17A fate reporter mice	35
2.2.4 Gel electrophoresis	36
2.2.5 Nephrotoxic nephritis (NTN)	37
2.2.6 Urine sample collection in metabolic cage	38
2.2.7 Enzyme-linked immunosorbent assay (ELISA) of albumin	39
2.2.8 Urine creatinine quantification (Jaffee analysis)	41
2.2.9 T cell isolation from the kidneys	42
2.2.10 Erythrocyte lysis	42
2.2.11 Manual and automated cell-counting	42
2.2.12 Fecal Yale microbiome transplantation into Rag1 KO mice	43
2.2.13 Induction of CD45RBhi colitis	43
2.2.14 Flow cytometric cell sorting	44
2.2.15 Mice evaluation during CD45RBhi colitis (colitis scoring)	45
2.2.16 T cell isolation from the colon	45
2.2.17 Preparation of tissue slices for histopathological analysis	46
2.2.18 Periodic acid-Schiff reaction	46
2.2.19 Hematoxylin and eosin stain	46
2.2.20 Ex vivo stimulation of T cells from kidney and colon	47
2.2.21 Surface- and intracellular staining for FACS analysis	47
2.2.22 Surface- and intranuclear staining for FACS analysis	48
2.2.23 Histological scoring in the cGN model	48
2.2.24 Histological scoring in CD45RBhi Colitis	48
2.2.25 10x Genomics scRNAseq pipeline	49
2.2.26 Analysis of scRNAseq data	52
2.2.26.1 Alignment	52
2.2.26.2 Preprocessing workflow	52
2.2.26.3 Merging of datasets	53
2.2.26.4 Batch correction	53
2.2.26.5 Cell cycle scoring	53
2.2.26.6 Differential expression analysis	53
2.2.26.7 Module scores	54
2.2.26.8 Heatmaps	54
2.2.26.9 Boxplots	54
2.2.27 Statistical Analysis	54

<b>3 Results</b>	<b>55</b>
3.1 Results of crescentic glomerulonephritis experiments	55
3.1.1 Clinical parameters in crescentic glomerulonephritis	55
3.1.2 Histology of renal sections	56
3.1.3 FACS analysis of renal lymphocytes	57
3.1.4 scRNAseq in crescentic glomerulonephritis	60
3.2 Results of Crohn's disease experiments	69
3.2.1 Clinical parameters in Crohn's disease	69
3.2.2 Histology of colonic sections	72
3.2.3 FACS analysis of intestinal lymphocytes	73
<b>4. Discussion</b>	<b>78</b>
4.1 The role of T-bet in Th17 IFN- $\gamma$ production	80
4.2 Is T-bet necessary for pathogenicity?	81
4.3 T-bet's impact on Th17 migration	83
4.4 Outlook	84
<b>5. Summary</b>	<b>86</b>
5.1 English summary	86
5.2 German summary (Zusammenfassung)	86
<b>6. List of Abbreviations</b>	<b>88</b>
<b>7. Bibliography</b>	<b>91</b>
7.1 Literature	91
7.2 Online	102
<b>8. List of Tables</b>	<b>103</b>
<b>9. List of Figures</b>	<b>104</b>
<b>10. Acknowledgements</b>	<b>106</b>
<b>11. Curriculum Vitae</b>	<b>107</b>
<b>12. Affidavit</b>	<b>108</b>

# 1. Introduction

## 1.1 The immune system

Every day we are in contact with huge quantities of molecules and microorganisms like viruses, bacteria, fungi and parasites that may be pathogenic or non-pathogenic. To identify and deal with those potential threats, we are well equipped with a broadly specialized immune system consisting of a wide range of effector cells and molecules. The role of the immune system is to prevent intrusion of pathogens, quickly identify invading microorganisms or tissue injury, precisely distinguish pathogens from endogenous cells and to inhibit their reproduction and eliminate pathogens. After overcoming an infection, the immune system possesses a memory of faced pathogens to react quicker in the case of reinfection. All these tasks are carried out by multiple highly specialized cell types.

The human immune system includes the unspecific innate immunity which represents the first barrier for infiltrating pathogens. The innate immune system is especially relevant in early stages of infection or tissue damage. The adaptive immune system needs more time to operate effectively. But when it does it delivers a very specific and effective response. These two systems are described in more detail in the following.

### 1.1.1 The innate immune system

Innate immunity is a fast-acting system with great importance in the first hours of pathogen infiltration or tissue damage. This first line of defense is executed by lymphoid cells as well as myeloid cells. Over the last years several newly explored innate lymphoid cells like  $\gamma\delta$  T cells, intraepithelial lymphocytes (IELs), mucosa-associated invariant T cells (MAIT cells) and innate lymphoid cells (ILC) were added to the already described classical natural killer cells (cNK cells) (Diefenbach *et al.*, 2014). The innate myeloid cells include macrophages, monocytes, granulocytes and dendritic cells (DC). Despite the number of players innate immunity is considered to be unspecific.

Innate immune cells are equipped with so called pattern recognition receptors (PRR) that can either recognize pathogen-associated molecular patterns (PAMP) on intruding microorganisms or damage-associated molecular patterns (DAMP) which are released from endogenous tissue during inflammation or injury. Toll like receptor (TLR) are the best characterized subclass of these germline encoded PRRs (Takeuchi and Akira, 2010). Effector mechanisms of innate cells include cellular mechanisms like cytotoxicity and phagocytosis, production of humoral antimicrobial peptides and complement factors that target pathogens and secretion of chemokines and cytokines that recruit and activate other key players of immunity (Medzhitov, 2007).

Adaptive and innate immunity should not be considered two separate systems but in fact show many interactions. To give an example granulocyte-macrophage colony-stimulation factor (GM-CSF) inducing the generation of the name giving subsets is produced by several subsets of the adaptive immune system (Codarri *et al.*, 2011; Becher *et al.*, 2016). DCs and macrophages act as professional antigen presenting cells and are crucial for induction of adaptive immunity.

### 1.1.2 The adaptive immune system

The adaptive immune system delivers a very specific response. As in innate immunity this response is carried out by cellular and humoral components. The cellular actors in adaptive immunity are antigen specific lymphocytes called B cells and T cells. Both originate from lymphoid progenitor cells that are descendants of hematopoietic stem cells of the bone marrow. The names of these cells are linked to the organs of their maturation, as B cells mature in the bone marrow and T cells migrate from the bone marrow to the thymus where they complete their development. To identify the huge number of antigens these cells are equipped with specific antigen receptors on their surface. These receptors are not uniform in all the B and T cells but in fact are highly variable due to genetic and somatic recombination of variable, diverse and junction segments (V(D)J-recombination) during their generation. The T and B cell receptors are not only crucial for antigen recognition but are also important for T and B cell activation.

B cells, just as DCs and macrophages, are professional antigen presenting cells. Further, B cells secrete cytokines that influence the immune response. Once activated their primary function is the production of antibodies (AB) They are then called plasma cells. The AB execute the humoral response of the adaptive immune system via noncovalent antigen-specific binding to a specific region on the pathogen surface, named epitope. The AB bound agents are thereby either neutralized, opsonized or eliminated via complement activation or AB dependent cellular cytotoxicity.

Surface molecules of a variety of cells including B and T cells are described with the so-called cluster of differentiation (CD) nomenclature. T cell progenitors in the thymus at first are CD4<sup>-</sup>CD8<sup>-</sup> (double negative) and then become CD4<sup>+</sup>CD8<sup>+</sup> (double positive). Before acquiring an either CD4<sup>+</sup> or CD8<sup>+</sup> single positive phenotype T cells with TCRs that recognize major histocompatibility complex (MHC) or human leukocyte antigen (HLA) in humans are positively selected. Then T cells that recognize endogenous antigens are negatively selected in order to prevent autoimmunity (Carpenter and Bosselut, 2010). Positive and negative selection assures the proper function of the newly generated TCRs.

CD4<sup>+</sup> T cells interact with HLA class II molecules presenting extracellular antigens. CD8<sup>+</sup> T cells recognize HLA class I loaded with endogenous protein fragments digested by the proteasome. Whether a double positive cell becomes CD4<sup>+</sup> or CD8<sup>+</sup> single positive depends on the affinity of the TCR towards HLA I or HLA II (Germain, 2002). Once mature T cells leave the thymus and migrate to secondary lymphoid organs via the bloodstream.

CD8<sup>+</sup> T cells are also called cytotoxic T cells due to their effector functions. If they interact with an infected cell presenting altered protein on HLA class I or that has no HLA class I on its surface CD8<sup>+</sup> T cells induce apoptosis via perforin and granzyme (Lowin *et al.*, 1995). HLA/MHC class I is present on the surface of all healthy cells with a nucleus, whereas HLA/MHC class II can only be found on specialized antigen presenting cells.

CD4<sup>+</sup> T cells are also referred to as T helper cells as they activate other cell types like macrophages and cytotoxic T cells. They further “help” B cells to become plasma cells and produce antibodies. These processes are carried out via HLA class II and T cell receptor interaction, interaction of costimulatory receptors and costimulatory ligands and the release of cytokines.

## 1.2 CD4<sup>+</sup> T cell subsets

CD4<sup>+</sup> cells are grouped according to the expression of certain surface receptors, production of effector molecules like cytokines and chemokines and upregulation of certain transcription factors (TF) that affect cell fate (Mosmann *et al.*, 1986). Cytokines produced by epithelial, stromal and immune cells determine the fate of a naïve CD4<sup>+</sup> T cell.

The first T cells subsets were described by Mossmann and Coffmann. They proposed a dichotomy of Th1 and Th2 cells based on differences in secreted molecules and activation patterns (Mosmann *et al.*, 1986; Mosmann and Coffman, 1989). Now more than 30 years later this assumption is outdated and several new CD4<sup>+</sup> T cell subsets have been added. In the following several CD4<sup>+</sup> T cell subsets are presented in more detail.

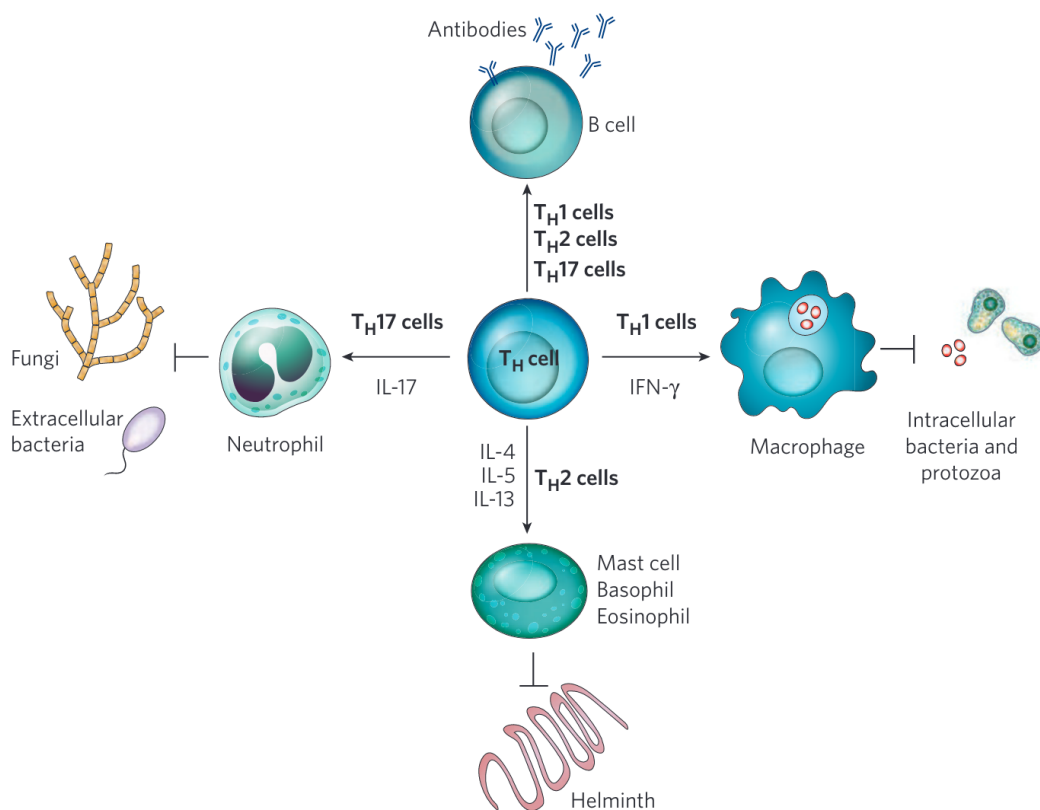


**Figure 1: Effector TH cell lineage and pathogen class**

Th1 cells induce macrophages to clear intracellular bacteria via IFN- $\gamma$ . Facing helminths TH2 cells produce IL-4, IL-5 and IL13 which induce eosinophilic inflammation. Th17 cells lead to neutrophil activation via IL-17 when facing fungi and extracellular bacteria (Illustration adopted from Medzhitov, 2007).

### 1.2.1 Th1 cells

Th1 cells are important for the clearance of intracellular pathogens like viruses, intracellular bacteria and protozoa. IFN- $\gamma$  and IL-2 are the subset defining cytokines. In addition, Th1 cells express tumor necrosis factor (TNF)  $\alpha$  and  $\beta$  as well as GM-CSF. Macrophages are stimulated by these cytokines and upregulate phagocytosis (phagocyte-dependent immunity) (Grifka-Walk *et al.*, 2015; Becher *et al.*, 2016).

To exert their effects, T cells have to reach the site of injury. Special chemokine receptors on the surface guide the cells along a gradient of chemokine concentration towards inflammation. The

chemokine receptors of Th1 cells are CXC-motif chemokine receptor (CXCR) 3, C-C chemokine receptor (CCR) 5, and CXCR6 (Sallusto and Lanzavecchia, 2000).

The transcriptional program of Th1 cells is defined through the master TF T-box expressed in T cells (T-bet) (Szabo *et al.*, 2000). IL-12 and IFN- $\gamma$  drive differentiation of naïve T cells towards Th1 cells via activation of Signal transducer and activator of transcription (STAT) 4 and T-bet signaling pathways (Lazarevic *et al.*, 2013; Szabo *et al.*, 2000).

### **1.2.1.1 T-Bet / Tbx21**

The protein T-bet encoded by T-box transcription factor 21 (Tbx21) is an immune cells specific TF. T-bet was shown to be a potent inducer of Th1 polarization and one of the main drivers of IFN- $\gamma$  induction in Th1 cells (Szabo *et al.*, 2000). Due to the important role in Th1 polarization T-bet is considered the master TF of the Th1 lineage. Via inhibition of Gata3 and ROR $\gamma$ t T-bet inhibits Th2 and Th17 lineage commitment of naïve CD4<sup>+</sup> T cells. (Lazarevic *et al.*, 2013).

The cytokines IL-12 and IL-23 have been shown to upregulate T-bet expression (Lee *et al.*, 2009; Wang *et al.*, 2014). Induction of T-bet in polarized Th17 cells can induce transdifferentiation towards so called Th1-like and exTh17 T cells (Hirota *et al.*, 2011; Lee *et al.*, 2009). It has been proposed that due to bivalent histone methylation marks in the Tbx21 locus of Th17 cells they might be especially responsive to environmental changes (Lazarevic *et al.*, 2013; Mukasa *et al.*, 2010).

## **1.2.2 Th2 cells**

Type 2 immune response induced by Th2 cells depends mainly on the cytokines IL-4, IL-5, IL-9 and IL-13 (Yamaguchi *et al.*, 1988; Van Dyken and Locksley, 2013). This type of response is triggered facing infections with extracellular parasites such as helminths or during allergic reactions. Inflammation is driven by recruitment of eosinophils and production of IgG1 and IgE by B cells (Kopf *et al.*, 1993; Yamaguchi *et al.*, 1988).

Induction of Th2 cells is promoted by IL-2 and IL-4 and the absence of cytokines inducing Th1 and other CD4<sup>+</sup> subsets (Zhu, 2015). This is reflected in Gata3, the master TF of the Th2 lineage, which in contrast to T-bet is already expressed in naïve CD4<sup>+</sup> T cells (Zheng and Flavell, 1997). Further, T-bet expression redirects Th2 commitment towards Th1 cells and inhibits IL-4 and IL-5 expression (Szabo *et al.*, 2000). Th2 cells express the chemokine receptors CCR3, CCR4, and CCR8 (Sallusto and Lanzavecchia, 2000).

## **1.2.3 Th17 cells**

Th17 cells are responsible for controlling bacterial and fungal infections (Cua *et al.*, 2003; Murphy *et al.*, 2003). They have been discovered in 2005 and since then linked to pathogenicity in several autoimmune mediated disease (Harrington *et al.*, 2005; H. Park *et al.*, 2005; Hirota *et al.*, 2011; Harbour *et al.*, 2015; Krebs *et al.*, 2016).

Th17 cells acquire their phenotype under the effect of master TFs ROR $\gamma$ t and ROR $\alpha$  (Ivanov *et al.*, 2006; Yang *et al.*, 2008). The cytokines causing a differentiation towards a Th17 phenotype are IL-

1 $\beta$ , transforming growth factor- $\beta$  (TGF- $\beta$ ) and IL-6 (Bettelli *et al.*, 2006; Mathur *et al.*, 2007; Krebs *et al.*, 2017). Moreover IL-23 plays a critical role in maintaining the Th17 phenotype (Kleiner *et al.*, 2022; Stritesky *et al.*, 2008). Polarized Th17 cells are defined by expression of the cytokines IL-17A, IL-17F, IL-21 and the chemokine receptor CCR6 (Ivanov *et al.*, 2006; Wang *et al.*, 2009). Further, Th17 cells can express GM-CSF and IL-22 which have been linked to pathogenicity (Chung *et al.*, 2006; Sonderegger *et al.*, 2008; El-Behi *et al.*, 2011; Paust and Song *et al.*, 2023).

STAT3 regulates the expression of ROR $\gamma$ t, ROR $\alpha$ , IL-17A, IL-17F and IL-21 (Durant *et al.*, 2010; Mathur *et al.*, 2007). Once a T helper cell has acquired a Th17 phenotype it remains prone to change its transcriptional and cytokine profile in a process called transdifferentiation. This plasticity of Th17 cells towards other T helper subsets is triggered by the cytokine milieu which can push Th17 towards regulatory T cells, Th1 cells or T follicular helper cells (Tfh) (Lee *et al.*, 2009; Hirota *et al.*, 2013; Gagliani *et al.*, 2015; Krebs and Panzer, 2018).

### **1.2.3.1 Th17-Th1 transdifferentiation**

Fate mapping revealed that in certain conditions Th17 cells can cease IL-17A production and start production of IFN- $\gamma$  (Hirota *et al.*, 2011). This Th17-Th1 axis includes IL-17A<sup>+</sup>IFN- $\gamma$ <sup>-</sup> bona fide Th17 cells (Th17), IL-17A<sup>+</sup>IFN- $\gamma$ <sup>+</sup> Th1-like Th17 (Th1-like) cells and IL-17A<sup>-</sup>IFN- $\gamma$ <sup>+</sup> Th1-like exTh17 (exTh17) cells (Hirota *et al.*, 2011; Brucklacher-Waldert *et al.*, 2016).

The Th17-Th1 axis is involved in several autoimmune disease (AID) like multiple sclerosis (MS), rheumatoid arthritis (RA) and intestinal bowel disease (IBD) (Lee *et al.*, 2009; Nistala *et al.*, 2010; Hirota *et al.*, 2011; Harbour *et al.*, 2015).

Both IL-12 and IL-23 can upregulate Tbx21 and Stat4 and induce IFN- $\gamma$  production in Th17 cells (Lee *et al.*, 2009; Wang *et al.*, 2014). IL-23 however seems to be a more potent inducer as IL12rb2 gene knockout (KO) targeting IL-12 signaling did not significantly alter the Th17-Th1 axis in murine IBD (Harbour *et al.*, 2015).

Co-expression of TFs ROR $\gamma$ t and T-bet was reported in Th17 transdifferentiation towards Th1 cells. CD4<sup>+</sup> T cells retrovirally transduced with T-bet did not expand towards a Th17 phenotype, while transduction with ROR $\gamma$ t led to an expansion of the Th17 population. Simultaneous retroviral transduction showed that co-expression of T-bet and ROR $\gamma$ t was not enough to induce a Th1-like phenotype (Kleiner *et al.*, 2022; Lazarevic *et al.*, 2011; Wang *et al.*, 2014). Runt-related proteins (RUNX) 1 and RUNX3 are upregulated in transdifferentiating Th17 cells after stimulation with IL-12 and have been shown capable to induce Th1-like cells (Wang *et al.*, 2014).

In recent work Bartsch *et al.* showed that *S. aureus* infection induces a strong IL-17A and IFN- $\gamma$  response in the kidney with pronounced plasticity of Th17 towards the Th1 lineage. Further, exTh17 cells expressing Tbx21 were shown to play an important role in bacterial clearance in the kidney (Bartsch *et al.*, 2022). However, the factors driving plasticity within the Th17-Th1 axis and pathogenicity of these cells remain incompletely understood.

### 1.2.4 Regulatory T cells

Besides effector CD4<sup>+</sup> T cells subsets that induce inflammation facing the threat of a pathogen an opposing group of CD4<sup>+</sup> T cells has developed in the evolutionary process. Regulatory T cells (Tregs) play an important role in the counter-regulation of inflammatory processes, self-tolerance and auto-immune defense (Kim *et al.*, 2007). These cells express the IL-2 receptor alpha chain (CD25) (Sakaguchi *et al.*, 1995).

CD4<sup>+</sup>CD25<sup>+</sup> Tregs can be found both in rodents and in humans (Ng *et al.*, 2001). The TF Forkhead box protein 3 (Foxp3) is the crucial TF for generation of Tregs (Fontenot *et al.*, 2003). IL-10 produced by Tregs acts on several immune cells and hence not only CD4<sup>+</sup>CD25<sup>-</sup> conventional T cells (Tconv) but also B cells, CD8<sup>+</sup> T cells, NK cells, monocytes and DCs can be suppressed (Roncarolo and Battaglia, 2007). Other cytokines contributing to immunosuppression are TGF- $\beta$  and IL-35 (Shevach, 2009). On their surface Tregs express cytotoxic T lymphocyte-associated antigen 4 which limits dendritic stimulation of naïve T cells (Shevach, 2009; Takahashi *et al.*, 2000). In addition to CD4<sup>+</sup>CD25<sup>+</sup> Tregs other regulatory CD4<sup>+</sup> T cells have been described.

Type 1 regulatory T cells (Tr1) do neither express CD25 nor Foxp3 but as Tregs produce IL-10 as their main suppressive cytokine (Roncarolo and Battaglia, 2007). CD49b and Lag-3 is co-expressed on the cellular surface of Tr1 cells (Gagliani *et al.*, 2013; Soukou-Wargalla *et al.*, 2023). Tr17 cells co-express ROR $\gamma$ t and Foxp3, the respective TFs of Th17 cells and Tregs. They can be found in the gut and peripheral lymph nodes. They seem to derive from Tregs following IL-6/Stat3 signaling and are possible inhibitors of Th17 driven inflammation (Kim *et al.*, 2017).

As previously mentioned, transdifferentiation of Th17 cells towards a regulatory phenotype has been observed. These cells can therefore also be considered a regulatory T cell subset. Th17 cells in the gut can stop IL-17A and pick up IL-10 production and expression of Foxp3. Further, these cells downregulate CCR6 and ROR $\gamma$ t and express Tr1 marker Lag-3 (Gagliani *et al.*, 2015; Soukou-Wargalla *et al.*, 2023).

### 1.2.5 Th22 cells

Th22 cells have recently been discovered and are not yet precisely understood. They produce IL-22, IL-13 and TNF- $\alpha$ , while lacking expression of signature cytokines of other subsets (IL-17, IFN- $\gamma$  and IL-4) (Plank *et al.*, 2017). IL-22 is heavily implicated in a variety of AIDs with both proinflammatory and anti-inflammatory effects reported (Wolk *et al.*, 2004; Seiderer and Brand, 2009).

### 1.2.6 Th9 cells

Differentiation towards IL-9 producing Th9 cells is induced by TGF- $\beta$  and IL-4 (Veldhoen *et al.*, 2008). They require Stat6, Irf4, PU.1 and Gata3 for their differentiation (Kaplan, 2013). These cells have been shown to be implicated in tumorigenesis, allergy and inflammatory diseases possibly also by interacting with Th17 cells and Tregs (Elyaman *et al.*, 2009). However, several functions of this rather new subset and the cytokine IL-9 remain incompletely understood.

## 1.3 Autoimmunity

The complex structures of the immune system are designed to protect its host from a vast number of pathogens. If discrimination between endogenous and exogenous peptides is disturbed it can cause inflammatory responses directed against host tissue. This process is called autoimmunity.

Several mechanisms aim at preventing recognition of endogenous antigens as exogenous. During maturation in the thymus, T cells with a TCR recognizing endogenous antigen are negatively selected and enter apoptosis (Carpenter and Bosselut, 2010). Alongside the central tolerance, T cells are further selected in the periphery. Mechanisms of peripheral tolerance include putting autoreactive T cells in an unresponsive state called anergy, deletion of those cells via apoptosis or induction of induced regulatory T cells from Tconv cells (Roncarolo and Battaglia, 2007; ElTanbouly and Noelle, 2021).

Even if some autoreactive cell are not neutralized through mechanisms of central and peripheral tolerance, it might not directly have to result in a pathological autoimmune response (Salinas *et al.*, 2013). The etiology of autoimmunity is not fully understood but genetic and environmental factors contribute to its development. Genome wide association studies identified MHC/HLA and non-MHC/HLA loci associations within several AID. Most of these AID have a multigenetic background and cannot be attributed to a single mutation (Sollid *et al.*, 2014). Studies with monozygotic twins showed a strong correlation but not a full penetration in the emergence of AID. This points at an important role for environmental and epigenetic factors in AID (Quintero-Ronderos and Montoya-Ortiz, 2012). Environmental factors include the microbiota, infections, tobacco smoke and pharmaceutical agents (Wang *et al.*, 2015).

Following infections with microorganisms that resemble host epitopes, in a process called “molecular mimicry” activated lymphocytes might not only attack the pathogen but also host tissue with similar epitopes (Guilherme *et al.*, 2001). T cell effector mechanisms directed against host tissue then result in organ damage and inflammation. Among CD4<sup>+</sup> T cells Th1 and Th17 cells have been linked to several AIDs like MS, RA, IBD and glomerulonephritis (GN) (Langrish *et al.*, 2005; H. Park *et al.*, 2005; Hirota *et al.*, 2011; Harbour *et al.*, 2015; Krebs *et al.*, 2017). The role of Th17 cells in selected AIDs will be described in more detail in the following sections of the thesis.

## 1.4 The kidneys

### 1.4.1 Anatomy and function of the kidneys

The paired kidneys are a bean-shaped organ situated retroperitoneally within the abdomen. Their main functions are the maintenance of physiological electrolyte levels and the clearance of toxic substance from the blood into the urine. Furthermore, they produce hormones like renin and erythropoietin (EPO). Renin is produced in hypotension and catalyzes the first reaction of the renin-angiotensin-aldosterone system leading to a vasoconstriction and production of aldosterone via Angiotensin II. This is called the renin-angiotensin system (RAS) and its activation results in rising blood pressure. EPO stimulates the erythropoiesis within the bone marrow and production is

stimulated by declining partial pressure of oxygen within the kidneys. In addition, the second hydroxylation step of cholecalciferol (vitamin D) takes place in the kidneys. They are also involved in pH regulation as they excrete excess protons in form of ammonium and hydrogen phosphate as well as it absorbs and synthesizes bicarbonate.

In relation to its weight, the kidney is the best perfused organ in the human body. Blood enters the kidney via the paired renal arteries and eventually reaches the glomerulus over the afferent arteriole. Here filtration of the primary urine takes place. The blood then leaves via the efferent arteriole. The kidney is drained by the paired renal veins (see *Figure 2 (A) and (C)*).

Functionally, the kidney can be divided into the urine producing renal parenchyma and the calyces and renal pelvis that drain the urine. The parenchyma consists of an outside cortex and the inside medulla. Parts of the functional units of the kidney, the nephrons, are situated in both cortex and medulla (see *Figure 2 (B)*). The renal corpuscles are situated in the cortex of the kidney. These are responsible for filtration of water, electrolytes and toxic substances. The proximal and distal tubules lie in the cortex. Electrolytes, water and other substances can be secreted or absorbed in these structures. The medulla contains the loop of Henle and the collecting ducts.

The filtration barrier between the blood and the urine is formed by the endothelial cells of the glomerulus, the glomerular basement membrane (GBM) and the podocytes (see *Figure 2 (D) and (E)*). Due to the slit membrane of the filter and its negative charge small positively charged molecules pass it with ease, while negatively charged larger molecules like albumin (68kDa) stay in the blood. The amount that is filtered depends on the pressure in the glomerulus. The pressure is a result of the width of the afferent and efferent arteriole. The filtered primary urine is collected by the Bowman's capsule and drained into the tubular system. Passing through the tubular system the primary urine is concentrated and some small proteins and electrolytes are secreted into or absorbed from the urine. This happens via formation of a high osmotic gradient in the medulla of the kidney and by active transport. After the passage through the tubular system the urine reaches the collecting duct and is then passed to the renal pelvis and the ureter.

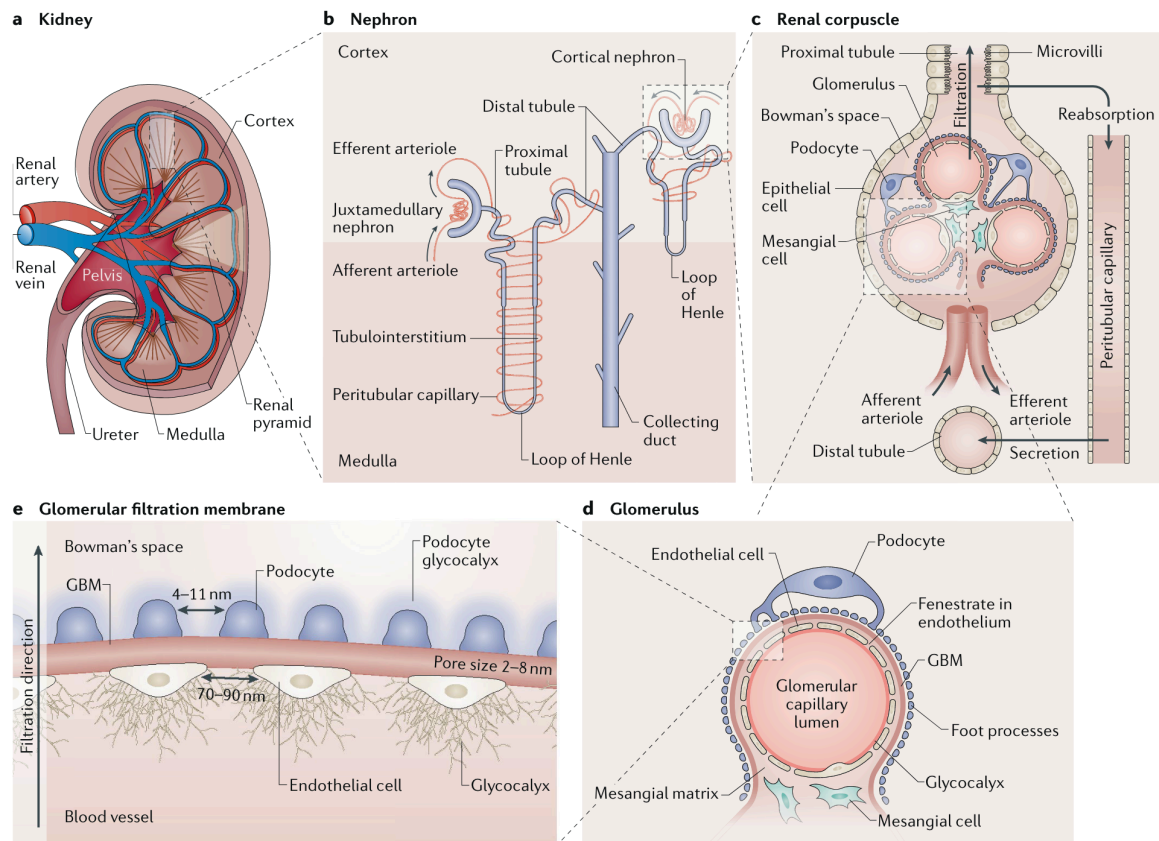


**Figure 2: Kidney anatomy**

(A) Kidney cross section showing the macroscopic kidney anatomy. Renal artery and vein supply and drain blood from the kidney. The parenchyma consists of the cortex and medulla. Renal corpuscles, proximal and distal tubule are situated in the cortex and loop of Henle, collecting duct and peritubular capillaries within the medulla. Produced urine is drained into the pelvis via the papilla of one of multiple renal pyramids. (B) Nephrons are the functional units of the kidney. Primary urine is filtered in the renal corpuscle and then passes the proximal tubule, loop of Henle, distal tubule and collecting ducts where it is concentrated. Further, substances are secreted and reabsorbed to eliminate toxic materials and maintain physiological blood electrolyte levels. (C) The renal corpuscle is the place of filtration. Blood reaches the glomerulus over the afferent arteriole. Discrepancies in the lumen or pressure between afferent and efferent arteriole cause sideways pressure responsible for filtration into the Bowman's space. Filtered blood leaves the renal corpuscle over the efferent arteriole. Reabsorption and secretion take place in the proximal and distal tubule respectively which are in proximity to peritubular capillaries. (D) The glomerular filtration membrane (from blood to urine) consists of endothelial cells, GBM and podocytes plus the respective glycocalyx. (E) The size of the pores (GBM) and slit membrane (podocytes) as well as the negative charge of components of the endothelial glycocalyx and GBM (proteoglycans and heparin sulfate) cause the size and charge selective filtration. The GBM consists mainly of type IV collagen. (Illustration adopted from Du *et al.*, 2018).

#### 1.4.2 Immune mediated crescentic glomerulonephritis

Immune mediated crescentic glomerulonephritis (cGN) is an aseptic immune mediated inflammatory disease affecting the glomeruli of both kidneys. There are several forms of glomerulonephritis (GN) with crescentic/rapid progressive GN (cGN/RPGN) being the most destructive. Further, GN can be divided into diseases that result from systemic disorders like lupus nephritis in the context of systemic lupus erythematosus (SLE) and GN that is restricted to the kidney like IgA nephropathy (Krebs and Panzer, 2018).

cGN is characterized by a rapidly advancing restriction of kidney function as depicted by decreased glomerular filtration rate (GFR). The histological finding of crescents in cGN describes epithelial cell proliferates within the otherwise empty Bowman's capsule (Jennette and Thomas, 2001). The

histological appearance of crescents is described in *Figure 3*. The 3 most prevalent entities of cGN are immune-complex GN (ICGN), anti-GBM GN and pauci-immune GN. Due to high levels of anti-neutrophil cytoplasmic autoantibodies (ANCA) pauci-immune GN is also called ANCA-GN (Couser, 1988; Jennette and Thomas, 2001). These three are described in brief below.

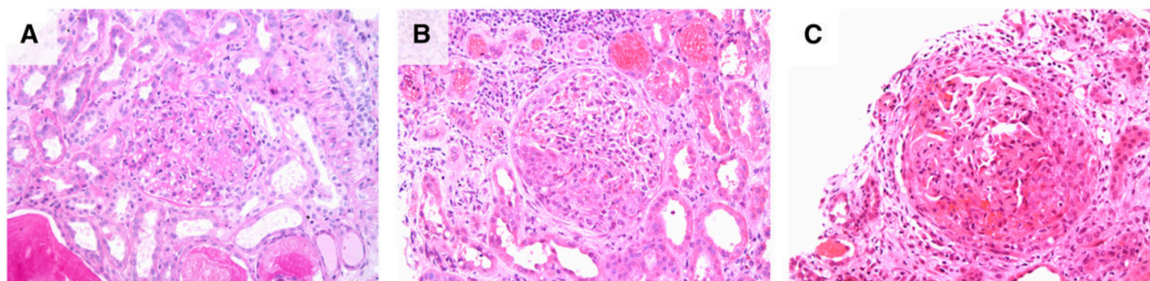


**Figure 3: Histological correlates of crescentic glomerulonephritis**

Hematoxylin/eosin stained sections of kidney tissue (A) Necrotizing lesion with fibrin (B) Small cellular crescent (C) Large circumferential crescent (Illustration adopted from McAdoo and Pusey, 2017).

#### **1.4.2.1 Immune-complex glomerulonephritis**

ICGN includes post- / para-infectious (e.g. poststreptococcal) GN, IgA nephropathy, lupus nephritis and membranoproliferative GN (Krebs and Panzer, 2018). In general crescents are less prevalent in ICGN compared to entities of cGN. This indicates a milder course of disease (Jennette and Thomas, 2001). It has been shown that the percentage of crescents correlates with the severity and the prognosis of disease (Haas *et al.*, 2017).

#### **1.4.2.2 Anti-glomerular basement membrane glomerulonephritis**

Autoantibodies against the non-collagenous domain 1 of the alpha 3 and alpha 5 chain of type IV collagen ( $\alpha 3/5(IV)NC1$ ) can trigger anti-GBM GN (Kalluri *et al.*, 1995; Pedchenko *et al.*, 2010). This induces a very aggressive clinical course which often includes pulmonary impairment due to expression of  $\alpha 3(IV)NC1$  in both kidneys and lungs (Kalluri *et al.*, 1995). The vasculitic syndrome including renal disease and pulmonary hemorrhage is termed Goodpasture's syndrome and can be found in 50% of the patients (Jennette and Thomas, 2001; Jennette, 2003; McAdoo and Pusey, 2017). Anti-GBM GN makes up around 15 % of total cGN cases (Jennette, 2003).

#### **1.4.2.3 Pauci-immune glomerulonephritis**

Pauci-immune GN describes an immune mediated renal disease lacking immunoglobulins (Ig) which are typical for immune complex or anti-GBM disease. Lack of Ig in immunohistochemical staining is in 80-90% accompanied by the finding of ANCA. ANCA can further be divided into proteinase 3 specific (PR3-ANCA) and myeloperoxidase specific (MPO-ANCA) ANCA (Jennette and Falk, 1997, 1998). These can be distinguished via indirect immunofluorescence assays as PR3-ANCA causes cytoplasmic (C-ANCA) and PR3-ANCA perinuclear (P-ANCA) staining of neutrophils (Jennette and Thomas, 2001).

Histological analyses of pauci-immune GN show fewer crescent formations compared to other types of cGN (Jennette and Thomas, 2001). In pauci-immune GN pulmonary-renal syndrome is even more prevalent than in anti-GBM GN as up to 75 % do suffer ANCA GN based on ANCA-small vessel vasculitis. Overall ANCA-associated vasculitis is the most frequent origin of RPGN (Rovin *et al.*, 2021). This includes three entities: (1) Granulomatosis with polyangiitis (GPA), (2) Microscopic polyangiitis (MPA) (3) Eosinophilic granulomatosis with polyangiitis (EGPA) (Couser, 1988; Jennette and Falk, 1997). Findings in GPA are necrotizing granulomatous inflammation paired with necrotizing vasculitis of small vessels. Necrotizing granulomatous inflammation can often be found in the lungs. MPA patients show systemic vasculitis of small vessel (arteries, capillaries, veins, venules). Patients suffering EGPA often have history of asthma and increased levels of eosinophils (Jennette and Falk, 1997).

#### **1.4.2.4 Diagnosis and course of crescentic glomerulonephritis**

Clinical symptoms of cGN include reduced urine production or anuria, flank pains, fatigue and edema. Blood analysis may reveal elevated creatinine levels paired with increased general inflammation markers. In earlier stages of disease hyperfiltration and glomerular hypertrophy may condition normal creatinine levels. This compensation may disguise glomerular injury (Helal *et al.*, 2012).

In cases of rapid declining kidney function, urinalysis for blood and protein is the first step to a RPGN diagnosis. If positive, this should be followed up by urine sediment. The finding of dysmorphic erythrocytes called acanthocytes (glomerular hematuria), urinary casts and aseptic pyuria in urine sediment can support a possible RPGN diagnosis. This is followed up by autoimmune serology including ANCA, antinuclear antibodies (ANA), anti-GBM antibodies and complement (Rovin *et al.*, 2021).

Kidney biopsy remains the gold standard in RPGN diagnosis. In anti-GBM GN direct immunofluorescence on frozen kidney slices reveals linear IgG deposits on the GBM level (McAadoo and Pusey, 2017). ICGN displays complexes of antigen (AG) and AB between the GBM and capillary endothelium. In pauci-immune GN there are typically few or no findings in immunohistology (Kurts *et al.*, 2013). Conclusive cases allow induction of treatment prior to biopsy results. This may limit kidney damage (Rovin *et al.*, 2021). Further, serological testing with commercially available bead-based immunofluorescence assays may be performed (McAadoo and Pusey, 2017). In addition to immunofluorescence, classic histological analysis is performed. Here the focus is on tubulointerstitial inflammation, sclerosis, necrosis and especially crescent formation.

Due to the rapid impairment of the complex filter function, glomerular inflammation leads to a high risk and restriction for the patient. Accurate diagnosis and immediate initiation of therapy are essential in order to ameliorate glomerular injury and prevent the need of renal replacement therapy (RRT) (Jennette, 2003; McAadoo and Pusey, 2017). RRT includes dialysis and kidney transplantation. With progression of the disease, glomerular and tubulointerstitial fibrosis increase and lead to an irreversible chronic kidney disease (CKD). CKD describes an abnormal kidney structure paired with health implications lasting for more than 3 months (Stevens *et al.*, 2013). By measuring the glomerular filtration rate (GFR), the kidney function can be assessed and a classification of CKD

severity can be made (see *Table 1*) (Gaitonde *et al.*, 2017; Levey *et al.*, 2020). The GFR describes the filtered volume of the whole kidney per time unit in ml/min. Ultimately, CKD can result in end-stage renal disease (ESRD), which describes kidney disease dependent on RRT.

RPGN is a frequent intrarenal cause of acute kidney injury (AKI). AKI describes a rapid decrease in kidney function, based on decreased urinary output and increased creatinine for less than 7 days. The loss of nephrons during AKI may cause a subsequent CKD (Kellum *et al.*, 2021).

**Table 1: Stages of CKD based on GFR**

Stage	GFR in ml/min/1,73 m <sup>2</sup>	Explanation
G1	≥ 90	Kidney damage* with normal to increased GFR
G2	60 - 89	Kidney damage* with mildly reduced GFR
G3a	45 - 59	Mildly to moderately reduced GFR
G3b	30 - 44	Moderately to severely reduced GFR
G4	15-29	Severely reduced GFR
G5	<15 or dialysis	Kidney failure

\*Markers of kidney damage required for diagnosis

(Adopted from Gaitonde *et al.*, 2017; Levey *et al.*, 2020)

**Table 2: Interpretation of Albumin/Creatinine-ratios (ACR)**

Stage	ACR	Explanation
A1	< 30 mg/g	Normal to mildly increased
A2	30 to 300 mg/g	Moderately increased
A3	> 300 mg/g	Severely increased
	> 2200 mg/g	Nephrotic range

(Adopted from Levey *et al.*, 2020)

#### **1.4.2.5 Treatment of crescentic glomerulonephritis**

The treatment of cGN is currently still unspecific and carries the risk of serious side effects under general immunosuppression. The drivers of kidney damage and pathways that lead to pathogenicity in earlier described diseases are not fully understood. Patients rely on lifestyle changes and immunosuppressive treatment to prevent a worsening of disease towards ESRD. Toxic substances like non-steroidal anti-inflammatory drugs (NSAID) must be avoided and strict control of the blood pressure is indicated. The blood pressure should be adjusted to below 120 mmHg with nephroprotective angiotensin converting enzyme (ACE) inhibitors or angiotensin 2 receptor blockers (ARBs) (Levey *et al.*, 2020). Clinical manifestations of cGN like edema need to be treated, preferably with loop diuretics and restriction of sodium intake (Levey *et al.*, 2020). Side effects of diuretics include hyponatremia, hypokalemia and volume depletion and should therefore be monitored

narrowly. Metabolic acidosis needs to be treated, if bicarbonate drops beneath 22 mmol/l (Rovin *et al.*, 2021).

ANCA GN is more prevalent than other entities of RPGN. The therapies of these other entities are therefore often based on experience from ANCA GN therapy. As noted previously, immunosuppressive treatment should not be delayed by kidney biopsy results (Levey *et al.*, 2020). Induction therapy in ANCA GN includes glucocorticoids with cyclophosphamide or rituximab. Due to a high risk of relapse in ANCA GN, this is followed up with a maintenance therapy including low dose glucocorticoids plus rituximab or azathioprine for at least 18 months. If long term RRT is necessary, kidney transplantation should not be performed before 6 months of clinical remission. A termination of maintenance therapy should consider risk factors for a relapse such as rising ANCA, more extensive disease, low serum creatinine or history of relapse (Rovin *et al.*, 2021).

Anti-GBM GN is treated with glucocorticoids and cyclophosphamides. In addition to immunosuppression, plasma exchange may be performed to clear pathogenic anti-GBM AB (McAdoo and Pusey, 2017). Imlifidase is a newly introduced enzyme with the ability to degrade IgG. It can therefore clear pathogenic AB and allows kidney transplant despite a positive crossmatch (Couzi *et al.*, 2023; Rovin *et al.*, 2021). In cases of successful initial therapy, a maintenance therapy is not necessary as anti-GBM GN has low rates of relapse. However, if patients test positive for ANCA a maintenance therapy as previously described in ANCA GN is indicated (Rovin *et al.*, 2021). Treatment in ICGN differs between the various entities. For example, in IgA nephritis immunosuppressive treatment is limited to glucocorticoids, although their clinical benefit has not been evaluated yet. The focus is on lifestyle changes, diet and blockage of the RAAS. In cases of rapid progressive IgA nephritis cyclophosphamide may be applied for additional immunosuppression (Rovin *et al.*, 2021). Further a series of biologicals is currently under investigation and may replace or supplement current therapy regimes in different entities of cGN in the future.

#### **1.4.2.6 Th17 cells in crescentic glomerulonephritis**

The discovery of Th17 cells challenged the proinflammatory role of Th1 cells in AID. Th17 were shown to play an important role in pathogenesis, pathogenicity and disease progression (Krebs *et al.*, 2017). T cells producing IL-17 were first identified in the kidney during acute urinary obstruction. Later, they were linked to cGN due to findings in the nephrotoxic nephritis mouse model (NTN) (see 2.2.4). NTN is frequently used to study cGN, as it resembles the disease of anti-GBM GN. Sheep anti-mouse GBM ABs are injected into mice that in the following suffer cGN. At first, kidney damage in this model was believed to be exclusively AB mediated. Later, it has been shown that CD4<sup>+</sup> T cells and especially Th17 cells are the key mediators of renal damage (Krebs *et al.*, 2017). Cessation of both IL-17A and IL-23 expression leads to ameliorated disease, proving the relevance of Th17 cells in cGN (Paust *et al.*, 2009). This was backed up by work from Steinmetz *et al.*, who showed that ROR $\gamma$ t KO mice cannot mount a Th17 response and do not suffer GN following the i.p. injection of NTN serum (Steinmetz *et al.*, 2011).

IL-17A produced by Th17 cells leads to upregulation of CXCL1 and CXCL5 in tubular cells. These attract neutrophils and leucocytes that increase kidney damage (Disteldorf *et al.*, 2015).

Th17 cells are not only present in the kidney during active GN. So called tissue resident Th17 cells (Trm17) can be found in the kidneys of healthy specimens. They differentiate facing a pathogen like *S. aureus* and then remain in the kidney after the infection. Trm17 cells can be reactivated during inflammation and then contribute to disease severity in cGN (Krebs *et al.*, 2020). Regarding Th17-Th1 plasticity, data so far suggests a stable Th17 phenotype in cGN (Hirota *et al.*, 2011; Krebs *et al.*, 2016).

## **1.5 The gastrointestinal tract**

### **1.5.1 Anatomy and function of the gastrointestinal tract**

The gastrointestinal tract includes the connected organs between mouth and anus that are involved in digestion. Food is mechanically crushed in the mouth and mixed with saliva. Saliva already contains enzymes like lipase and lysozymes that contribute in a small part to the digestion. Food then enters the stomach through the esophagus. Here the main enzymatic digestion starts. 2 liters of gastric juice are produced every day. The gastric juice contains hydrochloric acid from parietal cells and pepsin from main cells. The motility of the stomach is crucial for mixing the food with the gastric juice and production of the chyme. Digestion in the stomach usually takes between 1 and 3 hours. The chyme then small portioned enters the duodenum via the pyloric sphincter, where pancreatic derived enzymes are added. These enzymes produced in the acinar cells of the exocrine pancreas are lipases, RNases and DNases, proteases, cholesterol esterase, peptidases and  $\alpha$ -amylase. Afterwards, the chyme passes through the ileum and jejunum. Here most nutrients are absorbed from the chyme. Duodenum, ileum and jejunum form the small intestine. The small intestine reaches to the ileocecal valve (Bauhin's valve) and is followed by the colon. In the colon most of the water is absorbed and the chyme thereby thickened. Indigestible parts of the food are then transported towards the rectum and finally excreted via the anus.

### **1.5.2 Inflammatory bowel disease**

#### **1.5.2.1 Crohn's disease and ulcerative colitis**

Inflammatory bowel disease (IBD) is a chronic inflammatory disease of the intestine. The two most frequent examples of IBD are Crohn's disease (CD) and ulcerative colitis (UC). These are recurrent or permanent inflammations of the intestine, especially frequent in patients in their twenties and thirties. The prevalence of IBD is rising, which seems to be caused by environmental factors. A genetic susceptibility has been suspected early, as first-degree relatives of IBD patients are 5 times more likely to suffer IBD (Tysk *et al.*, 1988). Genome wide association studies revealed NOD2 as a susceptible locus for CD (Hugot *et al.*, 2001). NOD2 is implicated in the expression of antimicrobial defensins, whose reduction was observed in IBD (Wehkamp *et al.*, 2004). The loci IBD5, ATG6L1 and IL23R influence phagocytosis and innate immunity and were also associated with IBD (Xavier and Podolsky, 2007).

UC usually begins at the level of the rectum and then continuously ascends to more proximal sites within the colon. The main localization of CD is the terminal ileum and the adjacent colon. However, CD is not limited to the ileo-cecal region and can manifest itself throughout the entire intestinal tract. The pattern of inflammation in CD is patchy resulting in so called “skip lesions” (see *Figure 5 (A)*). Early lesions are often observed in proximity to Peyer’s patches (PPs). PPs are lymphoid follicles located in the subepithelial of the distal small intestine. Inflammation in UC is limited to the mucosal lamina propria. It is driven by neutrophilic inflammation and the formation of so-called crypt abscesses. CD in contrast is driven by macrophages forming granulomas (see *Figure 4*). In CD inflammation can affect all layers of the intestinal tract and is therefore called transmural inflammation. This conditions the frequent occurrence of fistulas and abscesses.

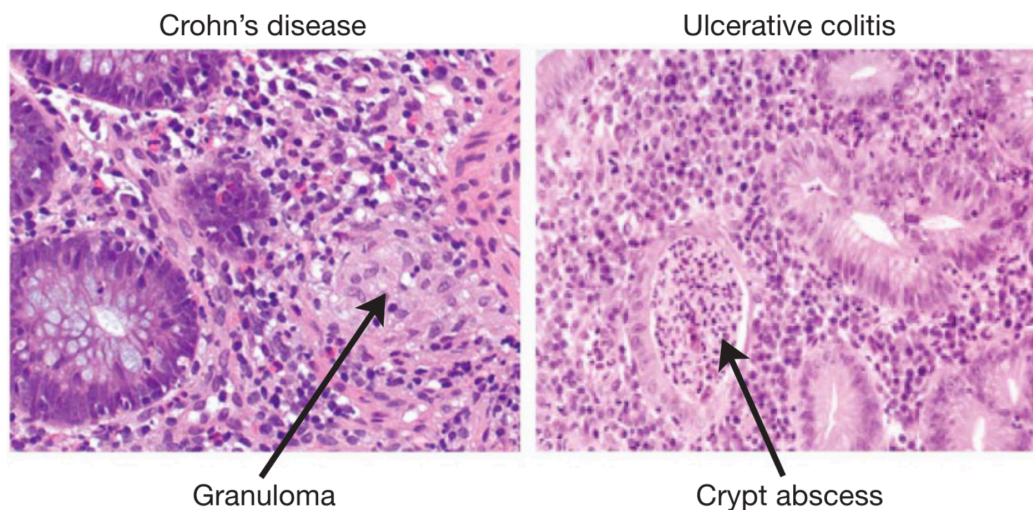


**Figure 4: Histological correlates of CD and UC**

Transmural inflammation in CD is driven by macrophages that lead to formation of granuloma. In UC neutrophilic infiltration into the intestinal lamina propria takes place. This results in crypt abscesses. (Illustration adopted from Xavier and Podolsky, 2007).

The etiology of IBD is incompletely understood. In addition to earlier described genetic and environmental factors, an impaired intestinal barrier function, decreased ability to recognize pathogens by lymphocytes and an altered mucus layer may contribute to the onset of IBD (Mizoguchi *et al.*, 2018; Söderholm *et al.*, 2002). All this leads to an increased permeability of the intestinal mucosa for pathogens.

The composition of the microbiome is an important factor contributing or even conditioning IBD. Not only does antibiotic alteration of the commensal flora ameliorate IBD, but there also specific germs inducing chronic colitis in murine models of IBD (Gkouskou *et al.*, 2014). Modification of the microbiome is therefore an interesting target in future therapies of IBD. Yet, our understanding of the microbiome and its interactions with the immune system in IBD is limited and needs further research. So far, antibiotic treatments cannot be recommended in a clinical context except for the treatment of IBD complications (Lamb *et al.*, 2019).

ILCs, macrophages, neutrophils and DCs mediate tissue damage in IBD. Apart from the infiltration of innate cells, leukocyte infiltration is observed in the inflamed mucosa of IBD patients (see *Figure 5 (D)*, Neurath, 2019)). In CD these infiltrating leukocytes are pathological Th1 or Th17 cells. UC shows predominant IL-4 and IL-13 producing Th2 cells (Heller *et al.*, 2002; Fujino *et al.*, 2003).

Effector memory T cells migrate among lymph nodes, the bloodstream and the gut. They can contribute to extra-intestinal manifestations and to intestinal tissue destruction after homing to the lamina propria (Neurath, 2019).

### **1.5.2.2 Diagnosis of inflammatory bowel disease**

The diagnosis of IBD starts with physical and stool examination. Diagnostic procedures include sonography, esophagogastroduodenoscopy, colo-ileoscopy, magnetic resonance imaging and histopathological analysis of material acquired during endoscopic examinations. Further, extraintestinal manifestations linked to IBD may be observed. Some examples are primary sclerosing cholangitis, skin disease like pyostomatitis vegetans, erythema nodosum and pyoderma gangrenosum as well as renal complications (see *Figure 5 (C)*, Levine and Burakoff, 2011; Neurath, 2019).

Once IBD is manifest, the endoscopic examinations may reveal macroscopically visible ulceration, erythema, granulosis and pronounced vascularity. In CD ulceration and adjacent inflamed mucosa termed “cobblestone-like relief” combined with aphthoid hemorrhagic lesions (“pinpoint lesions”) can be observed (see *Figure 5 (B)*). The macroscopic and microscopic findings translate to the clinical picture. This includes chronic diarrhea, weight loss, tenesmus and abdominal pain. In CD, patients report predominant pain in the right lower abdomen. UC patients localize the pain around the affected rectum in the left lower abdomen. Diarrhea in UC is usually bloody-slimy. IBD usually progresses in a chronic relapsing course. There can also be symptom-free periods. Patients suffering IBD report a significant reduction of the quality of life. This is represented in high prevalence of fatigue in IBD patients (van Langenberg and Gibson, 2010). In UC, 15-20% percent will require hospitalization in the course of disease due to complications like acute severe ulcerative colitis (ASUC) or toxic megacolon. Moreover, IBD leads to increased frequency of malignancies in the intestinal tract (Lamb *et al.*, 2019).

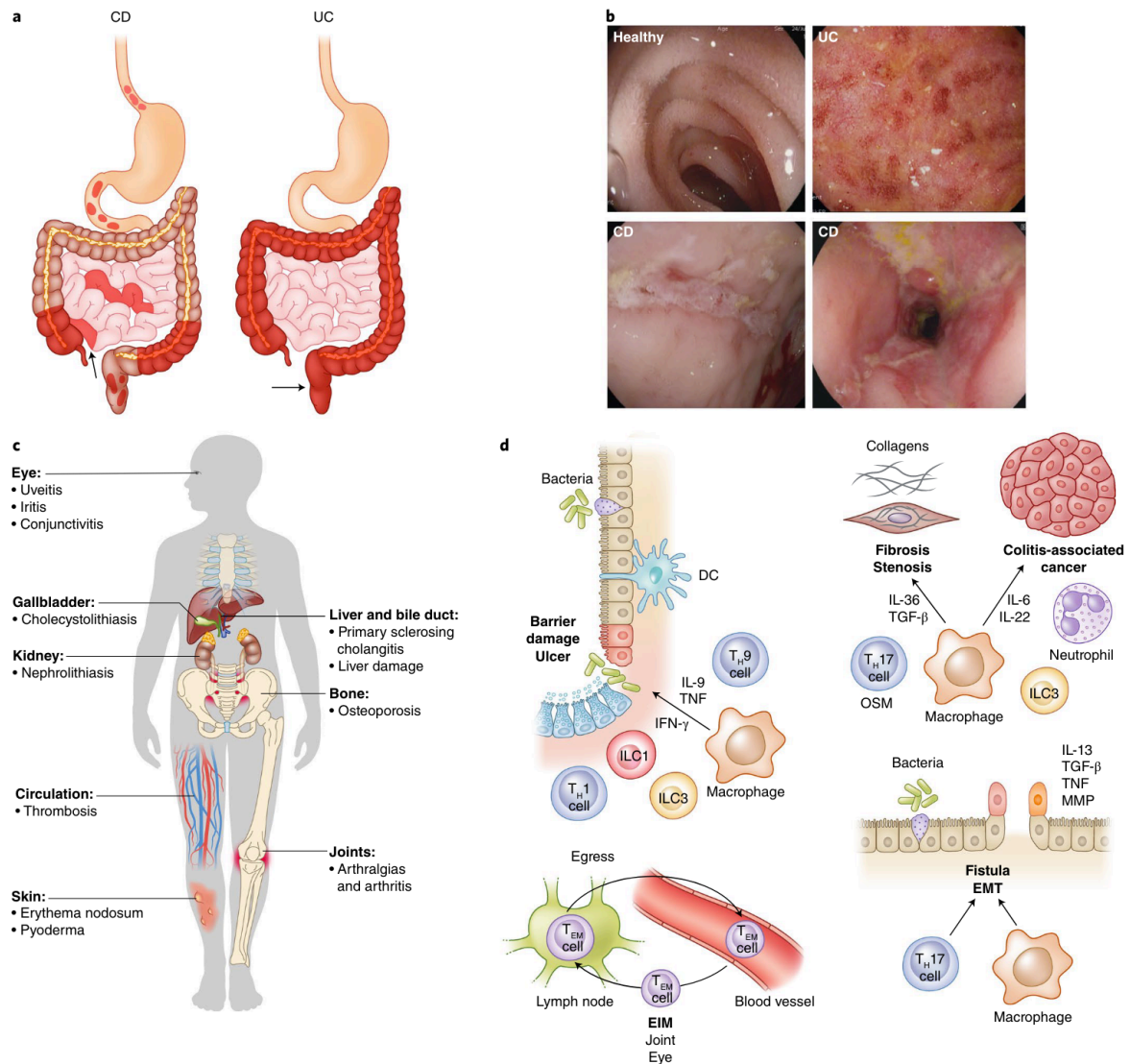


**Figure 5: Clinical features of IBD**

(A) Localization of inflammation in CD and UC. The inflammation pattern in CD is generally disconnected (skip lesions) and can affect the whole gastrointestinal tract. The main localization is the terminal ileum (arrow). UC begins at the level of the rectum and ascends continuously to more proximal sites within the colon. (B) Endoscopic findings in IBD. The pictures show a healthy patient (top left), erosions and bleeding in UC (top right), large ulcers in CD (bottom left) and ulcers with stenosis in CD (bottom right). (C) Manifestations of IBD in other organ systems. (D) Cellular mechanisms in IBD. Production of proinflammatory cytokines by immune cells contributes to the progression of IBD and generation of complications (e.g. fibrosis, stenosis, fistula, cancer and ulcers). Effector memory T cells migrate between bloodstream, gut and lymph nodes and can further aggravate extra-intestinal manifestations (Illustration adopted from Neurath, 2019).

### 1.5.2.3 Treatment of inflammatory bowel disease

Currently, IBD treatment relies on individual immune suppressive therapy and therapy of IBD complications (Lamb *et al.*, 2019). The treatment of both UC and CD is divided into two parts. The first part is the induction of remission. The second part is the following maintenance of the remission. Mucosal healing is the focus of these therapies. UC remission can be induced with 5-aminosalicylic acid or systemic corticosteroids (Feagan and Macdonald, 2012). Corticosteroids however should only be considered as a second option due to frequent side effects (Lennard-Jones *et al.*, 1960). In mild cases of CD, induction of remission can be achieved with local acting oral budesonide or systemic corticosteroids. Exclusive enteral nutrition (EEN) can have comparable effects to corticosteroid treatment, but is often poorly accepted by patients (Lamb *et al.*, 2019). In both UC and

CD, corticosteroids should not be considered as a long-term maintenance medication due to detrimental side effects. These include adrenal insufficiency, osteoporosis, hyperlipidemia and aseptic joint necrosis.

For the maintenance of remission, the biologicals Infliximab and Vedolizumab can be applied in both UC and CD. Infliximab is a monoclonal chimeric AB targeting proinflammatory tumor necrosis factor  $\alpha$  (TNF $\alpha$ ). The monoclonal AB Vedolizumab targets  $\alpha 4\beta 7$  and prevents association of  $\alpha 4\beta 7$  to mucosal addressin cell adhesion molecule-1, which is important for lymphocyte trafficking (Shyjan *et al.*, 1996; Lamb *et al.*, 2019). Ustekinumab targets both IL-12 and IL-23 signaling via the shared p40 subunit and can be used in the treatment of CD. Further, thiopurines and methotrexate are used in CD maintenance therapy. Due to decreasing cost and their overall less side effects, there is a tendency towards earlier application of biologicals. This is especially the cases in patients with high risk factors. For CD these include perianal fistula, structuring or penetrating disease; the need for steroids to control the first flare and age below 40 at disease onset (Beaugerie *et al.*, 2006; Loly *et al.*, 2008). Both corticosteroids and biologicals do not only reduce inflammation in IBD, but they also weaken the immune system. Patients are susceptible to opportunistic infection and reactivation of infectious disease like tuberculosis or hepatitis B virus. This underlines the relevance of a precise check-up before biological therapy. This includes anamnesis of infectious disease, immunization status, serology and tuberculosis screening (Lamb *et al.*, 2019).

In case of failure of the drug therapy or in case of complications, surgery might be beneficial. In the case of acute severe UC or toxic megacolon usually a subtotal colectomy with an end ileostomy with long rectal stump is performed (Hyman *et al.*, 2005). The 10 year colectomy rate in patients with extensive UC is around 19 % (Fumery *et al.*, 2018). In CD laparoscopic ileocecal resection can be performed in patients with terminal ileal disease with an exhausted drug therapy (Ponsioen *et al.*, 2017). Even though the risk of having to undergo surgery in CD decreased over the last decades, it remains high at around 30 % at the 5 year and 45 % at the 10 year mark (Frolkis *et al.*, 2013). This is also due to the earlier reported prevalent complications like fistulas and perforation.

Treatment of IBD patients includes the treatment of frequent comorbidities. 85 % of IBD patients are undernourished and diet must be adjusted accordingly or enteral nutrition must be considered (Vagianos *et al.*, 2007). An impaired iron resorption can cause hypochromic microcytic anemia, making a treatment with intravenous (i.v.) iron necessary.

#### **1.5.2.4 Th17 cells in inflammatory bowel disease**

With the discovery of the Th17 lineage, the role of Th1 cells as principal drivers of inflammation in IBD was challenged. Transdifferentiation of Th17 cells towards Th1-like Th17 and exTh17 cells has been shown to be detrimental in inducing and maintaining IBD (Lee *et al.*, 2009, Harbour *et al.*, 2015). Much of the data on the Th17 cells in IBD results from Th17 transfer colitis models and CD45RB<sup>hi</sup> colitis (see 2.2.13). The transfer of *in vitro* polarized Th17 cells into Rag<sup>-/-</sup> mice induces colitis. Fate mapping of those Th17 cells revealed that most of these cells acquired a Th1-like phenotype (Lee *et al.*, 2009).

Animals receiving *ex vivo* polarized Th17 cells deficient in IFN- $\gamma$  expression, retained the Th17 phenotype and did not suffer intestinal inflammation. This confirms the importance of Th1-like and

exTh17 cells for pathogenicity in IBD. Via IFN- $\gamma$  these cells support the differentiation of additional Th1 cells, which contribute to pathogenicity (Harbour *et al.*, 2015).

While there are many studies focusing on the pathogenic role of Th17 cells, IL-17 may also have protective capabilities via regulation of occludin. The protein occluding is part of tight junctions within the colonic crypts and detrimental for regulation of permeability within the colonic mucosa. These protective effects were observed in the absence of IL-23 (Lee *et al.*, 2009).

The cytokine IL-23 has been linked to pathogenicity in IBD. IL-23 is produced by DCs and was shown to be detrimental for the maintenance of Th17 cells in IBD. (Ahern *et al.*, 2010; Kullberg *et al.*, 2006, Langrish *et al.*, 2005; Hue *et al.*, 2006). Further, IL-23 has been linked to transdifferentiation of Th17 towards the Th1 lineage (Kleiner *et al.*, 2022, Hirota *et al.*, 2011).

The role of the microbiota in Th17 expansion and transdifferentiation is of increasing interest and may heavily contribute to disease severity in IBD (Niess *et al.*, 2008). Transfer of IBD donor microbiota into germ-free mice induced expansion of Th17 cells and leads to worsened disease in murine colitis. More Th1-like cells were found in murine colitis with IBD donor microbiota, than in mice with microbiota from healthy donors (Britton *et al.*, 2019).

## 1.6 Hypothesis and research goals

Th17 cells are a plastic CD4<sup>+</sup> T helper subset. Plasticity towards the Th1 lineage is depending on T-bet as the master TF controlling type 1 immunity. The amount of emerging Th1-like and exTh17 cells differs between different AIDs and so does their contribution to pathogenicity. However, the factors that drive pathogenicity of Th1-like Th17 and exTh17 cells are incompletely understood.

There has been a great progress in IBD and cGN therapy over the last decades, especially regarding the introduction of biologicals. High percentages of surgical interventions, dialysis and side effects of immunosuppression remain and reduce patients' quality of life. A better understanding of pathways and cellular subsets that drive disease is needed to identify new targets for specific therapies that reduce severe side effects.

Using a Th17 specific T-bet KO in models of Th17 driven autoimmunity, we want to better understand the role of T-bet in transdifferentiation towards the Th1 lineage and in pathogenicity. In the applied models of NTN and CD45RB<sup>hi</sup> colitis, contrasting percentages of Th17 to Th1 transdifferentiation have been reported. In cGN Th17 cells show minimal transdifferentiation towards the Th1 population (Hirota *et al.*, 2011; Krebs *et al.*, 2016). CD45RB<sup>hi</sup> colitis shows abundant Th17 to Th1 plasticity (Harbour *et al.*, 2015; Lee *et al.*, 2009).

We hypothesize, that the T-bet KO ameliorates disease in models with higher Th17 plasticity towards the Th1 lineage via decreased IFN- $\gamma$  expression. Further, we want to investigate the impact of the KO on several other canonical Th17 and Th1 lineage markers that might contribute to inflammation. The results of this work may identify possible targets for future treatments of cGN and IBD and help us to gain more knowledge about the Th17-Th1 plasticity.

## 2 Material and Methods

### 2.1 Material

#### 2.1.1 Mice

Mouse name	Background	Mutation	Supplier
wt	C57BL/6	-	The Jackson Laboratory
IL-17A Fate Reporter	C57BL/6	IL-17ACRE x R26eYFP	The Jackson Laboratory donation by B. Stockinger (Hirota <i>et al.</i> , 2011)
Tbx21 flox	C57BL/6	IL-17ACRE x R26eYFP x floxTbx21flox	The Jackson Laboratory donation by B. Stockinger / UKE
Rag1 <sup>-/-</sup>	C57BL/6	Rag1tm1Mom	The Jackson Laboratory

#### 2.1.2 Primers

Primer description	Nucleotide sequence	Length
17AypfF	CAA GTG CAC CCA GCA CCA GCT GAT C	25
17AypfRwt	CTT AGT GGG TTA GTT TCA TCA CAG C	25
17AypfiCreR	GCA GCA GGG TGT TGT AGG CAA TGC	24
3104 Rag1 common	CCG GAC AAG TTT TTC ATC GT	20
8162 Rag1 mut fw	TGG ATG TGG AAT GTG TGC GAG	21
1746 Rag1 WT fw	GAG GTT CCG CTA CGA CTC TG	20
Rosa26 Seq1	AAA GTC GCT CTG AGT TGT TAT	21
Rosa26 Seq2	GCG AAG AGT TTG TCC TCA ACC	21
Rosa26 Seq3	GGA GCG GGA GAA ATG GAT ATG	21
Tbet flox A	TAT GAT TAC ACT GCA GCT GTC TTC AG	26
Tbet flox B	CAG GAA TGG GAA CAT TCG CCT GTG	24

### 2.1.3 ELISA-Antibodies

Antibody	Clone	Supplier
Coating Antibody	Polyclonal	Bethyl Laboratories Inc. Cat. No. A90-134A
Goat anti-Mouse Albumin Antibody HRP Conjugated	Polyclonal	Bethyl Laboratories Inc. Cat. No. A90-134P

### 2.1.4 FACS Antibodies

Antibody	Conjugate	Isotype	Clone	Supplier	Antibody dilution
CD3	BV421	Syrian Hamster IgG2, κ	500A2	BD Cat: 740014	1 : 400
CD3	V500 / BV510	Syrian Hamster IgG2, κ	500A2	BD Cat: 560771	1 : 100
CD3	BV785	Rat IgG2b, κ	17A2	BioLegend Cat: 100232	1 : 200
CD4	APC	Rat IgG2a, κ	RM4-5	BioLegend Cat: 100530	1 : 100
CD4	BV650	Rat IgG2a, κ	RM4-5	BioLegend Cat: 100545	1 : 300
CD4	PE/Cyanine7	Rat IgG2a, κ	RM4-5	BioLegend Cat: 100528	1 : 400
CD8	BV785	Rat IgG2a, κ	53-6.7	BioLegend Cat: 100750	1 : 500
CD25	PE	Rat IgG1, λ	PC61	BioLegend Cat: 102008	1 : 200
CD25	BV650	Rat IgG1, λ	PC61	BioLegend Cat: 102037	1 : 200
CD45	AF700	Rat IgG2b, κ	30-F11	BioLegend Cat: 103128	1 : 1000
CD45	PerCP	Rat IgG2b, κ	30-F11	BioLegend Cat: 103130	1 : 100

CD45RB	APC	Rat IgG2a, κ	C363-16A	BioLegend Cat: 103312	1 : 400
CXCR3	BV421	Armenian Hamster IgG	CXCR3- 173	BioLegend Cat: 126529	1 : 100
CCR6	PE/Cyanine7	Armenian Hamster IgG	29-2L17	BioLegend Cat: 129816	1 : 150
Foxp3	AF700	Rat / IgG2a, κ	FJK-16s	eBiosciences Cat: 56-5773-80	1 : 100
GM-CSF	PE	Rat IgG2a, κ	MP1-22E9	BioLegend Cat: 505406	1 : 200
IL-10	APC	Rat / IgG2b, κ	JES5-16E3	Invitrogen Cat: 17-7101-81	1 : 100
IL-17A	PE	Lewis IgG1, κ	TC11- 18H10	BD Cat: 559502	1 : 100
IL-17A	BV421	Rat IgG1, κ	TC11- 18H10.1	BioLegend Cat: 506926	1 : 100
IL-17F	AF647	Mouse IgG1, κ	9D3.1C8	BioLegend Cat: 517004	1 : 100
IL-22	PerCP-Cy5.5	Goat Polyclonal IgG	Poly5164	BioLegend Cat: 516411	1 : 50
IFN-g	BV 711	Rat IgG1, κ	XMG1.2	BioLegend Cat: 505836	1 : 300
RORγt	PE	Mouse IgG2a, κ	Q31-378	BD Cat: 562607	1 : 100
T-bet	APC	Mouse IgG1, κ	4B10	BioLegend Cat: 644813	1 : 100
γδ -TCR	BV605	Armenian Hamster IgG	GL3	BioLegend Cat: 118129	1 : 300

## 2.1.5 Buffers, solutions and media

Buffer	Composition
Coating buffer (Albumin ELISA)	Content of one carbonate-bicarbonate buffer capsule in 100 mL aqua dest.
Collagenase solution	Add 55 ml 10 % FBS (heat-inactivated), 5.5 ml 100× HGPG, 1 ml of 0.5 M CaCl <sub>2</sub> and 1 ml of 0.5 M MgCl <sub>2</sub> to 500 ml RPMI 1640
Digestion medium (kidney)	500 ml RPMI-supplemented with 10 % (v/v) FCS, 1 % (v/v) HEPES, 1 % (v/v) penicillin/streptomycin
DTT solution	50 ml 10X Hanks balanced salt solution (HBSS), 50 ml 10X HEPES-bicarbonate buffer, 50 ml 10 % FBS (heat-inactivated), 350 ml H <sub>2</sub> O, 15.4 mg dithioerythritol (DTT; Calbiochem) per 100 ml of buffer (1 mM final)
Eosin solution	1 g eosin in 100 ml aq. dest, dilute with 100 ml 1 % acetic acid
Erythrocyte lysis buffer	NH <sub>4</sub> Cl 160 mM :Tris-HCL 170 mM (9:1 v/v), pH= 7,6
Hämalaun after Meyer	1 g Haematoxylin Serva 24420, 50 g potassiumalaun, 0,2 g potassium iodate, 50 g chloral hydrate in 1 L aq. dest.
HEPES-bicarbonate Buffer 10X	23.8 g HEPES (100 mM final), 21 g Sodium Bicarbonate (250 mM final). Fill with H <sub>2</sub> O to 1 L and adjust pH to 7.2 with HCL.
HEPES, L-Glutamine, Penicillin/Streptomycin and Gentamycin 100X (HGPG 100X)	59.6 g HEPES, 14.6 g L-Glutamine, 1x10 <sup>6</sup> U Penicillin (2000 U/ml final), 1g Streptomycin (2 mg/ml final) and 2.5 mg Gentamycin (5 µg/ml final). Add RPMI 1640 to 500 ml. and adjust pH to 7.5 using HCl. Filter using a 0.45 µm filter.
Paraformaldehyde (PFA) 4%	89 ml Sörensen buffer, 11 ml 37 % Paraformaldehyde
PBS, 1% FCS solution	Add 5 ml FCS to 500 ml PBS
PBS, 10% FCS solution	Add 50 ml FCS to 500 ml PBS
Percoll solution (100%)	Prepare a 1X stock solution by mixing 90 ml Percoll (GE Healthcare, Cat. No. 17-0891-01) with 10 ml of 10X PBS.
Percoll solution (67%)	Add 45,6 ml 100 % Percoll solution to 22,4 ml PBS/1 % FCS.
Percoll solution (40%)	Add 27,2 ml 100 % Percoll solution to 40,8 ml PBS/1 % FCS.
Percoll solution (37%)	106 ml H <sub>2</sub> O, 74 mL Percoll PLUS, 20 mL 10X DPBS
Perm Wash 1X	Mix 1 part 10X Permeabilization Buffer with 9 parts aqua dest.
Post-coat solution (Albumin ELISA)	1 package 50 mM Tris buffered saline in 1 L distilled water, 1 % BSA, pH 8,0

Sample / conjugate diluent (Albumin ELISA)	200 mL of post-coat solution, 1 ml 10 % Tween20
Sörensen Buffer	3,03 g NaHPO <sub>4</sub> + 14,14 g Na <sub>2</sub> HPO <sub>4</sub> add to 1 L with bi dest. H <sub>2</sub> O, pH= 7,2-7,4
Stimulation medium	20 ml X-vivo, 20 µl β-Mercaptoethanol, 1 µl PMA, 20 µl Ionomycin, 40 µl Brefeldin A
Wash solution (Albumin ELISA)	1 L aqua dest., content of one package 50 mM Tris buffered saline, 0,05 % Tween20, pH 8,0

## 2.1.6 Chemicals and consumables

Product	Supplier	Cat. no.
Carbonate-Bicarbonate Buffer Capsules	Sigma Aldrich, St. Louis, Missouri, USA	C3041
Creatinine, 10 g	Sigma Aldrich, St. Louis, Missouri, USA	C4255 – 10G
Dulbecco´s Phosphate Buffered Saline (DPBS(1x))	Thermo Fisher Scientific, Waltham, Massachusetts, USA	14190-094
eBioscience™ Permeabilization Buffer (10X)	Thermo Fisher Scientific, Waltham, Massachusetts, USA	00-8333
Fetal calf serum (FCS)	Thermo Fisher Scientific, Waltham, Massachusetts, USA	10500-064
Hanks´ Balanced Salt Solution	Thermo Fisher Scientific, Waltham, Massachusetts, USA	14170-088
Ionomycin, Free acid, (f. Streptomyces conglobatus)	Sigma Aldrich, St. Louis, Missouri, USA	407950-1MG
Phorbol 12-Myristate 13-Acetate (PMA)	Sigma Aldrich, St. Louis, Missouri, USA	P1585
TMB (substrate)	Bethyl Laboratories Inc., Montgomery, Texas, USA	E102
Tris buffered saline, with BSA, pH 8,0	Sigma Aldrich, St. Louis, Missouri, USA	T6789
Tris buffered saline, with Tween20, pH 8,0	Sigma Aldrich, St. Louis, Missouri, USA	T9039
RPMI-1640 medium	Thermo Fisher Scientific, Waltham, Massachusetts, USA	21875-034

10 % Tween 20	Bethyl Laboratories Inc., Montgomery, Texas, USA	E108
---------------	---	------

### 2.1.7 Plasticware

<b>Product</b>	<b>Supplier</b>	<b>Cat. no.</b>
C tube	Miltenyi Biotech, Bergisch Gladbach, Germany	130-093-37
Cell culture micro plate, 96- well, u-bottom	Greiner Bio-One Holding, Kremsmünster, Austria	650180
Cell culture micro plate, 96- well, v-bottom	Greiner Bio-One Holding, Kremsmünster, Austria	651160
Cell counting slides	Bio-Rad Laboratories Inc., Hercules, California, USA	145.0015
Falcon Round-Bottom Polypropylene Tubes, 5 mL, with cap	Stemcell Technologies, Vancouver, Canada	38057
Falcon Round-Bottom Polypropylene Tubes, 5 mL, without cap	Stemcell Technologies, Vancouver, Canada	38056
Falcon tubes, 15 mL	Greiner Bio-One Holding, Kremsmünster, Austria	188271
Falcon tubes, 50 mL	Greiner Bio-One Holding, Kremsmünster, Austria	227261
Micro tube, 1.5 ml	Sarstedt, Nümbrecht, Germany	72.690.001
Micro tube 1.5 ml with cap	Sarstedt, Nümbrecht, Germany	72.692
Micro tube, 1.3 mL (filled with K3 EDTA)	Sarstedt, Nümbrecht, Germany	41.1504.015
Micro tube 0.5 ml, PP	Sarstedt, Nümbrecht, Germany	72.699
Filter Tip, 10 µl	Sarstedt, Nümbrecht, Germany	70.1130.410
Filter Tip, 100 µl	Sarstedt, Nümbrecht, Germany	70.760.12
Filter Tip, 200 µl	Sarstedt, Nümbrecht, Germany	70.760.211
Filter Tip, 1000 µl	Sarstedt, Nümbrecht, Germany	70.762.411
Serological pipette, 50 ml	Sarstedt, Nümbrecht, Germany	86.1256.001
Serological pipette, 25 ml	Sarstedt, Nümbrecht, Germany	86.1685.001

Serological pipette, 10 ml	Sarstedt, Nümbrecht, Germany	86.1254.001
Serological pipette, 5 ml	Sarstedt, Nümbrecht, Germany	86.1253.001
T175 Cell culture flask	Sarstedt, Nümbrecht, Germany	83.3912

### 2.1.8 Kits

Product	Supplier	Cat. no.
XNAT2 Extract-N-Amp Tissue PCR Kit	Sigma Aldrich, St. Louis, Missouri USA	(Lamb <i>et al.</i> , 2019)
BD Cytotfix/Cytoperm™ Fixation/Permeabilization Solution Kit	BD (Becton, Dickinson and Company), Franklin Lakes, New Jersey, USA	554714
CD4 <sup>+</sup> T Cell Isolation Kit (anti-mouse)	Miltenyi Biotech, Bergisch Gladbach, Germany	130-104-454
LIVE/DEAD Fixable Near-IR Dead cell staining Kit	Thermo Fisher Scientific, Waltham, Massachusetts, USA	L34975
Creatinine Jaffe Kinetic Fluid (5+1)	Hengler Analytik, Steinbach, Germany	114444
Chromium Next GEM Single Cell 5' GEM Kit v2	10x Genomics, Inc., Pleasanton, California, USA	PN-1000266
Library Construction Kit	10x Genomics, Inc., Pleasanton, California, USA	PN-1000196
Chromium Next GEM Single Cell 5' Gel Bead Kit	10x Genomics, Inc., Pleasanton, California, USA	PN-1000267

### 2.1.9 Equipment

Equipment	Supplier
BD LSR II	BD (Becton, Dickinson and Company), Franklin Lakes, New Jersey, USA
BD LSRFortessa	BD (Becton, Dickinson and Company), Franklin Lakes, New Jersey, USA
BD FACSAria IIIu	BD (Becton, Dickinson and Company), Franklin Lakes, New Jersey, USA
Biological safety cabinet Nuair KS12	Thermo Scientific / Heraeus, Waltham, Massachusetts, USA
C1000 Touch Thermal Cycler	Bio-Rad Laboratories Inc., Hercules, California, USA

Centrifuge 5417R	Eppendorf, Hamburg, Germany
Centrifuge C1008-B my Fuge mini centrifuge	Greiner Bio-One, Kemsminster, Austria
Citadel Tissue Processor Shandon 1000	Thermo Fisher Scientific, Waltham, Massachusetts, USA
CO <sub>2</sub> -Incubator HERAcell 240	Thermo Scientific / Heraeus, Waltham, Massachusetts, USA
CO <sub>2</sub> -Incubator, B 5042	Thermo Scientific / Heraeus, Waltham, Massachusetts, USA
Freezer (-20 °C)	Liebherr, Bulle, Switzerland
Fridge, CP 43 CPel 4313-20	Liebherr, Bulle, Switzerland
GentleMACS Dissociator	Miltenyi Biotech, Bergisch Gladbach, Germany
Siemens Multistix 10 SG	Siemens Healthcare Diagnostics Inc., Tarrytown, New York, USA
Counting chamber Neubauer	Carl Roth, Karlsruhe, Germany
Cutfix one-use scalpel	B. Braun, Melsungen, Germany
Pipet Boy	INTEGRA Biosciences AG, Zizers, Switzerland
Syringe Omnifix-F	B. Braun, Melsungen, Germany
Syringe Injekt-F	B. Braun, Melsungen, Germany
Syringe needle, Sterican 23G	B. Braun, Melsungen, Germany
Syringe needle, Sterican G20	B. Braun, Melsungen, Germany
Surgical instruments (Scissors, clamps, tweezers, sharp spoon)	Carl Roth, Karlsruhe, Germany
Vortexer V1 S000	IKA, Staufen, Breisgau, Germany
Water bath incubator, Typ 1012	Gesellschaft für Labortechnik, GFL, Burgwedel, Germany
Zeiss light microscope IM35	Carl Zeiss AG, Jena/ Oberkochen, Germany
10x Vortex Adapter	10x Genomics, Inc., Pleasanton, California, USA
Chromium Next GEM Secondary Holder	10x Genomics, Inc., Pleasanton, California, USA
10x Magnetic Separator	10x Genomics, Inc., Pleasanton, California, USA

## 2.1.10 Software

<b>Software</b>	<b>Developer</b>
Adobe Illustrator CS6; version 25.4.1	Adobe Inc., San Jose, California, USA
Adobe Photoshop; version 22.5.3	Adobe Inc., San Jose, California, USA
BD FACS Diva software; version 8.0.1	BD Biosciences, Franklin Lakes, New Jersey, USA
FlowJo; version 10.5.3	Tree Star, Ashland, Oregon, USA
GraphPad Prism; versions 6, 7, 8 and 9	GraphPad Software Inc., La Jolla, California, USA
Microsoft® Word, 16.54	Microsoft Corporation, Redmond, Washington, USA
Microsoft® Excel, 16.54	Microsoft Corporation, Redmond, Washington, USA
R, versions 4.0.2, 4.0.3, 4.2.3, 4.0.4, 4.0.5	R Foundation for Statistical Computing, Vienna, Austria
T-Base; version 14.3	4D SAS, 60 Rue d'Alsace, 92110 Clichy, France

## 2.1.11 R and python packages

<b>package</b>	<b>Developer/paper</b>
Seurat, versions 3.2, 4.0.2	Hao <i>et al.</i> , 2021
Harmony 0.1.1	Korsunsky <i>et al.</i> , 2019
Cellranger	Dobin <i>et al.</i> , 2013
RColorBrewer 1.1.2	Erich Neuwirth, 2022

## 2.2 Methods

### 2.2.1 Ethics statement and handling of laboratory animals

The performed mouse experiments were in accordance with the National Institutes of Health Guide for the Care and Use of Laboratory Animals, as well as the German law for the welfare of animals. They were approved by local health authorities of the BGV Hamburg (G20/43).

In all experiments, if not stated different mice between the age of 9 and 12 weeks were used. Littermate mating of heterozygous mice ensured, that wildtype and (conditional) knock-out animals from one breeding (littermates) could be compared in the experiments.

The mice used in experiments, were held under specific-pathogen-free (SPF) hygiene measures. Mice were fed with standard dry food and received water ad libitum. The burden of the animals in experiment was examined daily by checking parameters like general appearance, fur, eyes, nose hairs, movement, social behavior and drinking to name a few. Depending on the experiment performed special parameters were investigated. Those were bodyweight, proteinuria and endoscopic colitis score. Further, usage of the metabolism cage and the collection of data was carried out according to the animal experiment application.

To extract the murine organs, the animals were anaesthetized with an 4 % (v/v) isoflurane/ oxygen mixture under a fume hood in the animal facility. Before sacrificing the mice by performing cervical dislocation the toe pinch reflex in the murine leg was checked to ensure sufficient anesthesia depth. Afterwards, mice were sacrificed by cervical dislocation and organs were removed.

### 2.2.2 Genotyping of transgenic mice

The genotype of transgenic mice used in the experiment was validated by PCR. DNA was extracted and amplified from murine tail biopsies using the XNAT2 Extract-N-Amp Tissue PCR kit according to the manufacturers protocol.

First, 100 µl Extraction Solution and 25 µl of Tissue Preparation Solution was mixed and added to the biopsy. The DNA was extracted from the murine tail during a 10min incubation at 55 °C in the thermal cycler. By adding 100 µl of Neutralizing Solution the DNA extraction was stopped. The DNA was now ready for further PCR amplification and could be stored at 4 °C for 6 months.

The PCR mix for DNA amplification contained the reagents listed in *Table 3*. Different primers were used to investigate the various genes of interest.

**Table 3: PCR mix for genotyping**

Gene	Reagent/ Primer	Volume
Tbx 21-flox	10x Dream Taq MasterMix	2 µl
	dNTPs (10 mM)	0,4 µl
	DreamTaq Polymerase	0,1 µl
	Tbx21 flox A primer (10 µM)	1 µl

	Tbx21 flox B primer (10 $\mu$ M)	1 $\mu$ l
	Nuclease free H <sub>2</sub> O	14,5 $\mu$ l
<b>AA cre</b>	Taq Mix	10 $\mu$ l
	IL17Acre.1 (20 $\mu$ M)	1 $\mu$ l
	IL17Acre.2 (20 $\mu$ M)	1 $\mu$ l
	IL17Acre.3 (20 $\mu$ M)	1 $\mu$ l
	Nuclease free H <sub>2</sub> O	16 $\mu$ l
<b>R26 YFP</b>	Taq Mix	10 $\mu$ l
	Primer 1 (20 $\mu$ M)	1 $\mu$ l
	Primer 2 (20 $\mu$ M)	1 $\mu$ l
	Primer 3 (20 $\mu$ M)	1 $\mu$ l
	Nuclease free H <sub>2</sub> O	16 $\mu$ l
<b>Rag1 ko</b>	Taq Mix	10 $\mu$ l
	Rag1 common (10 $\mu$ M)	1 $\mu$ l
	Rag1 wt Fw (10 $\mu$ M)	1 $\mu$ l
	Rag1 mut Fw (10 $\mu$ M)	1 $\mu$ l
	Nuclease free H <sub>2</sub> O	16 $\mu$ l

**Table 4: Programs for genotyping (Thermal cycler)**

Gene	Step	Temperature [°C]	Time [h:min:s]	Notes
<b>IL17A cre</b>	1	94	00:01:00	
	2	94	00:00:30	
	3	61	00:00:40	
	4	72	00:00:50	
	5	Go to step 2 x30 cycles		
	6	72	00:03:00	
	7	4	$\infty$	Mutant band: 597 bp WT band: 304 bp
<b>R26 YFP</b>	1	94	00:05:00	

	2	94	00:00:30	
	3	51	00:00:30	
	4	72	00:00:30	
	5	Go to step 2 x33 cycles		
	6	72	00:05:00	
	7	4	∞	Transgen band: >250 bp WT band: 600 bp
<b>Tbx 21 flox</b>	1	94	00:05:00	
	2	94	00:00:30	
	3	60	00:00:30	
	4	72	00:01:00	
	5	Go to step 2 x34 cycles		
	6	72	00:05:00	
	7	4	∞	WT band: 298 bp Tbet null: 400 bp Tbet flox: 440 bp
<b>Rag1 ko</b>	1	95	00:03:00	
	2	95	00:00:30	
	3	58	00:00:30	
	4	72	00:01:00	
	5	Go to step 2 x35 cycles		
	6	72	00:03:00	
	7	4	∞	Knock-out: 530 bp WT band: 474 bp

### 2.2.3 Conditional Tbx21 KO in IL-17A fate reporter mice

In order to evaluate the role of T-bet in the Th17-Th1 axis, we used a previously described mouse line that permanently marks Th17 cells (Hirota *et al.*, 2011). To generate IL-17A<sup>CRE</sup> x R26<sup>eYFP</sup> x floxTbx21<sup>flox</sup> mice, IL-17A<sup>CRE</sup> x R26<sup>eYFP</sup> were crossed with Tbx21 floxed mice (2.1.2).

The principle of the IL-17A<sup>CRE</sup> x R26<sup>eYFP</sup> mouse line is shown in *Figure 6* (Krebs and Panzer, 2018). If the IL-17A promoter is activated, the locus of crossover in P1 (loxP) flanked stop codon upstream of eYFP is cut out (Hirota *et al.*, 2011). This is carried out by expression of Cre recombinase following the activation of the IL-17A promoter. Cre and loxP originate from the bacteriophage P1 (Sternberg

and Hamilton, 1981). The result is a continuous expression of eYFP due to the housekeeping-type Rosa26 (R26) promoter, which is now upstream of eYFP.

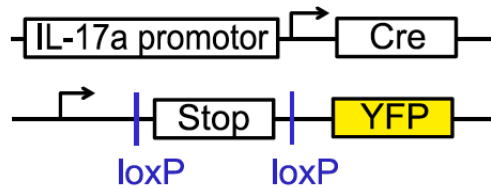


**Figure 6: IL-17A fate reporter mice**

Cre-recombinase is expressed under the control of the IL-17A promoter, resulting in permanent YFP expression through the removal of a floxed stop-codon (Illustration adopted from Krebs and Panzer, 2018).

By crossing these IL-17A fate reporter mice with Tbx21 floxed mice ( $^{loxP}Tbx21^{loxP}$ ), cells are not only permanently eYFP marked once expressing IL-17A, but further lack Tbx21 due to Cre driven excision of loxP flanked Tbx21 (see Figure 7).

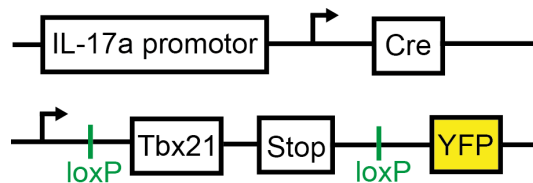


**Figure 7: IL-17A fate Tbx21 flox reporter mice**

Following the expression of Cre-recombinase induced by the IL-17A promoter loxP flanked Tbx21 as well as the Stop codon upstream of YFP are cut. This results in permanently YFP marked cells lacking Tbx21 expression.

## 2.2.4 Gel electrophoresis

Depending on the number of samples, a casting tray was chosen and the fitting amount of 1,5 % agarose gel was prepared. The casting tray was filled with the liquid agarose gel and left to cool with a comb placed in the upper third of the gel. Once cooled down, the comb was removed, and the gel was placed in the electrophoresis chamber. The chamber was filled with electrophoresis buffer. Then the amplified nucleic acid together with 4  $\mu$ l loading buffer was carefully pipetted into the wells produced by the comb. One well was loaded with aqua dest. as a negative control, one well with C57/Black6 positive control and one well with a 1000 bp DNA ladder.

By applying a voltage, an electrical field forms in the chamber. In this electrical field molecules travel according to their charge. Due to the phosphate backbone, DNA is negatively charged and therefore pulled towards the positive charge. The DNA can be separated as it migrates through the gel at a certain speed according to the size of the fragment. Smaller proteins migrate quicker through the agarose matrix and are therefore closer to the positive charge. Larger molecules remain closer to the wells.

The voltage was set to 120 mV and 400 mA and maintained for approx. 30 min. A visible band reaching the end of the gel indicated the end of the run. Afterwards pictures of the gel were taken with a gel image system and the bands of the samples were compared to the DNA ladder.

## 2.2.5 Nephrotoxic nephritis (NTN)

The NTN mouse model resembles the clinical picture of cGN. ABs against the murine GBM induce an inflammation that is driven by Th17 cells during the first 10 days of disease. Later, Th1 and Tregs are involved in pathogenicity and resolving the disease (Krebs and Panzer, 2018). Sheep anti-mouse GBM ABs (S-anti-M GBM ABs) are produced as illustrated in *Figure 8*.

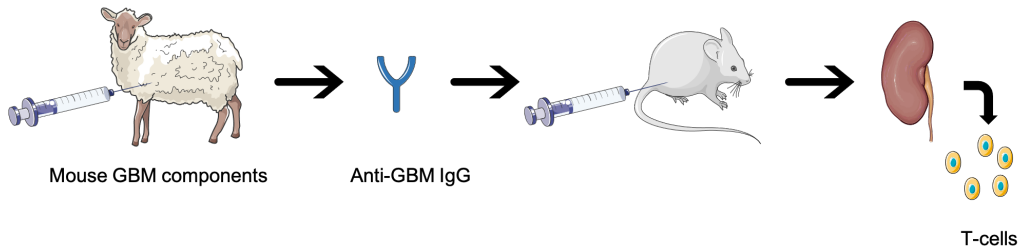


**Figure 8: Generation of sheep-anti-mouse GBM ABs**

Components of the murine GBM were injected into sheep, which then produced IgG antibodies directed against these components. These ABs were purified, and the resulting nephrotoxic serum was injected i.p. into mice. Following the onset of nephritis, kidney or other organs were removed to study the role of T cells in cGN. The Figure was partly generated using Servier Medical Art, provided by Servier, licensed under a Creative Commons Attribution 3.0 unported license.

On day 0 age-matched (6 to 10 weeks old) male mice were intraperitoneally injected 150  $\mu$ l sheep anti mouse glomerular basement membrane antibodies. Mice were held in a heating cabinet for 3 days and fed with soft food. On day 3 albuminuria of the mice was assessed via Multistix as described in 2.2.6 to make sure that the injection was successful. Animals with low proteinuria (trace/+) were excluded from the experiment. On day 9 of the experiment murine urine was collected for further analysis as described in 2.2.6. On day 10 mural blood was taken via cardiac puncture and the mice were sacrificed by cervical dislocation. During the organ extraction the capsule of the kidney was removed to improve later tissue digestion. A slice of the middle of the kidney was put into 4 % PFA for histological analysis and a piece of the pole of the organ was cut and put on dry ice for later RNA isolation.

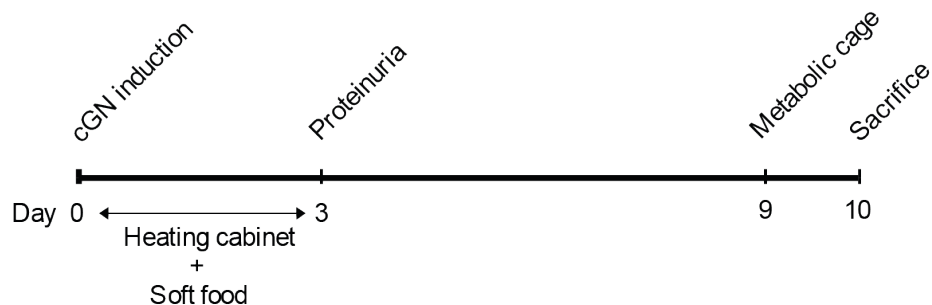


**Figure 9: Experimental outline of cGN experiments**

Animals received 150  $\mu$ l sheep anti mouse glomerular basement membrane serum on day 0. At day 3 albuminuria of the mice was assessed via Multistix. At day 9 urine was collected for ACR quantification. On day 10 mural blood was taken and the mice were sacrificed. Kidneys were removed for histological and FACS analysis.

## 2.2.6 Urine sample collection in metabolic cage

Metabolic cages for urine sample collection were constructed by attaching the lid of a pipet tip box on top of a 96-well plate using adhesive tape. The holes in the lid ensured proper ventilation of the cage. 6 wells were filled with water, to guarantee the water supply of the animals (see *Figure 10*). Mice were held in metabolic cages for maximum 4 h and afterwards put back into their normal cages. Urine was collected from the 96-well plate with a 1000  $\mu$ l pipet. Proteinuria was tested directly after sample collection using Siemens Multistix 10 SG. 10  $\mu$ l murine urine was pipetted onto the test square for proteinuria of the urine stick. The color change of the test square correlated with the proteinuria. Yellow color indicated negative or no detectable proteinuria (“-“symbol), light green indicated traces or low amount of protein in the urine (“+/-“ symbol) and richer and darker greens up to petrol color correlated with higher proteinuria (“+”, “++”, “+++”, “++++” symbols). The symbols indicated protein concentrations in the urine as shown in *Figure 11*.



**Figure 10: Murine urine collection in metabolic cage**

Mice were held in metabolic cages made from pipet tip boxes on top of a 96-well plate for maximum 4 h. During this time sufficient water was provided. Afterwards urine was collected from the 96-well plate with a 1000  $\mu$ l pipet. The Figure was partly generated using Servier Medical Art, provided by Servier, licensed under a Creative Commons Attribution 3.0 unported license.

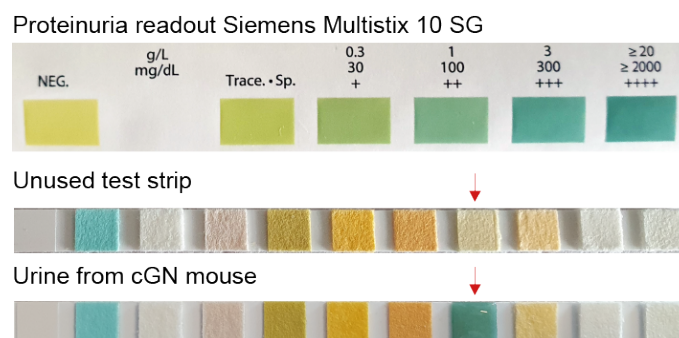


**Figure 11: Proteinuria quantification with Siemens Multistix**

Murine urine was pipetted onto the proteinuria test square (marked with red arrow). Concentration of albumin in murine urine was quantified with the help of the color code readout. Yellow color indicated negative or no detectable proteinuria and green/petrol color change indicated high proteinuria.

### 2.2.7 Enzyme-linked immunosorbent assay (ELISA) of albumin

The ELISA reaction was used to indirectly quantify the amount of albumin and was performed on the surface of a 96-well plate coated with an anti-murine, anti-albumin antibody.

The horseradish peroxidase (HRP-) which is coupled to the murine albumin antibody (detection antibody) reacts with the 3, 3', 5, 5'-tetramethylbenzidine (TMB) substrate solution. In the process peroxide ( $H_2O_2$ ) is being reduced to water ( $H_2O$ ). This results in a change of color of the solution towards blue (absorption maximum of 650 nm). The reaction is stopped by addition of sulfuric acid ( $H_2SO_4$ ) to prevent precipitation of oxidized TMB, which would distort measurements. Stopping the reaction with  $H_2SO_4$  results in another change of color towards yellow at a wavelength of 450 nm due to electron transfers (Martin *et al.*, 1984). The greater the color change, the more detection antibody has bound, thus the more albumin is in the sample.

The buffers used for the albumin ELISA were prepared one day in advance according to 2.1.5. The murine urine samples were collected as described in 2.2.6 and the albuminuria was quantified with urine sticks. The albumin ELISA was carried in the period of 2 days.

On the first day 100  $\mu$ l of anti-murine albumin antibody was diluted in 9900  $\mu$ l of coating buffer (1:100 dilution). A high-binding 96-well plate was coated by pipetting 100  $\mu$ l diluted antibody into each well of the plate by the help of a multichannel pipette. The covered plate was placed in the fridge (4 °C) to coat overnight.

On the second day each well was washed three times with 200  $\mu$ l washing buffer. Following each washing step, the plate was tapped on the laboratory bench laid out with tissues to remove remnants of buffer. This is important to assure correct pre-sample dilutions. 200  $\mu$ l of post coat solution per well was added and incubated for 30 min at room temperature (RT) to block unspecific binding sites. Sample dilutions and standard dilutions were prepared according to *Table 5* and *Table 6*. Sample dilutions resulted from proteinuria quantification by urine sticks as described in 2.2.6. Dilution factors according to the urine Multistix readout are shown in *Table 7*.

Once again, each well was washed three times with 200  $\mu$ l washing buffer as in the previous washing step. 100  $\mu$ l of either diluted sample or standard was pipetted into the plate according to *Table 8*. The plate incubated for 1 h at RT in which the albumin in the samples and standards was bound by the anti-murine albumin antibody. Afterwards, each well was washed five times with 200  $\mu$ l washing buffer. 1  $\mu$ l HRP-coupled detection antibody was diluted in 50 ml of sample diluent (1:50.000 dilution) and mixed thoroughly. 100  $\mu$ l diluted HRP-coupled detection antibody was pipetted into each well of the plate. The plate was covered and incubated for 1 h at RT. The detection antibody bound to the albumin, which was earlier bound by the anti-murine albumin antibody. Another washing step with five repetitions followed.

100  $\mu$ l of tetramethylbenzidine substrate solution was added to each well and the plate was put in the dark for an incubation of 15 min at RT. During the time of the substrate reaction, the photometer was switched on and the layout of the plate with the dilutions of the samples and standards was entered. The addition of 100  $\mu$ l 2 M  $H_2SO_4$  per well under the hood stopped the substrate reaction. After stopping the reaction, the plate was directly measured in the photometer at 450 nm and the quantities of albumin in the murine urine samples were determined.

**Table 5: Sample dilutions for ELISA**

Dilution factor	Sample + Diluent	Sample + Diluent	Sample + Diluent
1 : 1000	10 µl + 90 µl	5 µl + 495 µl	
1 : 20 000	10 µl + 90 µl	10 µl + 190 µl	5 µl + 495 µl
1 : 50 000	10 µl + 90 µl	10 µl + 190 µl	5 µl + 495 µl
1 : 100 000	10 µl + 90 µl	5 µl + 495 µl	5 µl + 495 µl

**Table 6: Standard dilutions for ELISA**

	Dilution	Standard + Diluent
<b>S0</b>	10 000 ng/ml	2 µl stock solution in 198 µl sample diluent
<b>S1</b>	1000 ng/ml	100 µl S0 in 900 µl sample diluent
<b>S2</b>	500 ng/ml	300 µl S1 in 300 µl sample diluent
<b>S3</b>	250 ng/ml	300 µl S2 in 300 µl sample diluent
<b>S4</b>	125 ng/ml	300 µl S3 in 300 µl sample diluent
<b>S5</b>	62.5 ng/ml	300 µl S4 in 300 µl sample diluent
<b>S6</b>	31.25 ng/ml	300 µl S5 in 300 µl sample diluent
<b>S7</b>	15.625 ng/ml	300 µl S6 in 300 µl sample diluent
<b>S8</b>	7.8125 ng/ml	300 µl S7 in 300 µl sample diluent

**Table 7: Readout of albuminuria quantification with Multistix**

Proteinuria (Urine Multistix)	Dilution factor
Trace	1 : 1000
+	1 : 1000
++	1 : 20 000
+++	1 : 50 000
++++	1 : 100 000

**Table 8: Plate design for ELISA**

	1	2	3	4	5	6	7	8	9	10	11	12
<b>A</b>	S1	S1	BI	BI	P8	P8						
<b>B</b>	S2	S2	P1	P1	P9	P9						
<b>C</b>	S3	S3	P2	P2	...	...						

<b>D</b>	S4	S4	P3	P3								
<b>E</b>	S5	S5	P4	P4								
<b>F</b>	S6	S6	P5	P5								
<b>G</b>	S7	S7	P6	P6								
<b>H</b>	S8	S8	P7	P7								

### 2.2.8 Urine creatinine quantification (Jaffee analysis)

For determination of creatinine from urine the Creatinine-Kit Jaffee Kin was used (see 2.1.8). Standards S1-S5 were prepared as shown in *Table 9*. Reagent was produced by mixing 1 part of picric acid with 5 parts of alkaline buffer as specified by the manufacturer. 10 µl of either NaCl as blank (BI), standard or urine was pipetted into the wells of a 96-well plate as shown in *Table 10*. 50 µl reagent was added to each well with a multichannel pipette. After 1 min of incubation at RT, the plate was read in a plate reader at 430 nm and then once again 5min later.

**Table 9: Standard dilutions for Jaffee creatinine quantification**

	Dilution	Standard + Diluent
S0	1 g/l in NaCl	
S1	0.5 g/l	500 µl S0 + 500 µl NaCl
S2	0.4 g/l	300 µl S0 + 300 µl NaCl
S3	0.3 g/l	350 µl S0 + 350 µl NaCl
S4	0.2 g/l	100 µl S0 + 400 µl NaCl
S5	0.1 g/l	50 µl S0 + 450 µl NaCl

**Table 10: Plate design for Jaffee creatinine quantification**

	1	2	3	4	5	6	7	8	9	10	11	12
<b>A</b>	BI	BI	P3	P3	P11	P11						
<b>B</b>	S1	S1	P4	P4	P12	P12						
<b>C</b>	S2	S2	P5	P5	...	...						
<b>D</b>	S3	S3	P6	P6								
<b>E</b>	S4	S4	P7	P7								
<b>F</b>	S5	S5	P8	P8								
<b>G</b>	P1	P1	P9	P9								
<b>H</b>	P2	P2	P10	P10								

### 2.2.9 T cell isolation from the kidneys

The kidneys were harvested as described in 2.2.5. The organs were minced in a petri dish using a scalpel and then transferred into a C tube (GentleMACS dissociator) filled with 5 ml digestion medium (see 2.1.5). 20 $\mu$ l Collagenase D (2 mg/dl) and 10  $\mu$ l DNase I (200  $\mu$ g/ml) was added into the C tube, mixed and then incubated in the water bath at 37 °C for 40 min. Following this digestion, the C tubes were put onto the GentleMACS dissociator and the programs mSpleen 1.01” followed by “mLung 2.01” were run to process the tissue. After centrifugation of the cell suspension (300 x g, 8 min, 4 °C), the supernatant was discarded carefully. To enrich for leukocytes, a density gradient was performed. This step removed fat and other tissue remains. Cells were centrifuged (500 x g with slow break, 20 min, RT) in 37 % Percoll (see 2.1.5). Supernatant was discarded and the tube without turning it back around placed in a tube stand to remove remaining Percoll. Cells were then washed one more time and transferred into a 1.5 ml micro tube in a suitable medium for further staining or stimulation. If there were too many erythrocytes in the cell pellet instead of washing the cells directly erythrocyte lysis as described in 2.2.10 was performed.

### 2.2.10 Erythrocyte lysis

Depending on the severity of bleeding during organ removal, there can be large amounts of erythrocytes in the cell pellet during lymphocyte purification. These erythrocytes may interfere with detection of lymphocytes in FACS.

Erythrocytes lysis buffer was newly produced (see 2.1.5). 1 ml of erythrocytes lysis buffer was added to the cell pellet and incubated at RT for 3-5 min depending on the quantity of erythrocytes in the cell pellet. Adding 5 ml PBS (4 °C) stopped the lysis. Cells were centrifuged at 350 x g for 5 min at 4 °C and washed two times with 2 ml PBS.

### 2.2.11 Manual and automated cell-counting

For counting the cells, a 10  $\mu$ l aliquot of the cell suspension was used. 10  $\mu$ l trypan blue staining dye was added and incubated for 1 min at RT. Dead cells have non-intact cell membranes and the trypan blue can pass into their cytosol staining these cells blue. Living cells with intact cell membranes can be distinguished by their unlabeled cytosol.

10  $\mu$ l of cell suspension, consisting of the aliquot and the trypan blue, were added onto a counting slide (for automated cell counting) or onto the Neubauer cell chamber (for manual cell counting). In case of the automated cell counting, the slide was now inserted into the cell counter and the size of the cells of interest (4-12  $\mu$ m) was selected. The cell counter calculated the total amount of cell, the living cells and gave the proportion of living cells in relation to total cells.

While automated cell counting is a lot quicker, manual counting is more accurate in terms of the number of living cells. After cleaning the Neubauer cell chamber with water and alcohol, a coverslip was put onto the chamber. Then 10  $\mu$ l of the incubated aliquot and trypan blue suspension was pipetted between coverslip and the chamber.

The total number and the number of live cells in the four corner squares of the chamber were counted using a microscope with 20-fold magnification. The cell number was calculated by multiplying the mean sum of counted cells per square with the dilution factor times 10.000 as the factor of the Neubauer counting chamber (see *Figure 12*).

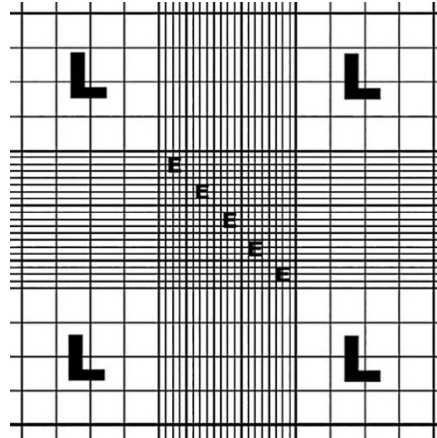


**Figure 12: Counting areas of a Neubauer cell chamber**

The cell trypan blue suspension was pipetted between coverslip and the chamber. All four corner squares marked with the letter “L” were counted (Illustration adopted from <https://www.carlroth.com/com/en/counting-cells/counting-chamber-neubauer-improved-bright-lines/p/t735.1>).

#### 2.2.12 Fecal Yale microbiome transplantation into Rag1 KO mice

The donor mouse with the Yale flora (kindly provided by AG Huber S) was sacrificed and the stool in the colon and caecum was taken. Stool was directly put into thioglycolate medium.

Stool was then passed through a 70  $\mu\text{m}$  sieve, and afterwards the filter was rinsed with 15ml brain heart infusion (BHI). The stool was centrifuged at 500 x g for 10 min and then the supernatant was discarded carefully. After this step, the stool could either be gavaged directly or prepared for freezing for later use.

For freezing 3 ml of 20 % glycerol in PBS was added to the stool and it was then stored at  $-80\text{ }^{\circ}\text{C}$ . To gavage the stool it was diluted in 3 ml BHI. To prepare the frozen aliquots for transplantation, the frozen stool was heated in a  $37^{\circ}\text{C}$  water bath for 3 min and then dissolved in 13 ml BHI. After spinning down at 500 x g for 10 min the supernatant was discarded as earlier described. After adding 2 ml BHI, the stool was ready for transplantation. The Rag1<sup>-/-</sup> mice in the experiments were gavaged 200  $\mu\text{l}$  of Yale flora. After a period of 2-3 weeks for the flora to establish itself in the new host, CD45RB<sup>hi</sup> colitis was induced as described in 2.2.13.

#### 2.2.13 Induction of CD45RB<sup>hi</sup> colitis

CD45RB<sup>hi</sup> Colitis was induced in Rag1<sup>-/-</sup> mice, that prior to cell transfer, were gavaged a colitogenic flora. CD45RB<sup>hi</sup> cells were obtained from IL17A<sup>CRE</sup> x R26R<sup>eYFP</sup> x T-bet<sup>flox</sup> and IL17A<sup>CRE</sup> x R26R<sup>eYFP</sup> mice. 1 donor mouse was sacrificed per 4 recipients. Spleen and lymph nodes of the donor were collected in PBS 1X and the fat was removed. Spleen and lymph nodes were smashed through a 100  $\mu\text{m}$  cell strainer, washed with MACS buffer and then centrifuged for 7 min at 350 x g at  $4\text{ }^{\circ}\text{C}$ . Supernatant was discarded. Mouse CD4 MACS beads were diluted 1:10 in MACS buffer and 200  $\mu\text{l}$  diluted CD4 MACS beads per donor mouse was added to the cell pellets. The beads incubated at 4

°C for 30 min in the fridge. Up to 20 ml MACS buffer was added and after centrifugation at 350 x g for 7 min at 4 °C the supernatant was discarded. MACS columns were placed onto the magnet and pre-wet with 3 ml MACS buffer. 1 ml MACS buffer was added, and cells were passed through a 40 µm cell strainer.

The cells were then applied onto the MACS column and the flow-through was collected in a 15 ml tube. The MACS column was washed 3 times with 3 ml MACS buffer. The CD4<sup>-</sup> cells were in the flow-through collected in the 15 ml Falcon, while the CD4<sup>+</sup> cells stayed in the column. CD4<sup>-</sup> cells were discarded and the columns were taken out of the magnet and placed on top of a new tube. 5 ml MACS buffer was added on top of the column and using a plunger pressure was applied. This step was repeated twice. The tube now contained the CD4<sup>+</sup> cells and was centrifuge at 350 x g for 7 min at 4 °C. Then the supernatant was discarded.

The surface staining master mix was prepared, and cells were stained in 100 µl/per donor for 30 min at 4°C in the dark. After centrifugation at 350 x g for 7 min at 4 °C the supernatant was discarded and 160 µl MACS buffer was added to the pellet.

Cells were then sorted into 15 ml tubes containing 500 µl RPMI/ 1 % FBS at the FACS device. It was gated for lymphocytes and doublet discrimination was performed. Next CD3<sup>+</sup>CD4<sup>+</sup>CD25<sup>-</sup> cells were selected. CD45RB<sup>hi</sup> cells were sorted as the third with the highest CD45RB expression of previously gated cells.

After sorting the cells, they were centrifuge for another 5 min at 250 x g and 4 °C and the supernatant was discarded. PBS 1X was added and the cells were counted manually using the Neubauer counting chamber. The volume of the cell suspension was adjusted with PBS 1X, so that 100 µl contain 200.000 cells. Receiver mice (Rag1 KO Yale mice) were weighed and injected 100 µl (= 200.000 cells) of sorted CD45RB<sup>hi</sup> T cells i.p.. Progress of disease was monitored by regular weighing and weekly endoscopy. As soon as the mice developed colitis they were sacrificed and colons and spleens were harvested for further analysis.

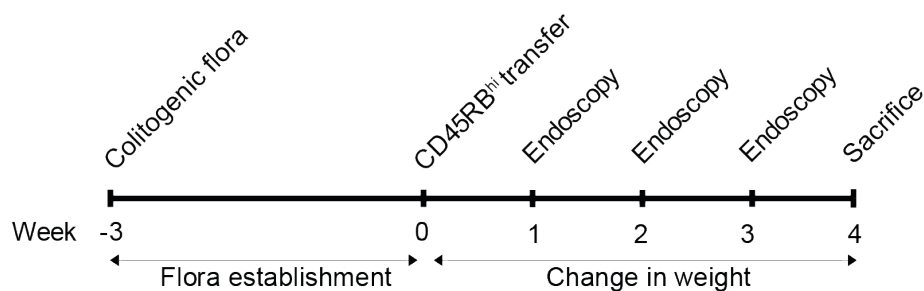


**Figure 13: Experimental outline of CD45RB<sup>hi</sup> Colitis**

Animals received colitogenic flora 2-3 weeks prior to CD45RB<sup>hi</sup> cell transfer via gavage. At day 0 200.000 CD45RB<sup>hi</sup> cells were injected i.p. Weekly endoscopy evaluating the inflammation of the colon was conducted and change in weight was assessed regularly. After the onset of colitis, animals were sacrificed. Then the colon was removed for histological and FACS analysis.

## 2.2.14 Flow cytometric cell sorting

The cell sorting was performed with the BD FACSAria IIIu and the BD FACS Fusion according to the manufacturer. Cell sorting was performed by the UKE FACS Core Facility.

### 2.2.15 Mice evaluation during CD45RB<sup>hi</sup> colitis (colitis scoring)

Disease severity during the experiment was monitored by regular weighing every 2-3 days, checking the general condition of the mice (social behavior, stool, condition of the after, eyes and fur, expression of pain etc.) and by weekly endoscopy of the colon. If the body weight of the mice dropped beneath 80 % of the body weight at day 0, mice were sacrificed according to the animal welfare agreement. Mice were furthermore sacrificed, if there was a heavy load or a prolonged medium load (more than 3 days).

Blinded weekly coloscopy was performed using the Coloview system (Karl Storz, Germany; see *Figure 14*; Becker *et al.*, 2006). Parameters observed during coloscopy were translucency of the colon, granularity of the mucosa, stool consistency, fibrin and the vascular pattern. 0-3 points were given per category making 18 the highest possible colitis score as previously described (Kamanaka *et al.*, 2011).

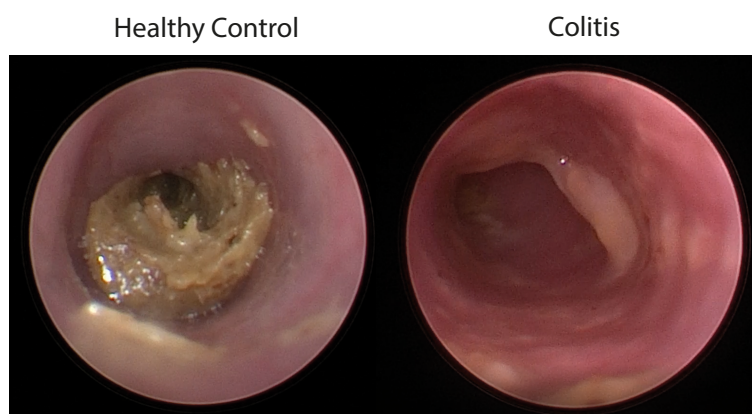


**Figure 14: Endoscopic evaluation of disease in CD45RB<sup>hi</sup> Colitis**

Translucency, vascularity and granularity of the colonic mucosa as well as consistency of the stool and presence of fibrin were observed parameters during evaluated endoscopy. The left picture of a healthy murine colon shows solid stool and inconspicuous mucosa whereas the left colon section shows increased granularity and vascularity and soft stool and thereby clear signs of colonic inflammation.

### 2.2.16 T cell isolation from the colon

The mouse abdomen was opened cutting through the skin and anterior abdominal wall. Pubis bone was cut to reach the rectum. The intestine was followed from the stomach to the rectum. The colon was harvested by disconnecting the gut after the caecum and close to the rectum. The fat was removed. Colon size was measured and 0.5 cm of the colon were separated for each histology and RNA isolation. Material for histology was placed in 4 % formalin for 24 hours and material for RNA analysis was frozen at -80 °C. The colon was transferred into PBS 1X and cut open longitudinally to wash off the colonic content. Colon tissue was cut to pieces of about 0.5 cm and then shaken horizontally for 20 min at 37 °C in 10 mL DTT solution. Tissue pieces were placed on a 70 µm strainer and rinsed with PBS/1 % FBS. Tissue was minced with surgical scissors and placed in 4 ml of collagenase buffer. 40 µl of Collagenase (100 mg/ml) and 8 µl DNase I (100 mg/ml) per tube was added and tubes were shaken horizontally for 45 min at 37 °C. Digested tissue was smashed through metal strainer, washed with PBS/1 % FBS and then centrifuged at 500 x g for 10 min at 4 °C. Supernatant was discarded and 4 ml 40 % Percoll was added. The cells were laid carefully on top of

4 ml 67 % Percoll in a 15 ml tube and then centrifuged at 400 x g, 20 min at RT with slow acceleration and break. After discarding the fat layer on top of the Percoll, the interphase containing the lymphocytes was taken with a 1 ml pipet and put in a new tube filled with 5 ml PBS/1 % FBS. Cells were centrifuged at 400 x g for 5 min at 4 °C. Supernatant was discarded and 1 ml PBS/1 % FBS was added. T cells were now ready to count and proceed with the staining.

### 2.2.17 Preparation of tissue slices for histopathological analysis

Removed tissue during the organ extraction was put into 4 % paraformaldehyde (PFA) for 24 h at 4 °C. Afterwards, tissue was washed 3 times with phosphate buffered saline for 30 min on a shaker. Tissue was then put in EtOH (50 % v/v) for two hours at RT to reduce the amount of water in the samples for the following embedding. A histological citadel containing EtOH (60 %, 70 %, 96 %, 100 % v/v), paraffin and xylene in various baths and at different temperatures was used to further process the tissue. After passing through the citadel tissue was embedded in paraffin and cooled down to -15 °C. 0.5 µm -1 µm thick tissue slices were cut with a microtome and transferred onto a microscope slide. Tissue was now ready for further histopathological staining and could be deparaffinized and hydrated to proceed with PAS staining (see 2.2.18) or HE stain (see 2.2.19).

### 2.2.18 Periodic acid-Schiff reaction

Periodic acid-Schiff (PAS) stain was used for kidney histological cuts from the NTN experiments. At first, the cuts embedded in paraffin were deparaffinized with xylene and then rehydrated using a descending alcohol series.

Cuts were put into periodic acid (0,5 % v/v) for 15 min at RT. The periodic acid oxidizes the samples, so that the Schiff reagent can later react with it and produce the magenta color. After oxidation, cuts were washed with tap water for 3 min and then with aqua dest.. Cuts were then put in a cuvette filled with Schiff reagent for 40 min at RT. It is important to note that the Schiff reagent was already warmed up to RT previously. Afterwards, cuts were washed with warm tap water for 7 min and then with aqua. dest.. Next, the sections were stained in hematoxylin solution for 1-2 min at RT (Böhmer, 1865). The intensity of the staining was checked under the light microscope. If necessary, staining was repeated. Stained samples were then washed with tap water for 2-3 min. Samples then were briefly dipped 2-3 times into hydrochloric acid/EtOH for differentiation. After another washing step, the ready dyed cuts were dehydrated using an ascending alcohol series. Using Eukitt mounting media the tissue was then covered with a coverslip.

### 2.2.19 Hematoxylin and eosin stain

Hematoxylin and eosin (HE) stain was used for colon histological cuts from the CD45RB<sup>hi</sup> colitis experiments. The eosin dyes the cytoplasm and extracellular matrix pink/red. The hematein (oxidized hematoxylin) dyes the cell nuclei and the endoplasmic reticulum purple/blue.

As described previously in 2.2.18, the cuts were first deparaffinized with xylene and then rehydrated using a descending alcohol series. Sections were then put in haemalum stain for 1-2 min, followed

by a washing step (tap water for 8 min, then aq. dest.). Cuts afterwards were put in eosin (0,5 % v/v) for 15 s and then quickly dipped into aq. dest.. Next, tissue was shortly dipped once into 96 % EtOH and twice into 100 % EtOH to improve staining contrast. The tissue was washed twice with xylene. Using Eukitt mounting media the tissue was then covered with a coverslip.

#### 2.2.20 *Ex vivo* stimulation of T cells from kidney and colon

Phorbol 12-myristate 13-acetate (PMA), ionomycin and Brefeldin A were used for *ex vivo* stimulation. PMA and ionomycin induce cytokine production, while Brefeldin A inhibits intracellular protein transport and therefore allows better intracellular FACS staining (Nylander and Kalies, 1999).

Stimulation medium was prepared according to 2.1.5. Following the T cell isolation (see 2.2.9 and 2.2.16), the cell suspension was centrifuged (370 x g, 5 min, 4 °C). Cells were incubated for 3 h in 1 ml medium at 37 °C in an incubator with 4 % CO<sub>2</sub>. After a washing step with MACS buffer, cells were subjected to FACS staining.

#### 2.2.21 Surface- and intracellular staining for FACS analysis

For easier handling, the surface- and intracellular staining was performed in a 96-well plate. Washing steps were performed with the aid of a multichannel pipette. During the staining the cells were protected from light whenever possible to avoid photobleaching.

Following *ex vivo* stimulation (see 2.2.20), cells were centrifuged at 350 x g for 7 min at 4 °C. Supernatant was discarded and cells were transferred in 200 µl MACS onto a 96-well plate. Then the cell suspension was centrifuged at 350 x g for 2 min at 4 °C. Supernatant was discarded and 100 µl of prediluted near-infrared (NiR) (1:1000 dilution) was added. NiR incubated for 10 min in the dark at RT. Then 200 µl MACS buffer was added and the cell suspension was centrifuged (350 x g, 2 min at 4 °C). Supernatant was discarded and 50 µl of MACS and 5 µl of mouse serum was added and mixed thoroughly. The mouse serum, that blocks unspecific binding sites of murine monoclonal ABs, incubated for 5 min at RT. First chemokine receptors were stained in concentrations as specified in 2.1.4. After adding the ABs directed against the chemokine receptors the well mixed cell suspension incubated for 15 min at 37 °C to improve the staining results (Berhanu *et al.*, 2003). In the next step, antibodies targeting extracellular antigens were added and incubated for 15 min at RT. One more washing step with 100 µl MACS buffer and centrifugation at 350 x g for 2 min at 4 °C was performed. Supernatant was removed and 100 µl 3,7 % paraformaldehyde (PFA) was added to the cell pellet. Cells incubated for 17 min in the dark in PFA. Another washing step followed. Then 100 µl 0,1 % IGEPAL was added and cells incubated for 4 min. IGEPAL as a detergent can perforate the cell membrane and therefore makes staining of intracellular antigens like cytokines possible. Yet another washing step was performed. 50 µl MACS buffer and the ABs directed against intracellular antigens were added (for concentrations see 2.1.4). After 30 min of incubation at 4 °C, cells were washed and 250 µl PBS was added.

### 2.2.22 Surface- and intranuclear staining for FACS analysis

Surface and intranuclear staining was performed in a 96-well plate. Washing steps were performed with the aid of a multichannel pipette. During the staining the cells were protected from light whenever possible to avoid photo bleaching.

Following T cell isolation (see 2.2.9 and 2.2.16) cells were centrifuged at 350 x g for 7 min at 4 °C. Cells were transferred onto a 96-well plate in 200 µl MACS and then centrifuged at 350 x g for 2 min at 4 °C. Supernatant was discarded and 100 µl of prediluted near-infrared (NiR) (1:1000 dilution) was added. NiR incubated for 10 min in the dark at RT. Then, 200 µl MACS buffer was added and the cell suspension was centrifuged (350 x g, 2 min at 4 °C). Supernatant was discarded and 25 µl of MACS and 5 µl of mouse serum was added and mixed thoroughly. The mouse serum, that blocks unspecific binding sites of murine monoclonal ABs, incubated for 5 min at RT. First, chemokine receptors were stained in concentrations as listed in 2.1.4. After adding the ABs directed against the chemokines, the well mixed cell suspension incubated for 15 min at 37 °C to improve the staining results. In the next step ABs targeting extracellular antigens were added and incubated for 15 min at RT. One more washing step with 100 µl MACS buffer and centrifugation at 350 x g for 2 min at 4 °C was performed. Supernatant was removed and 100 µl 3,7 % paraformaldehyde (PFA) was added. Cells incubated for 20 min at RT in PFA for fixation. 1X Perm Wash was produced according to 2.1.5. Cells were washed with 100 µl 1X Perm Wash and following centrifugation (370 x g, 2 min, RT). 200 µl 1X Perm Wash was added and cells incubated for 20 min at RT. 1X Perm Wash perforates the cell and nucleus membrane and thereby makes staining of intranuclear TFs possible. After centrifugation of the cell suspension, ABs directed against intranuclear antigens were pipetted to the return flow and stained overnight in the fridge at 4 °C. The next day cells were washed with 200 µl 1X Perm Wash, centrifuged and then 250 µl PBS was added to the pellet. Cells were now ready for FACS analysis.

### 2.2.23 Histological scoring in the cGN model

The histological glomerulonephritis score (GN-Score) or crescent score was assessed as previously described in Krebs *et al.*, 2013. Crescent formation was assessed in 30 glomeruli per mouse in a blinded fashion in PAS-stained paraffin sections.

### 2.2.24 Histological scoring in CD45RB<sup>hi</sup> Colitis

HE stained sections of colons of CD45RB<sup>hi</sup> mice were scored for mononuclear inflammation, crypt hyperplasia, epithelial injury, neutrophilic inflammation and depth of inflammation. The grading within these 5 items is shown in *Table 11*. The total colitis score is the sum of the score for the 5 items. For the item crypt hyperplasia, a crypt to villus ratio of 1 : 3-4 in mature mice was considered normal (=absent). Elongated crypts with increased mitoses were then scored from mild to severe crypt hyperplasia. Assessing mononuclear inflammation, normal GALT and lymphoid aggregates were excluded.

**Table 11: Histological Colitis Score**

Score	0	1	2	3	4
<b>Mononuclear inflammation</b>	absent	diffuse increase in lamina propria, usually with plasma cells	lamina propria increased with basal localization aggregates displacing crypts	lamina propria with submucosal infiltration	-
<b>Crypt hyperplasia</b>	absent	mild	moderate	severe	-
<b>Epithelial injury</b>	absent	crypt dropout/ distortion or surface epithelial damage	focal ulceration	multifocal or extensive ulceration	-
<b>Neutrophilic inflammation</b>	absent	lamina propria only	+ cryptitis or crypt abscesses	sheet-like or submucosal infiltrate	-
<b>Depth of inflammation</b>	mucosa	submucosa	1 spot transmural	2-5 spots transmural	diffuse

### 2.2.25 10x Genomics scRNAseq pipeline

The 10x scRNAseq pipeline for generation of a 5'v2 Gene expression library for sequencing was carried out according to the manufacturers protocols and in line with provided recommendations. In the following, the general principles and procedures from sorting the cells to sequencing are briefly described. More detailed information on the workflow is provided in the 10x genomics protocol (see [https://assets.ctfassets.net/an68im79xiti/57JaTECQNBSPyDz8oucdi/ced6aa8eaf73d6ee18dea8fd945faa/CG000331\\_Chromium\\_Next\\_GEM\\_Single\\_Cell\\_5-v2\\_UserGuide\\_RevD.pdf](https://assets.ctfassets.net/an68im79xiti/57JaTECQNBSPyDz8oucdi/ced6aa8eaf73d6ee18dea8fd945faa/CG000331_Chromium_Next_GEM_Single_Cell_5-v2_UserGuide_RevD.pdf)).

After sorting the cells as described in 2.2.14 the gel beads in emulsion (GEM's) were generated according to the 10x Genomics protocols. During this step, cells were captured in an oil droplet together with a unique feature barcode from a repertoire of approximately 750.000. All the cDNA obtained from a single cell will in further steps have the same 10x Barcode. After library construction, it can therefore be mapped to its origin. The process of GEM generation is illustrated in *Figure 15*.

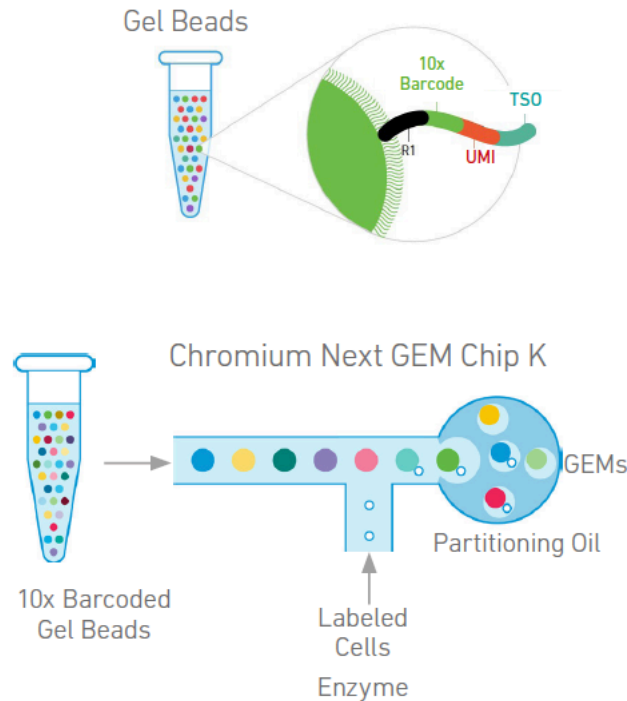


**Figure 15: Generation of GEM'S (scRNAseq)**

GEMs were generated using the Chromium Next GEM Chip K. It combines one Single Cell VDJ 5' Gel beads with a unique 10x Barcode, a single cell and a master mix containing enzymes for following steps in the scRNAseq pipeline inside an oil droplet. (Illustration adopted from 10x Genomics Chromium Next GEM Single Cell 5' Reagent Kits v2 (Dual Index) protocol. (see [https://assets.ctfassets.net/an68im79xiti/57JaTECQNBPSpYDz8oucdi/ced6aa8eaf73d6ee18dea8fdbd945faa/CG000331\\_Chromium\\_Next\\_GEM\\_Single\\_Cell\\_5-v2\\_User\\_Guide\\_RevD.pdf](https://assets.ctfassets.net/an68im79xiti/57JaTECQNBPSpYDz8oucdi/ced6aa8eaf73d6ee18dea8fdbd945faa/CG000331_Chromium_Next_GEM_Single_Cell_5-v2_User_Guide_RevD.pdf)))

Once a GEM was generated, the 10x Gel Bead dissolved and lysis of the captured cell was induced. Released mRNA is reverse transcribed into cDNA (see *Figure 16*). The master mix contains needed reagents for reverse transcription (RT) and poly(dT) primers. Dissolved 10x Gel Beads contain Gel Bead primers which ensure that produced cDNA is 10x Barcoded.

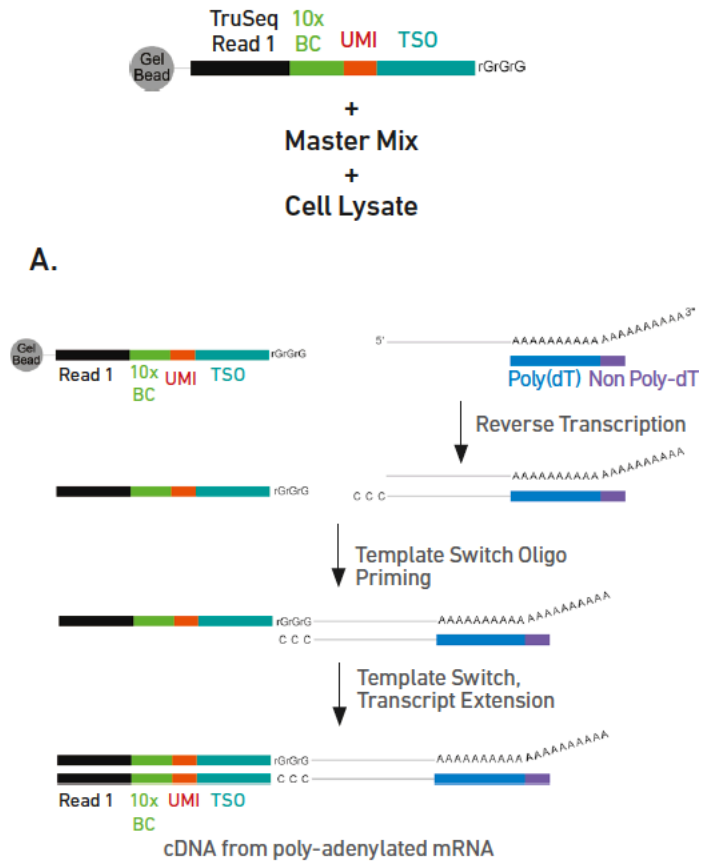


**Figure 16: Reverse transcription inside GEM (cDNA generation)**

10x Gel Bead primers contain a 10x barcode, a unique molecular modifier (UMI) and template switch oligos (TSO). Poly-adenylated mRNA of the lysed cells is reverse-transcribed and associated with a 10x Gel Bead primer. (Illustration adopted from 10x Genomics Chromium Next GEM Single Cell 5' Reagent Kits v2 (Dual Index) protocol (see [https://assets.ctfassets.net/an68im79xiti/57JaTECQNBPSpyDz8oucdi/ced6aa8eaf73d6ee18dea8fdbd945faa/CG000331\\_Chromium\\_Next\\_GEM\\_Single\\_Cell\\_5-v2\\_UserGuide\\_RevD.pdf](https://assets.ctfassets.net/an68im79xiti/57JaTECQNBPSpyDz8oucdi/ced6aa8eaf73d6ee18dea8fdbd945faa/CG000331_Chromium_Next_GEM_Single_Cell_5-v2_UserGuide_RevD.pdf)))

Following the generation of barcoded cDNA, the GEMs were dissolved and its content, except for the cDNA, was extracted with magnetic beads. Purified cDNA was then amplified with PCR using common 3' and 5' end primers. This step is needed to provide sufficient cDNA for the construction of different libraries. In our experiments a 5' Gene expression library (GEX) as well as a V(D)J library was constructed according to the manufacturers protocol. As the analysis in this work is only based on sequencing data from the Gene expression library further steps of the V(D)J library construction are spared. For further information, see the manufactures protocol (see [https://assets.ctfassets.net/an68im79xiti/57JaTECQNBPSpyDz8oucdi/ced6aa8eaf73d6ee18dea8fdbd945faa/CG000331\\_Chromium\\_Next\\_GEM\\_Single\\_Cell\\_5v2\\_UserGuide\\_RevD.pdf](https://assets.ctfassets.net/an68im79xiti/57JaTECQNBPSpyDz8oucdi/ced6aa8eaf73d6ee18dea8fdbd945faa/CG000331_Chromium_Next_GEM_Single_Cell_5v2_UserGuide_RevD.pdf))).

Following the PCR, the cDNA was fragmented and P5, P7, i5 and i7 sample indexes, and a second read primer sequence were added. P5 and P7 are priming sites needed for the following sequencing. The GEX library was now constructed, and the material was sent to Novogene UK for sequencing. The detailed steps leading to the final construct are illustrated in *Figure 17*.

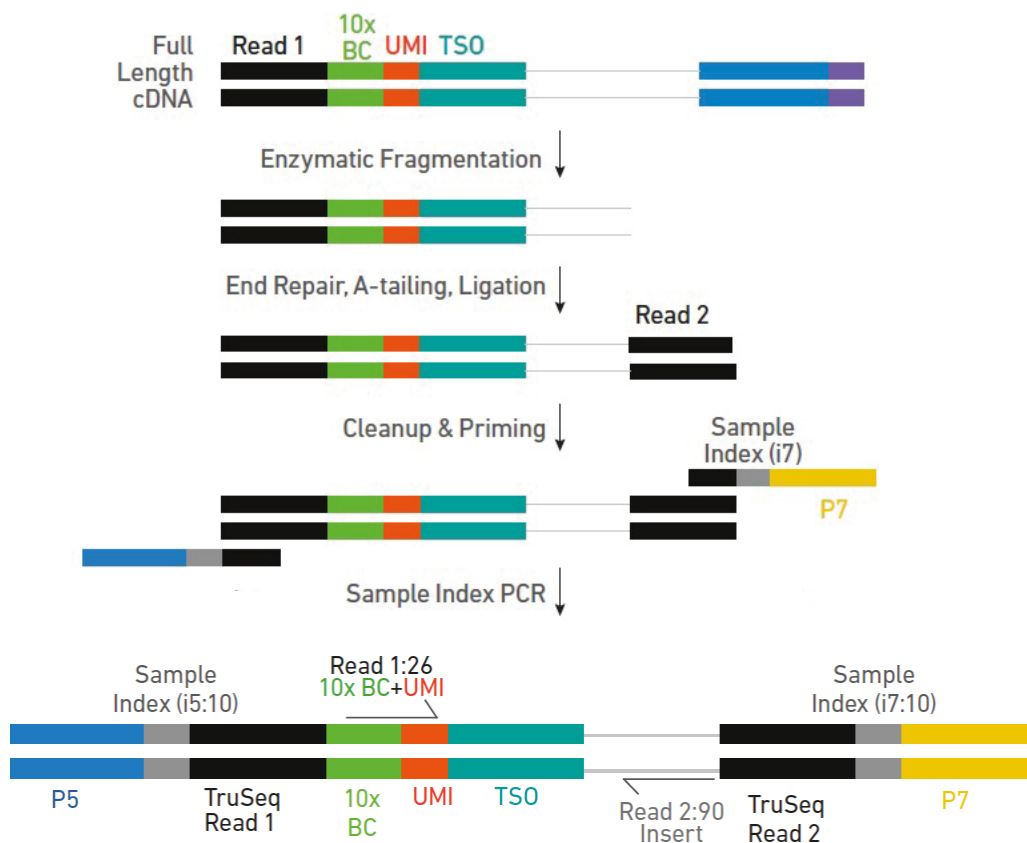


**Figure 17: Generation of 5' Gene Expression Library**

After cDNA fragmentation, the second Read sequence is added via end repair, A-tailing and ligation. Then during another PCR, the sample indices are conjugated. The final construct contains the P5 and P7 priming sites and is ready for Illumina sequencing. (Illustration adopted from 10x Genomics Chromium Next GEM Single Cell 5'Reagent Kits v2 (Dual Index) protocol (see [https://assets.ctfassets.net/an68im79xiti/57JaTECQNBPSpyDz8oucdi/ced6aa8eaf73d6ee18dea8fdbd945faa/CG000331\\_Chromium\\_Next\\_GEM\\_Single\\_Cell\\_5v2\\_UserGuide\\_RevD.pdf](https://assets.ctfassets.net/an68im79xiti/57JaTECQNBPSpyDz8oucdi/ced6aa8eaf73d6ee18dea8fdbd945faa/CG000331_Chromium_Next_GEM_Single_Cell_5v2_UserGuide_RevD.pdf)))

## 2.2.26 Analysis of scRNAseq data

Analysis of the sequenced data was performed with R packages named in 2.1.11. The workflow is shortly described in the following in chronological order.

### 2.2.26.1 Alignment

Sequencing data was aligned with Cell Ranger 4.0. Prior to alignment the TSO sequence is trimmed from the 5' end and the poly-A from the 3' end to improve sensitivity and efficiency. Cellranger makes use of STAR, an aligner carrying out splice-aware alignment (Dobin *et al.*, 2013).

### 2.2.26.2 Preprocessing workflow

Preprocessing of the data was performed according to the Seurat pipeline (Hao *et al.*, 2021). Cells with unique features counts over 2900 to 3800 depending on the batch, or under 200 were excluded from the analysis. As previously described in 2.2.23 during the 10x pipeline a single cell is captured within an oil droplet. Due to technical inaccuracies, it can happen that two cells at the same time, or no cell at all is captured within such a droplet. Excluding cells with very low or high feature counts

prevents, that doublets or empty droplets affect downstream analysis. Further, cells with mitochondrial counts higher than 5% were filtered. Afterwards, feature expression data of every cell was logarithmically normalized by the total expression using the “NormalizeData” function of the Seurat package. Using the “FindVariableFeature” function of Seurat, 2000 features with high differential expression within the data set were detected. Then linear transformation (“scaling”) with the “ScaleData” function was performed. The earlier found features from the “FindVariableFeature” function were then used to perform principal component analysis (PCA) with the “RunPCA” function. Using the function “FindNeighbors”, the similarity and heterogeneity of the cells within the dataset based on euclidian distances was assessed. With this information, the cells were then clustered using the Louvain algorithm included in the “FindClusters” function. Finally, using the “RunUMAP” function the cells were visualized in low dimensionality with similar cells in proximity to each other.

#### **2.2.26.3 Merging of datasets**

After performing the preprocessing workflow with the data of every batch individually, they were merged using the “merge” function implemented in the Seurat package. The merged dataset consisted of 53,285 cells.

#### **2.2.26.4 Batch correction**

To reduce the differences in gene expression level resulting from different treatment samples, batch correction was performed using the “Harmony” package. After finding the 2000 genes most variably expressed within the dataset with the FindVariableFeatures function of Seurat, this data was scaled and log transformed. Then PCA was performed and the top 20 PCs were kept. These PCs were then used to run harmony using the RunHarmony function of the harmony package. After this step the corrected Harmony embeddings were used in the “FindNeighbors”, “FindClusters” and “RunUMAP” functions earlier described to visualize the corrected similarity between the cells in low dimensionality and to illustrate clusters.

#### **2.2.26.5 Cell cycle scoring**

For exclusion of intercellular effects based on different cell cycle states, cell cycle scoring was performed. Using a list of DNA synthesis (S) and G2-Mitosis (G2M) phase genes from included in the Seurat packages, a S and G2M score was assigned to every cell within the dataset and on that basis the cells could be matched to either G1, G2M or S phase. Cells with either a S score under 0.25 or a G2M score under 0.2 were excluded from the dataset, leaving a total number of 52,252 cells.

#### **2.2.26.6 Differential expression analysis**

Using the “FindAllMarkers” function, marker genes upregulated within each of the earlier defined clusters in comparison to all other cells of the dataset were found. The 100 genes with the highest average logarithmic upregulation within each compared to the rest of the cells were saved in a csv

file and used for assigning the cell type to the found clusters. The expression level of those marker genes was then further visualized using the functions “VlnPlot” and “FeaturePlot”.

#### **2.2.26.7 Module scores**

Using the “AddModuleScore” function implemented in the Seurat package, an average expression level of a cellular program, meaning a combination of several genes typical for a specific cellular subset, in relation to control features can be added to each cell.

Using this function, a bcell\_feature, tcell\_feature and a myeloid\_feature score was added to the object meta data. The bcell\_feature module score contained the features “Cd19” and “Ms4a1”, the tcell\_feature score “Cd3d”, “Cd3e” and “Cd3g” and the myeloid\_feature score “Fcgr3”, “Cd68”, “Cd14” and “Cd74”. The module scores were then visualized with the “VlnPlot” function. These scores were considered when clusters for further subclustering of T cells were chosen.

#### **2.2.26.8 Heatmaps**

Heatmaps were made using the “DoHeatMap” function implemented in the Seurat package. The input was the average expression of chosen genes generated with the “AverageExpression” function of Seurat.

#### **2.2.26.9 Boxplots**

Boxplots were made using the “ggplot” function of the ggplot2 package. The color coding was carried out with the help of the RColorBrewer package.

### **2.2.27 Statistical Analysis**

Statistical analysis was performed using GraphPad Prism (see 2.1.10). The results are shown as the mean and standard deviation (SD), or standard error of the mean (SEM) as indicated in the graph description. Differences between two individual groups were compared by the help of two-tailed t-tests. For analysis of the change in weight in the three groups during CD45RB<sup>hi</sup> colitis a two-way ANOVA with Geisser-Greenhouse correction was used. This was followed up by Tukey-Kramer’s multiple comparison test to compute individual variances for each comparison. *P* values >0.05 were considered not significant (n.s.).

### 3 Results

The result section will give a sorted presentation of the experimental results starting with findings from cGN experiments and followed by CD45RB<sup>hi</sup> colitis data.

#### 3.1 Results of crescentic glomerulonephritis experiments

CGN was induced in IL17A<sup>CRE</sup> and IL17A<sup>CRE</sup> x Tbx21<sup>fl/fl</sup> animals and animals were sacrificed at day 10 as described in 2.2.5. A control group of IL17A<sup>CRE</sup> animals did not receive the nephrotoxic sheep serum.

##### 3.1.1 Clinical parameters in crescentic glomerulonephritis

Disease induction was evaluated in both runs of cGN by analysis of albumin-creatinine-ratio (ACR) (see *Figure 18*). Further the clinical markers cholesterol (CHOL2), triglycerides (TRIGL) and blood urea nitrogen (BUN) were assessed (see *Figure 19*).

Kidney function in IL17A<sup>CRE</sup> Control mice was normal and no albuminuria was present, whereas the two cGN groups showed elevated ACRs. Average ACR in the IL17A<sup>CRE</sup> x Tbx21<sup>fl/fl</sup> cGN group was slightly lower than in IL17A<sup>CRE</sup> cGN mice but did not reach statistical significance.

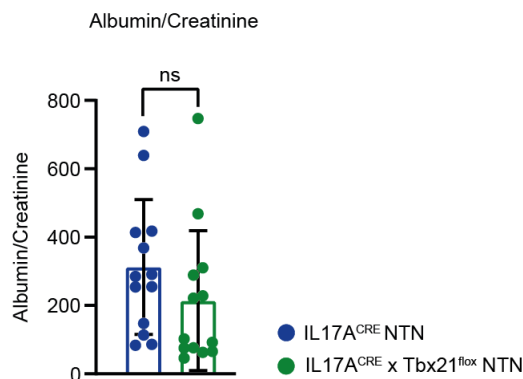


**Figure 18: Albumin/Creatinine-ratios in cGN**

Albumin/Creatinine ratio results from albumin ELISA data and results of urine creatinine quantification. Bar graphs show mean with SD. Significance was determined with the help of t-tests. Data was acquired from two separate experiments.

Apart from the histological and urinalysis, several plasma markers influenced by cGN were quantified. There was no significant difference in blood urea nitrogen (BUN) as a parameter of disease severity in the cGN groups. The same was observed for cholesterol. Interestingly there was a significant decrease in blood triglycerides in the IL17A<sup>CRE</sup> x Tbx21<sup>fl/fl</sup> cGN group compared to the IL17A<sup>CRE</sup> cGN group.

Overall blood and urine analysis showed elevated disease markers in both cGN groups. Yet, there was no ameliorated disease in IL17A<sup>CRE</sup> x Tbx21<sup>fl/fl</sup> cGN, with the exception of decreased triglyceride levels.

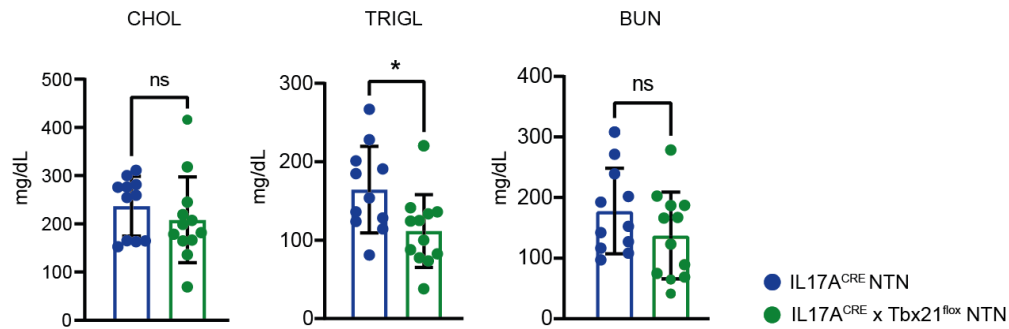


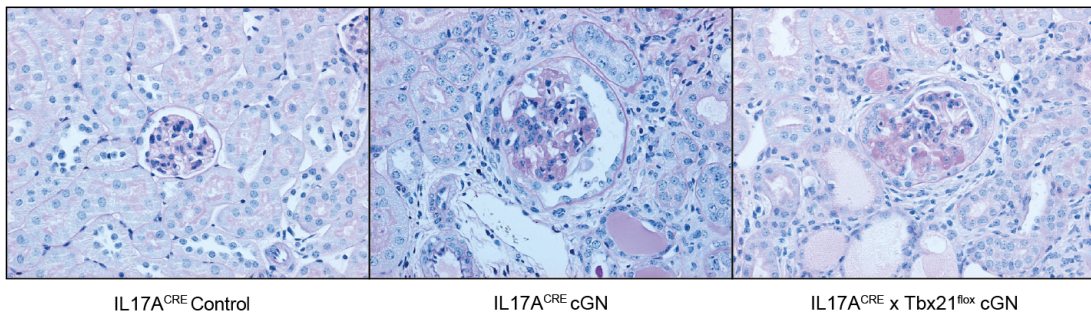
**Figure 19: Blood analysis of cholesterol, triglycerides and BUN in cGN**

Blood was taken on day 10 and put into EDTA tubes before animals were sacrificed. Blood samples were then centrifuged and plasma cholesterol, triglycerides and blood urea was determined by the laboratory at Campus Forschung N22, UKE. Bar graphs show mean with SD. Significance was determined with the help of t-tests. Data was acquired from two separate experiments.

### 3.1.2 Histology of renal sections

PAS-stained renal sections were scored as described in 2.2.23. While IL17A<sup>CRE</sup> Control animals showed no crescent formation, the GN-Scores of both cGN groups were elevated. IL17A<sup>CRE</sup> x Tbx21<sup>fllox</sup> cGN animals showed a tendency towards decreased GN-Scores compared to IL17A<sup>CRE</sup> cGN mice without reaching significance. This was in line with previous findings in clinical parameters (see 3.1.2). IL17A<sup>CRE</sup> x Tbx21<sup>fllox</sup> cGN animals were not protected from cGN onset (see Figure 20).

**A**



**B**

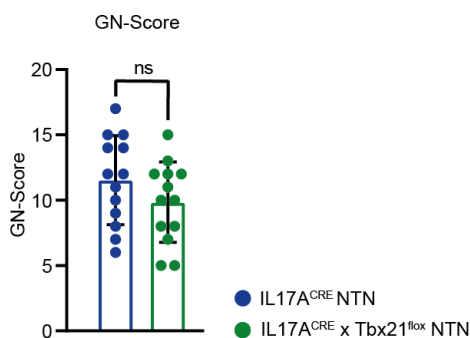


**Figure 20: Histological analysis of renal sections in cGN**

(A) PAS-stained sections of the kidney from day 10 of cGN. (B) GN-Score in cGN was assigned according to the PAS-stained sections of the kidney from day 10 of cGN. Bar graphs show mean with SD. Significance was determined with the help of t-tests. Data was acquired from two separate experiments.

### 3.1.3 FACS analysis of renal lymphocytes

Following the analysis of histological and clinical parameters, FACS analysis was conducted to assess the impact of the Th17 specific T-bet KO in cGN on a cellular level.

After purification, the renal cells were stained for FACS analysis according to 2.2.21 and 2.2.22. FACS analysis was performed with a BD LSR II Flow Cytometry Cell Analyzer. The gating strategy used in cGN experiments aimed at identifying CD45<sup>+</sup>CD3<sup>+</sup>CD4<sup>+</sup> Lymphocytes and further YFP<sup>+</sup> cells as depicted in *Figure 21*.

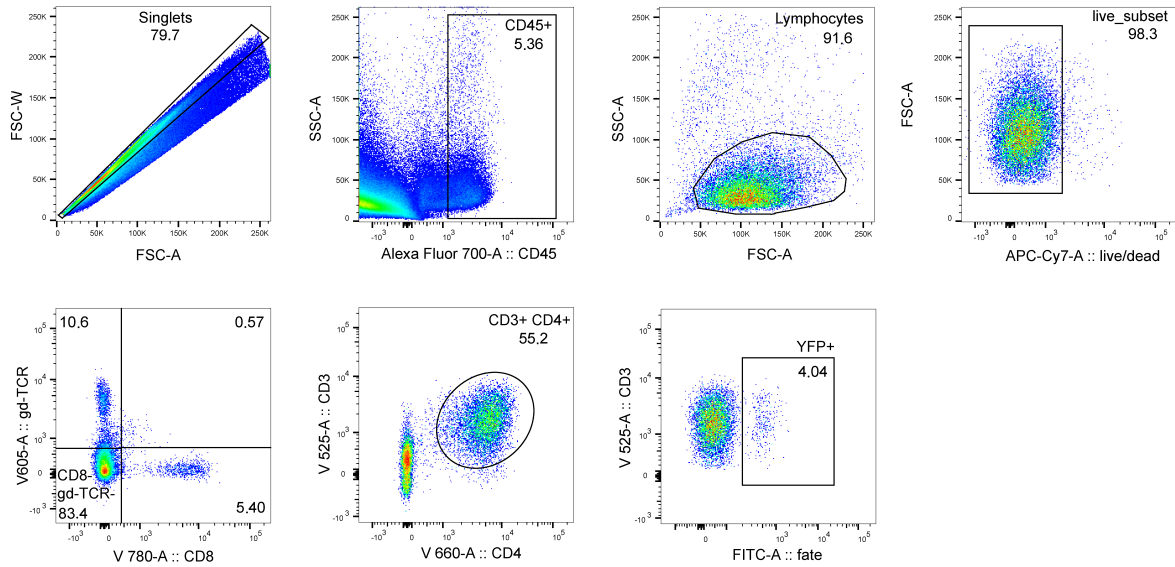


**Figure 21: FACS gating strategy in cGN experiments**

Cells were first gated for singlets, CD45<sup>+</sup>, Lymphocytes and then living cells. CD8<sup>+</sup> and gd-TCR<sup>+</sup> cells were excluded from the analysis and it was then gated on CD3<sup>+</sup>CD4<sup>+</sup> lymphocytes. YFP<sup>+</sup> cells (IL-17A fate<sup>+</sup>) were selected for further analysis.

The number of YFP<sup>+</sup> cells in IL17A<sup>CRE</sup> and IL17A<sup>CRE</sup> x Tbx21<sup>fllox</sup> mice was comparable (see *Figure 22*). As Th17 cells are the driver of pathogenicity within the cGN model the amount of YFP<sup>+</sup> cells represent a cellular marker of disease severity. Comparable numbers of YFP<sup>+</sup> cells are therefore in line with earlier findings from clinical and histological analysis.

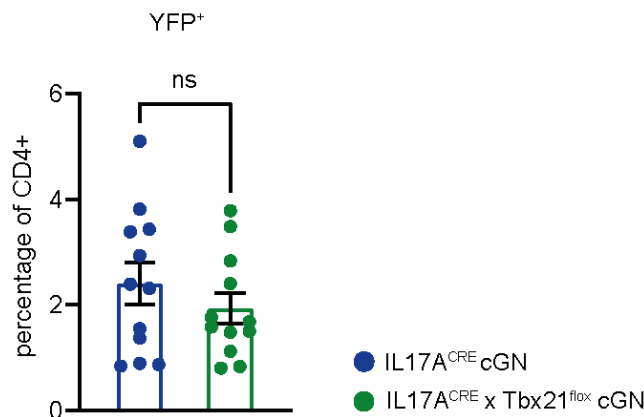


**Figure 22: Percentage of YFP<sup>+</sup> cells in IL-17A<sup>CRE</sup> Tbx21<sup>fllox</sup> cGN mice**

Cells were first gated for singlets, CD45<sup>+</sup>, Lymphocytes and then living cells. CD8<sup>+</sup> and gd-TCR<sup>+</sup> cells were excluded from the analysis and it was then gated on CD3<sup>+</sup>CD4<sup>+</sup> lymphocytes. YFP<sup>+</sup> cells (IL-17A fate<sup>+</sup>) were

selected for further analysis. Bar graph shows mean with SEM. Significance was determined with the help of t-tests. Data was acquired from two separate experiments.

At first, the T-bet expression of YFP<sup>+</sup> and YFP<sup>-</sup> cells in the two experimental groups was assessed. This ensured, that the Tbx21 KO only affects IL-17A fate<sup>+</sup> cells and no other T helper subsets. The baseline T-bet expression in YFP<sup>+</sup> cells of IL17A<sup>CRE</sup> animals was already low and was further reduced in IL17A<sup>CRE</sup> x Tbx21<sup>fllox</sup> animals (see Figure 23). Only in YFP<sup>+</sup> cells of IL17A<sup>CRE</sup> x Tbx21<sup>fllox</sup> animals, a significant decrease in T-bet expression was present. YFP<sup>-</sup> cells of IL17A<sup>CRE</sup> x Tbx21<sup>fllox</sup> animals showed no decreased T-bet expression. This confirms the T-bet KO to be Th17 specific in the performed cGN experiments.

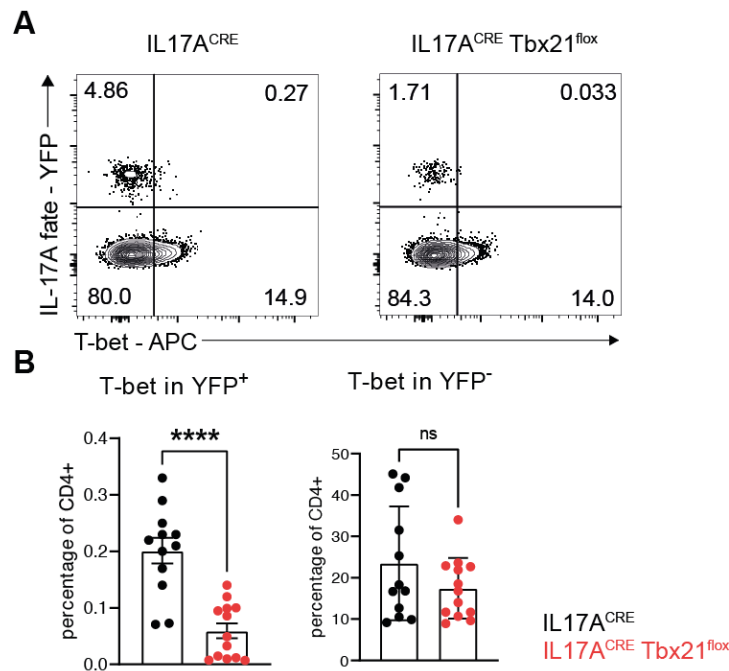


**Figure 23: T-bet expression in IL-17A<sup>CRE</sup> Tbx21<sup>fllox</sup> cGN mice**

(A) 10 days after cGN induction T-bet expression was analyzed in YFP<sup>+</sup> and YFP<sup>-</sup> renal lymphocytes via FACS analysis. It was previously gated on CD3<sup>+</sup>CD4<sup>+</sup> (B) Bar graphs show the resulting percentages of T-bet expression in YFP<sup>+</sup> and YFP<sup>-</sup> from FACS analysis with SEM. Significance was determined with the help of t-tests. Data was acquired from two separate experiments.

Following the verification of the IL17A fate<sup>+</sup> specific Tbx21 KO, its effect on the expression of Th1 lineage signature cytokine IFN- $\gamma$  and Th17 lineage signature cytokine IL-17A in Th17 cells was assessed.

The amount of IL-17A<sup>+</sup> IFN- $\gamma$ <sup>-</sup> YFP<sup>+</sup> cells (Th17 cells) did not differ between the two groups. We saw overall low numbers of Th1-like (IL-17A<sup>+</sup> IFN- $\gamma$ <sup>+</sup>) and exTh17 cells (IL-17A<sup>-</sup> IFN- $\gamma$ <sup>+</sup>) in the model of cGN. Th1-like and exTh17 cell populations were further decreased in the IL17A<sup>CRE</sup> x Tbx21<sup>fllox</sup> group (see Figure 24).

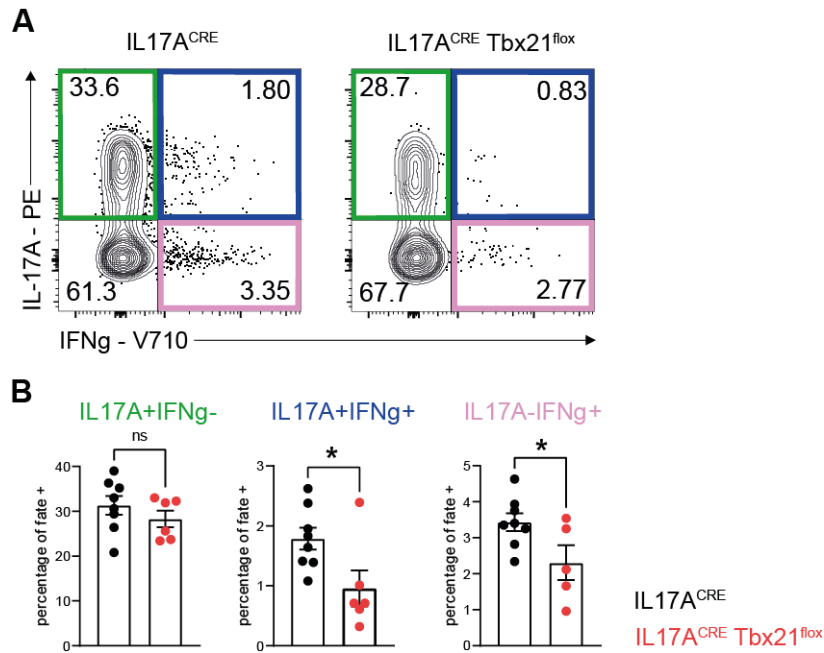


**Figure 24: Th17-Th1 axis in IL-17A<sup>CRE</sup> Tbx21<sup>flox</sup> cGN mice**

(A) IL-17A and IFN- $\gamma$  expression in IL-17A fate<sup>+</sup> cells of IL17A<sup>CRE</sup> and IL17A<sup>CRE</sup>Tbx21<sup>flox</sup> mice gated on CD3<sup>+</sup>CD4<sup>+</sup> as depicted in Figure 21. (B) Bar graphs show the resulting percentages of IL17A<sup>+</sup> IFN- $\gamma$ <sup>-</sup>, IL17A<sup>+</sup> IFN- $\gamma$ <sup>+</sup> and IL17A<sup>-</sup> IFN- $\gamma$ <sup>+</sup> of total YFP<sup>+</sup> cells from FACS analysis with SEM. Significance was determined with the help of t-tests.

Following the analysis of cytokine expression, the impact of the Tbx21 KO on the expression of Th1 and Th17 cell specific cytokine receptors CXCR3 and CCR6 was assessed.

CXCR3 is upregulated on Th1 cells and is crucial for their migration towards inflammation sites and subsequent tissue injury. This was also shown in previous work in our department with a CXCR3<sup>-/-</sup> in the model of NTN (Panzer *et al.*, 2007). It has previously been shown, that Tbet<sup>-/-</sup> Th1 cells express less CXCR3 (Lord *et al.*, 2005). CXCR3 expression in IL17A<sup>CRE</sup> x Tbx21<sup>flox</sup> mice was drastically downregulated while CCR6 expression was not significantly affected by the Tbx21 KO in cGN (see Figure 25).

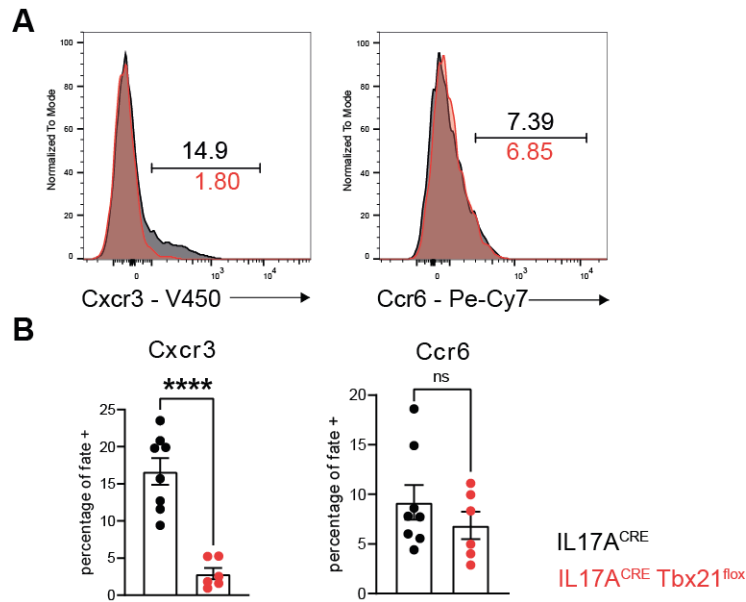


**Figure 25: Chemokine receptor expression in IL17ACRE Tbx21flox cGN mice**

(A) Gated on YFP<sup>+</sup> cells CXCR3 and CCR6 expression in IL-17A fate<sup>+</sup> cells of IL17ACRE and IL17ACRE Tbx21flox mice was assessed via Histogram. (B) Bar graphs show the resulting percentages of CCR6<sup>+</sup> and CXCR3<sup>+</sup> expression of total YFP<sup>+</sup> cells from FACS analysis with SEM. Significance was determined with the help of t-tests.

### 3.1.4 scRNAseq in crescentic glomerulonephritis

Due to the relatively low numbers of Th1-like Th17 and exTh17 cells in the FACS data, it was decided to sort lymphocytes from healthy animals and animals suffering cGN with a special focus on IL-17A fate positive (YFP<sup>+</sup>) cells and perform scRNAseq to precisely investigate Th17-Th1 transdifferentiation in cGN. CGN was induced in IL17A<sup>CRE</sup> animals and mice were sacrificed at day 10, as previously shown in *Figure 9*. The control group of IL17A<sup>CRE</sup> animals did not receive the NTN serum. Successful disease induction was verified by clinical parameters and histological analysis as in previous experiments. Control animals showed no development of cGN.

After the kidney extraction, renal lymphocytes were purified and stained for FACS sorting as described in 2.2.9 and 2.2.21. FACS analysis was then performed with FACS AriaIIIu. The sorting strategy used in cGN scRNAseq experiments aimed at 3 different populations as depicted in *Figure 26*. Sorted cell numbers are listed in *Table 12*.

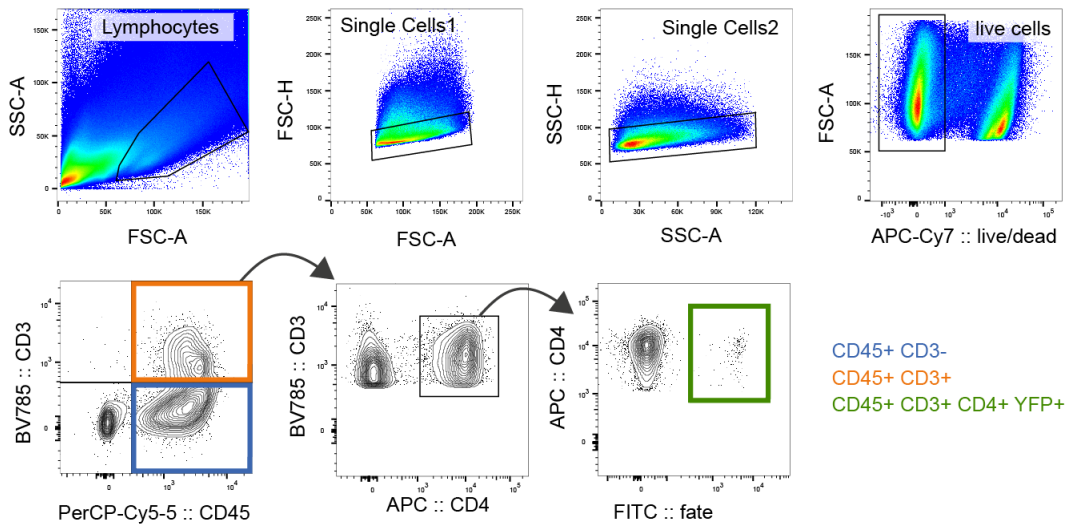


**Figure 26: Sorting strategy cGN scRNAseq**

Cells were first gated for Lymphocytes and then double doublet discrimination was performed. Living cells were selected. CD45+CD3- (blue gate) cells each were sorted from cGN and healthy condition. Further CD45+CD3+ (orange gate) cells each were sorted from cGN and healthy condition. Finally, CD45+CD3+CD4+YFP+ (green gate) were sorted from cGN animals.

**Table 12: Number of sorted cells for scRNAseq**

Sorting strategy	Condition	Cellnumber
CD45 <sup>+</sup> CD3 <sup>-</sup>	Control	40.400
CD45 <sup>+</sup> CD3 <sup>-</sup>	cGN	40.000
CD45 <sup>+</sup> CD3 <sup>+</sup>	Control	40.000
CD45 <sup>+</sup> CD3 <sup>+</sup>	cGN	40.000
CD45 <sup>+</sup> CD3 <sup>+</sup> CD4 <sup>+</sup> YFP <sup>+</sup>	cGN	5.937

After preparing the cells according to the 10x Genomics Single Cell Gene Expression pipeline (see 2.2.23), the cells were sent to Novogene UK for sequencing. The sequenced data of sorted CD45<sup>+</sup>CD3<sup>-</sup> and CD45<sup>+</sup>CD3<sup>+</sup> cells from healthy and NTN condition as well as CD45<sup>+</sup>CD3<sup>+</sup>CD4<sup>+</sup>YFP<sup>+</sup> cells (IL-17A fate<sup>+</sup> cells) from NTN animals was preprocessed as described in 2.2.24. *Figure 27* shows the QC metrics of the 5 datasets following preprocessing.

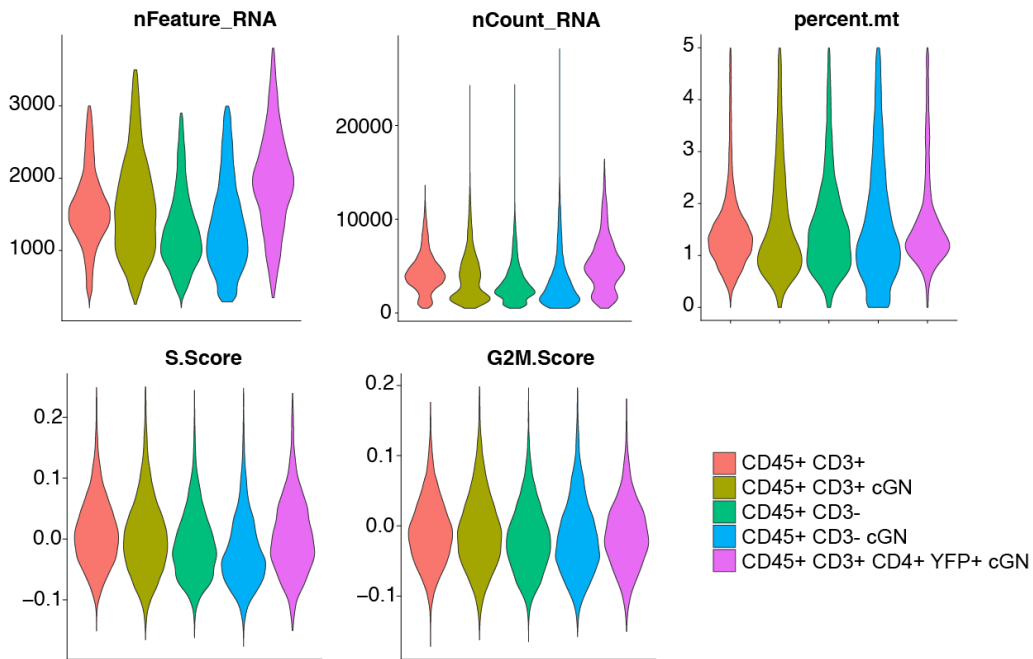


**Figure 27: QC metrics and cell cycle scoring (scRNAseq)**

Violin plots showing the number of unique genes per cell (nFeature\_RNA), number of UMI counts (molecules) per cell (nCount\_RNA), percentage of mitochondrial genes (percent.mt) and feature scores for S and G2M phase related genes of the 5 separately sorted datasets.

After preprocessing, the datasets were merged. Then batch correction was performed using the harmony package (see 2.2.24). As expected, 3 delimitable populations clustered in the UMAP which were identified as myeloid cells (blue colors), B cells (brown colors) and T cells (green colors) (see *Figure 28 (A)*). This was done via the comparison of expression levels of several marker genes (see *Figure 31 (A)*).

A subset containing only T cells was created and reclustering was performed. T cells now clustered as shown in *Figure 28 (C)*. Subclusters of T cells were determined by assessing CCR7 as marker of naïve T cells and CD4 and CD8 to distinguish between effector CD4<sup>+</sup> and CD8<sup>+</sup> T cells. IL17A expression was especially present in the effectorCD4cluster\_1 and in the gamma-delta T cell (gd-T) cluster. The gd-T cluster was identified through high expression of TRDV4 (see *Figure 28 (D) and (E)*). Naïve T cells with high CCR7 expression were especially prevalent in healthy condition mice. In the cGN group effector CD4<sup>+</sup> T cells were more frequent (see *Figure 31 (B) and (C)*).

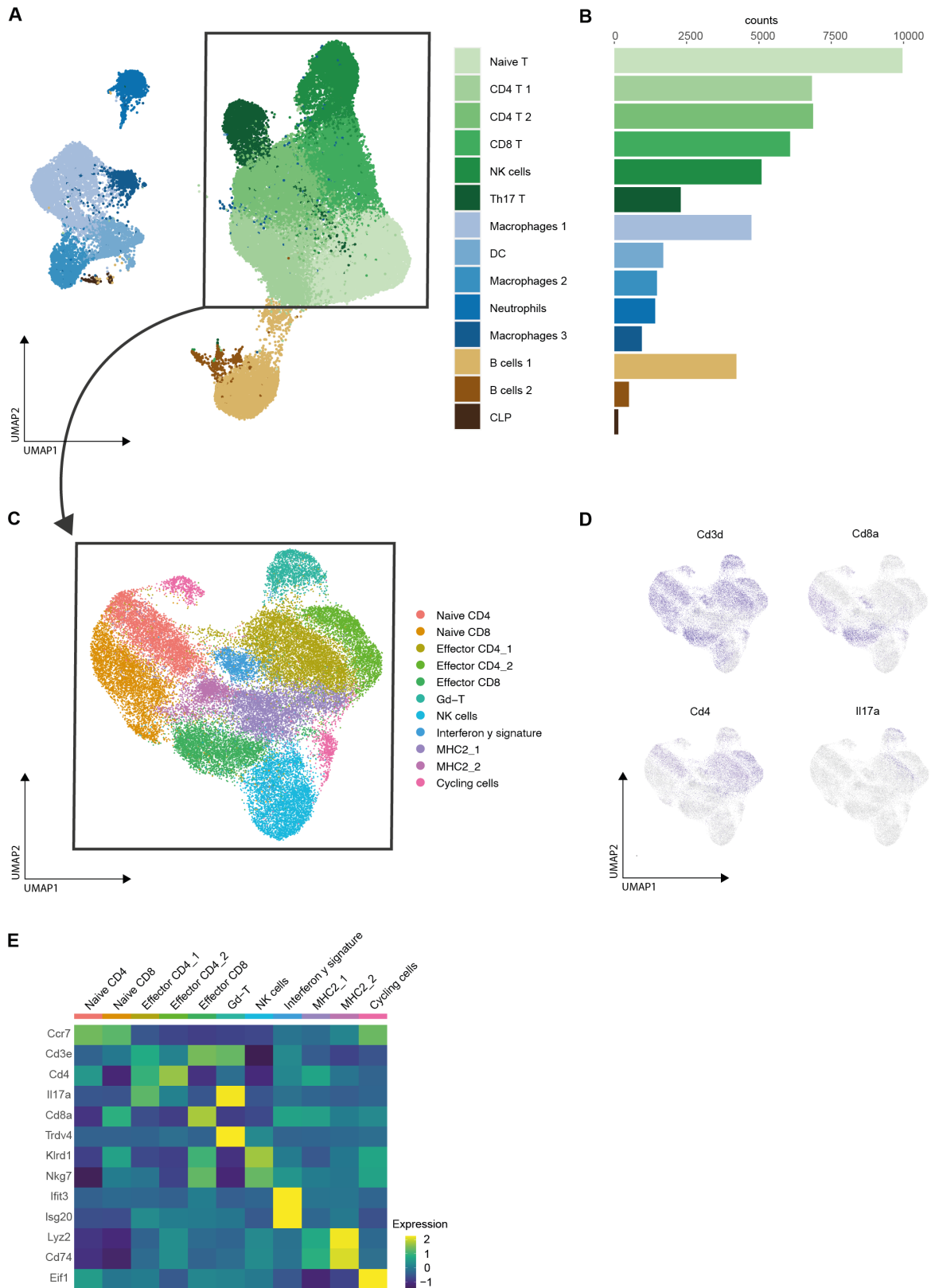


**Figure 28: Identification of T cell clusters (scRNAseq)**

(A) UMAP dimensionality reduction embedding of merged data from control and cGN condition (n=52.225) colored according to cell type determined by module scores and gene expression (B) Bar graph with cell numbers per cluster with equal color code as in (A) (C) UMAP dimensionality reduction embedding of reclustered T cell subset marked with a frame in (A) (D) Feature plot showing gene expression of T cell markers CD3, CD8A, CD4 and IL17A projected on UMAP dimensionality reduction embedding of T cell subset (E) Heatmap showing the average gene expression of cell type defying marker genes for the clusters in (C).

As the aim of the analysis was to investigate the expression of TBX21 and IFNG in Th17 cells and to look at Th17 plasticity within the CD4<sup>+</sup> populations, only the CD4<sup>+</sup> effector clusters and the gd-T cluster were chosen for detailed study (see *Figure 29 (A)*). Gd-T cells were not yet excluded as a clearer delineation was expected after repeated clustering.

As apparent in *Figure 29 (B) and (C)*, gd-T cells following repeated clustering now depicted more distant from the CD4<sup>+</sup> effector cells. In the following, they were excluded from the analysis. The remaining 9.677 cells were once more reclustered and they then grouped as shown in *Figure 29 (D)*. By assessing the average expression of TFs, effector cytokines and chemokine receptors of the different CD4<sup>+</sup> subsets the clusters could be allocated (see *Figure 29 (E)*).

There were two Th1 clusters identified by high expression of IFNG and TBX21. Cluster Th1.1 showed high expression of CXCR3, while cluster Th1.2 showed lower CXCR3 expression. Tregs were identified via high expression of IL10 and FOXP3 and clustered well delineated. Th17 cells clustered in proximity to the Th1.1 cluster. Within the bona fide Th17 cluster RORA/C, IL17A/F, CCR6 and IL22 were expressed above average. These are typical markers used for the classification of Th17 cells.

Three Th2 subsets were identified. Cluster Th2.1 showed high expression of Gata3, but lower expression of Th2 effector cytokines. Th2.2 had higher average expression of IL4 and IL13. The cluster Th2.3 showed high expression of Th2 cytokines IL4 and IL13, but at the same time of Th17 and Th1 markers. This cluster may therefore represent CD4<sup>+</sup> effector cells not yet fully committed to a distinct lineage, or it may contain transdifferentiating cells of several T cell subsets (see *Figure 29 (D) and (E)*).

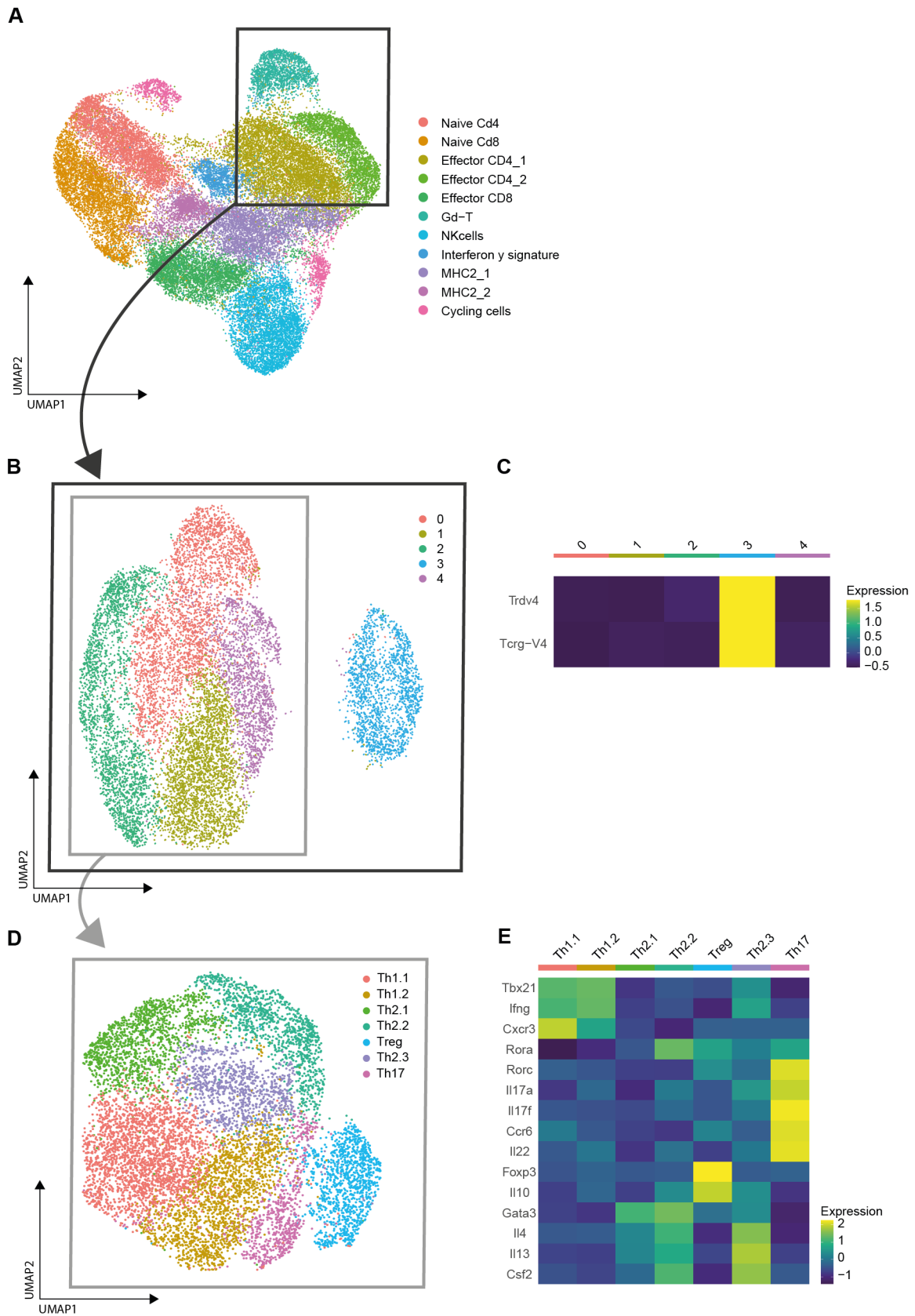


**Figure 29: Subclustering of CD4<sup>+</sup> T cells (scRNAseq)**

(A) UMAP dimensionality reduction embedding of reclustered T cell subset. Frame indicates the clusters used for further subclustering in (B) (B) UMAP dimensionality reduction embedding of reclustered T cell subset from (A). Frame indicates the clusters used for further subclustering in (D) (C) Heatmap showing the average expression of TRDV4 and TCRG-V4 markers in the clusters from (B) (D) UMAP dimensionality reduction embedding of reclustered CD4<sup>+</sup> T cells (E) Heatmap showing the average gene expression of CD4<sup>+</sup> subset markers for the clusters in (D).

After identification of the bona fide Th17 cells within our dataset, we used the information of our sorting strategy to track the IL-17A fate (YFP<sup>+</sup>) sorted cells within our dataset to see whether they clustered collectively or whether they spread out and therefore transdifferentiated towards other CD4<sup>+</sup> effector populations.

There was a total of 1.384 YFP<sup>+</sup> cells. Interestingly, the YFP<sup>+</sup> cells did not cluster just within the earlier defined Th17 cluster but spread out over all the CD4eff clusters (see *Figure 30 (A)*).

YFP<sup>+</sup> cells were especially prevalent in the pink cluster representing the bona fide Th17 cluster and within the two clusters that had earlier been defined as Th1 clusters (see *Figure 30(B)*).

Next, the average gene expression of YFP<sup>+</sup> cells within the earlier defined clusters was analyzed.

This revealed that YFP<sup>+</sup> cells in the red cluster showed TBX21, IFNG and CXCR3 expression without expression of Th17 markers except CCR6 (exTh17). Cells in the brown cluster had higher TBX21 and lower IFNG and CXCR3 expression and simultaneously expressed IL17A and RORC (Th1-like Th17). Average expression of Th17 markers within the pink bona fide Th17 cluster was in line with the preceding analysis with all CD4<sup>+</sup> effector T cells. Cells in the earlier undefinable purple cluster now essentially differed from bona fide Th17 cells by higher Csf2 expression (see *Figure 30 (C)*). These cells may therefore form a subset of especially active Th17 cells, as Csf2 was previously linked to Th17 driven inflammation in various models of AID (Sonderegger *et al.*, 2008; El-Behi *et al.*, 2011; Castro-Dopico *et al.*, 2020).

*Figure 30 (D) and (E)* further highlight, that YFP<sup>+</sup> cells expressing IFNG and TBX21 can be found in the model of cGN. Yet, in line with findings from the FACS analysis only few cells showed high expression of these two markers (see *Figure 23 and Figure 24*). Further, co-expression of IL17A and IFNG was visible in some cells.

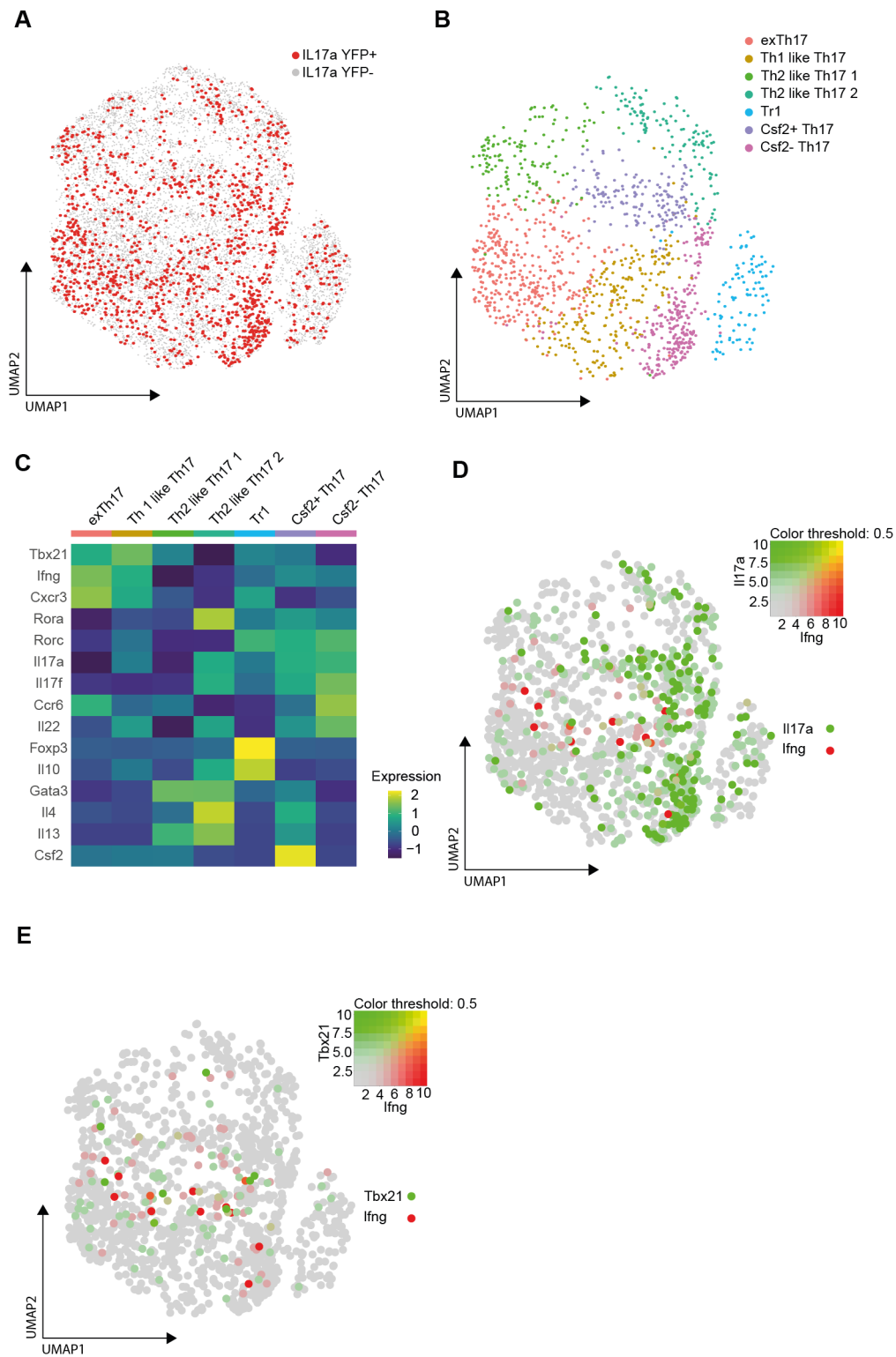


**Figure 30: Th17-Th1 axis in cGN (scRNAseq)**

(A) UMAP dimensionality reduction embedding of CD4<sup>+</sup> T cells resulting from earlier analysis (see Figure 29 (D)) with highlighted YFP<sup>+</sup> cells (B) UMAP dimensionality reduction embedding of YFP<sup>+</sup> cells (C) Heatmap showing the average expression of CD4<sup>+</sup> subset markers of YFP<sup>+</sup> cells in the clusters from (B) (D) Feature plot showing IL17A and IFNG co-expression projected on UMAP dimensionality reduction embedding of YFP<sup>+</sup> cells (E) Feature plot showing TBX21 and IFNG co-expression projected on UMAP dimensionality reduction embedding of YFP<sup>+</sup> cells.

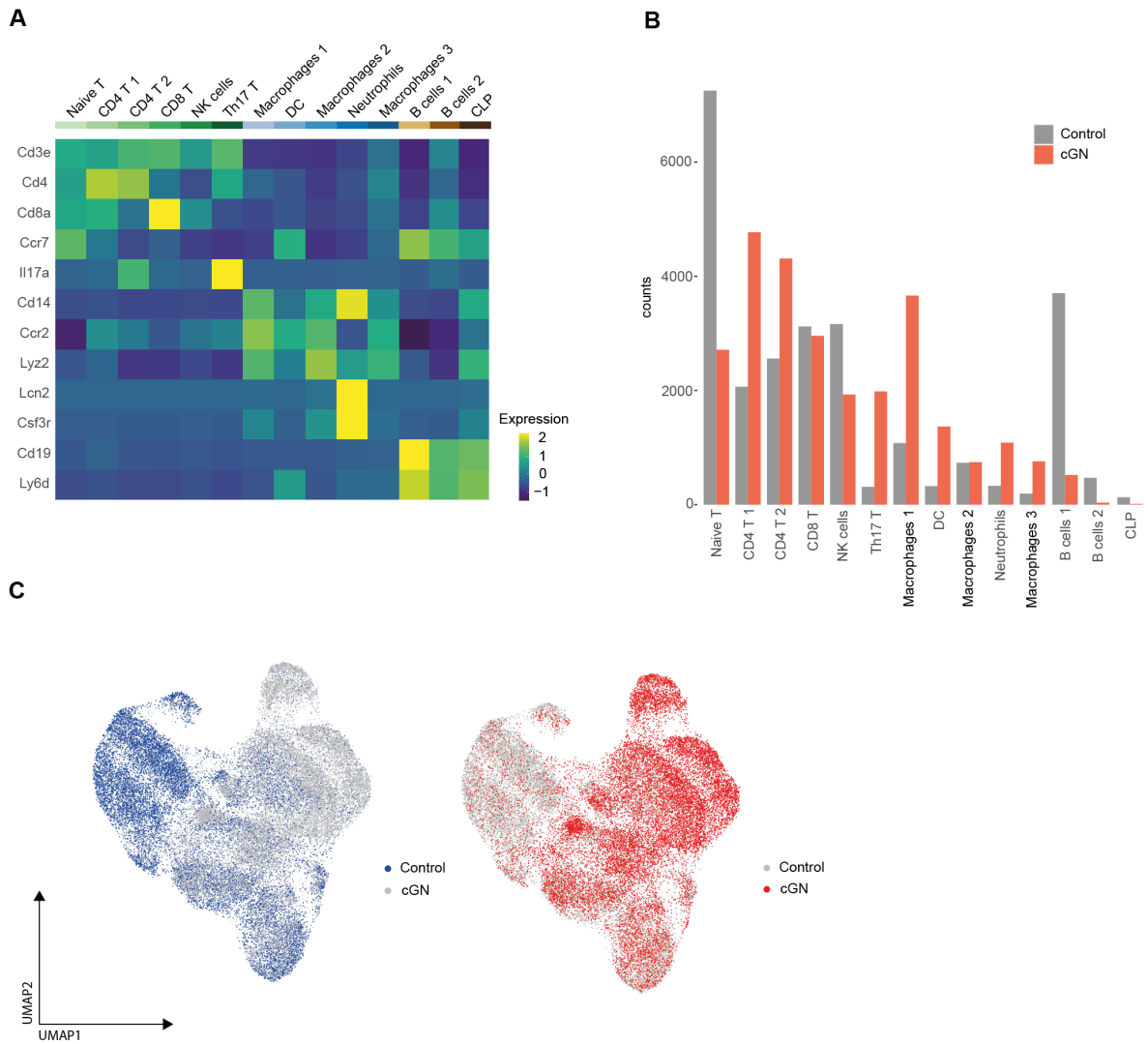


**Figure 31: Supplementary Figure 1 (scRNAseq)**

(A) Heatmap showing the average expression of subset defining markers in the clusters seen in *Figure 28 (A)*  
 (B) Bar graph with cell numbers per cluster split by condition of the clusters seen in *Figure 28 (A)*  
 (C) UMAP dimensionality reduction embedding of reclustered T cell subset (see *Figure 28 (C)*). Blue highlighted cells originate from control animals, red highlighted cells from cGN condition.

## 3.2 Results of Crohn's disease experiments

CD45RB<sup>hi</sup> Colitis was induced in Rag1<sup>-/-</sup> mice with donor cells from either IL17A<sup>CRE</sup> or IL17A<sup>CRE</sup> x Tbx21<sup>fllox</sup> animals. Experiments were conducted as described in 2.2.13. A control group was gavaged only the colitogenic flora but did not receive CD45RB<sup>hi</sup> cell transfer.

In the following, it will be referred to the group of Rag1<sup>-/-</sup> mice receiving CD45RB<sup>hi</sup> cells from IL17A<sup>CRE</sup> animals as IL17A<sup>CRE</sup> group and to the mice receiving IL17A<sup>CRE</sup> x Tbx21<sup>fllox</sup> cells as IL17A<sup>CRE</sup> x Tbx21<sup>fllox</sup> group.

### 3.2.1 Clinical parameters in Crohn's disease

Successful induction of disease in Rag1<sup>-/-</sup> animals was evaluated by weighing and endoscopic colitis scoring. After sacrificing the animals, colonic inflammation was assed via measurement of colon length and histological analysis of colon sections.

In the first experimental run, change in weight in the three groups was similar over week 1 of the experiment. 10 days into the experiment the two groups receiving the CD45RB<sup>hi</sup> cell transfer showed weight loss, while control animals did not. Between week 2 and 3 IL17A<sup>CRE</sup> x Tbx21<sup>fllox</sup> animals showed decreasing weight loss, which leveled out at around 5% below initial weight. In contrast, IL17A<sup>CRE</sup> animals continued to lose weight and lost on average more than 10% of their initial bodyweight. This discrepancy persisted until the end of the experiment as depicted in *Figure 32 (A)*. In the second run the weight development was analogous to the first run. Over the first week there was no notable change in weight in the three groups. After day 10 the animals receiving CD45RB<sup>hi</sup> cells started to lose weight. From day 10 to 30 weight loss in the IL17A<sup>CRE</sup> and IL17A<sup>CRE</sup> x Tbx21<sup>fllox</sup> showed the same tendency. After day 30 IL17A<sup>CRE</sup> x Tbx21<sup>fllox</sup> animals started to gain weight. IL17A<sup>CRE</sup> animals continued to lose weight. On average IL17A<sup>CRE</sup> x Tbx21<sup>fllox</sup> animals lost around 15% of their initial bodyweight (see *Figure 32 (B)*).

In both experimental runs significant differences in change in weight between IL17A<sup>CRE</sup> x Tbx21<sup>fllox</sup> and IL17A<sup>CRE</sup> colitis were observed. The significant individual values were seen in the first run at day 20 of the experiment and in the second run at the day 36.

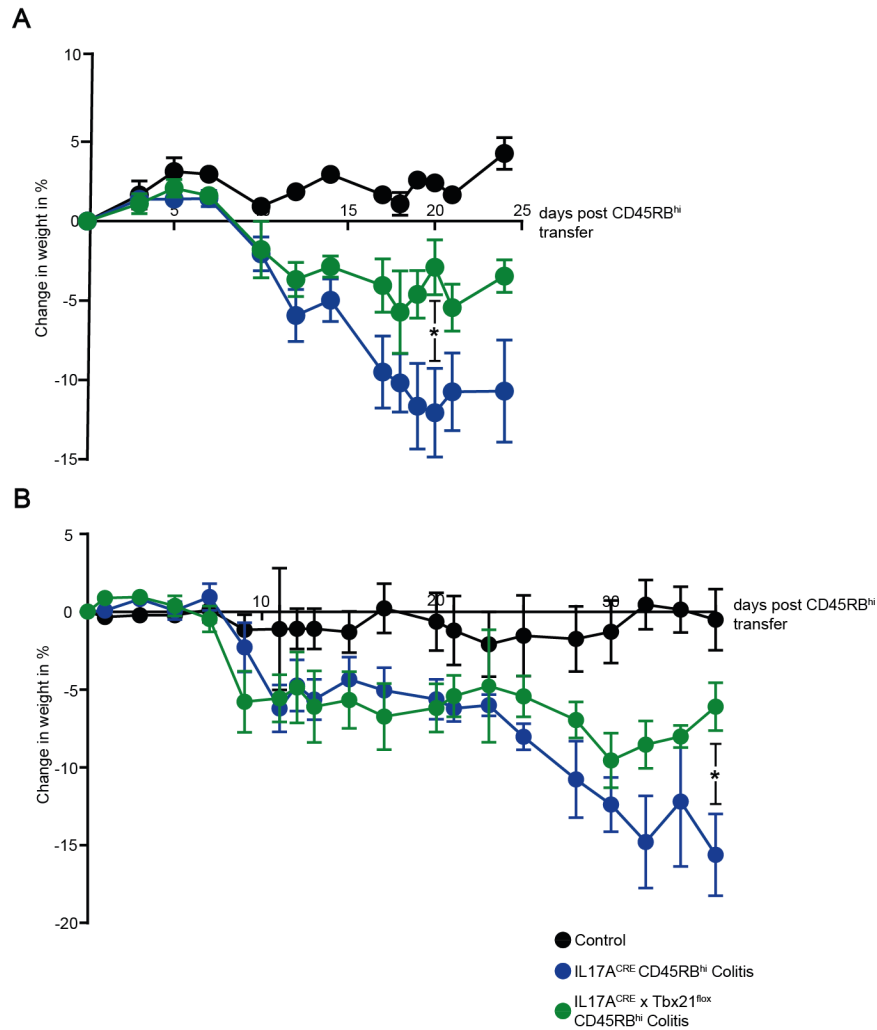


**Figure 32: Change in weight during CD45RB<sup>hi</sup>**

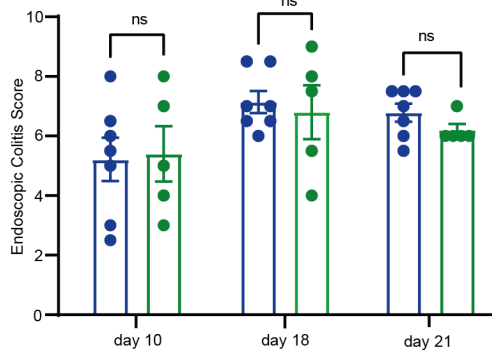
(A) Change in weight during the first run of CD45RB<sup>hi</sup> Colitis (B) Change in weight during the second run of CD45RB<sup>hi</sup> Colitis. The line graphs show the percentage weight loss in relation to the weight at day 0 (cell transfer) with SEM. Significance was determined by two-way ANOVA with Geisser-Greenhouse correction and a following Tukey-Kramer post-hoc test.

Weekly endoscopy during both experimental runs revealed that both groups receiving the cell transfer developed disease during the first or second week of the experiment. Macroscopic inflammation in both runs was the highest at day 18 of the experiment. No significant endoscopic difference between IL17A<sup>CRE</sup> and IL17A<sup>CRE</sup> x Tbx21<sup>flox</sup> animals was definable during the first and the second run of the experiment (see Figure 33 (B) and (C)).

A



B



C

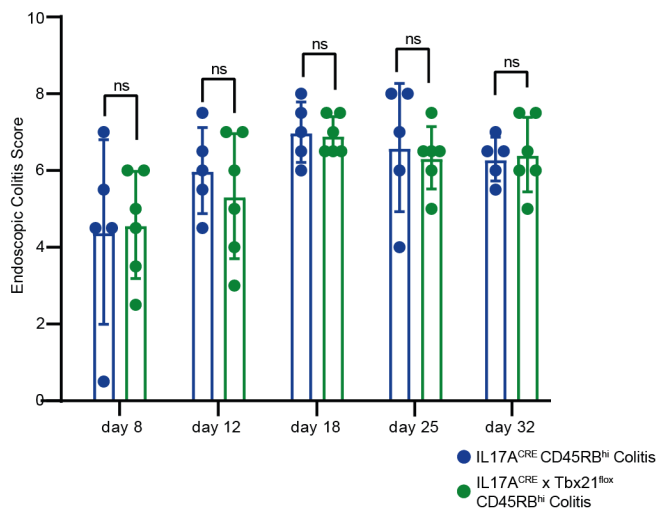


**Figure 33: Endoscopic scoring of CD45RB<sup>hi</sup> Colitis mice**

(A) Pictures of murine colons on day 21 of the experiment of animals receiving only the colitogenic flora (left), colitogenic flora and IL17A<sup>CRE</sup> CD45RB<sup>hi</sup> cells (middle) and colitogenic flora and IL17A<sup>CRE</sup> Tbx21<sup>fllox</sup> CD45RB<sup>hi</sup> cells (right) (B) Bar graphs of Endoscopic colitis score in run 1 of CD45RB<sup>hi</sup> Colitis with SEM at different timepoints of endoscopy. Significance was determined with the help of t-tests. (C) Bar graphs of Endoscopic colitis score in run 2 of CD45RB<sup>hi</sup> Colitis with SEM at different timepoints of endoscopy. Significance was determined with the help of t-tests.

Measurement of spleen size was conducted in order prove, that differences in colonic disease severity were not based on differences in systemic inflammation. IL17A<sup>CRE</sup> and IL17A<sup>CRE</sup> x Tbx21<sup>fllox</sup> mice overall had same sized spleens (see Figure 34 (A)). Comparable systemic inflammation therefore can be assumed in both groups. Further colon length as a local marker of inflammation was assessed (Ostanin *et al.*, 2009). There was no significant difference in colon length between IL17A<sup>CRE</sup> and IL17A<sup>CRE</sup> x Tbx21<sup>fllox</sup> transferred animals (see Figure 34 (B)).

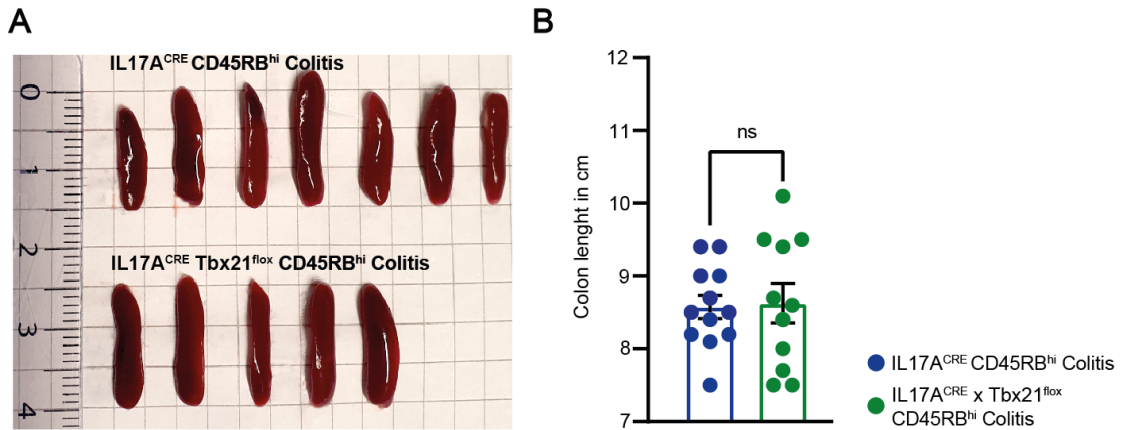


**Figure 34: Spleen size and colon length in CD45RB<sup>hi</sup> Colitis**  
 (A) Spleen size of IL17A<sup>CRE</sup> and IL17A<sup>CRE</sup> Tbx21<sup>flox</sup> CD45RB<sup>hi</sup> transferred animals at the day of sacrifice (B) Bar graph of colon length at day of sacrifice with SEM. Significance was determined with the help of t-tests. Results were obtained in two independent experiments.

### 3.2.2 Histology of colonic sections

HE-stained colon sections were scored as described in 2.2.24. While Control animals showed no signs of colonic inflammation, both CD45RB<sup>hi</sup> groups showed microscopically detectable colitis. IL17A<sup>CRE</sup> x Tbx21<sup>flox</sup> animals did not have a decreased colitis score (see Figure 35). While this was in line with the finding from the macroscopic analysis (see Figure 33 and Figure 34), it stood in contrast to previous findings in change in weight (see Figure 32). IL17A<sup>CRE</sup> x Tbx21<sup>flox</sup> mice were not protected from the onset of colitis.

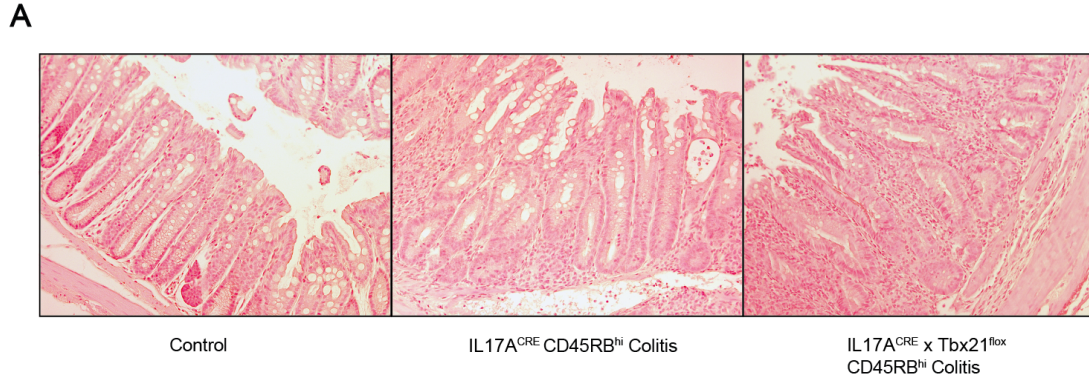


**Figure 35: Histological analysis of colon sections in CD45RB<sup>hi</sup> colitis**  
 (A) HE-stained sections of the colon from CD45RB<sup>hi</sup> mice. (B) Colitis score in CD45RB<sup>hi</sup> according to the HE-stained sections of the colon. Bar graphs show mean with SD. Significance was determined with the help of t-tests. Data was acquired from two separate experiments.

### 3.2.3 FACS analysis of intestinal lymphocytes

After evaluating the macroscopic and histological effects of the Tbx21 KO on disease severity, cellular effects were assessed.

Cells were stained for FACS analysis according to 2.2.21 and 2.2.22. The gating strategy was equivalent to the gating in NTN experiments and is shown in *Figure 36*.

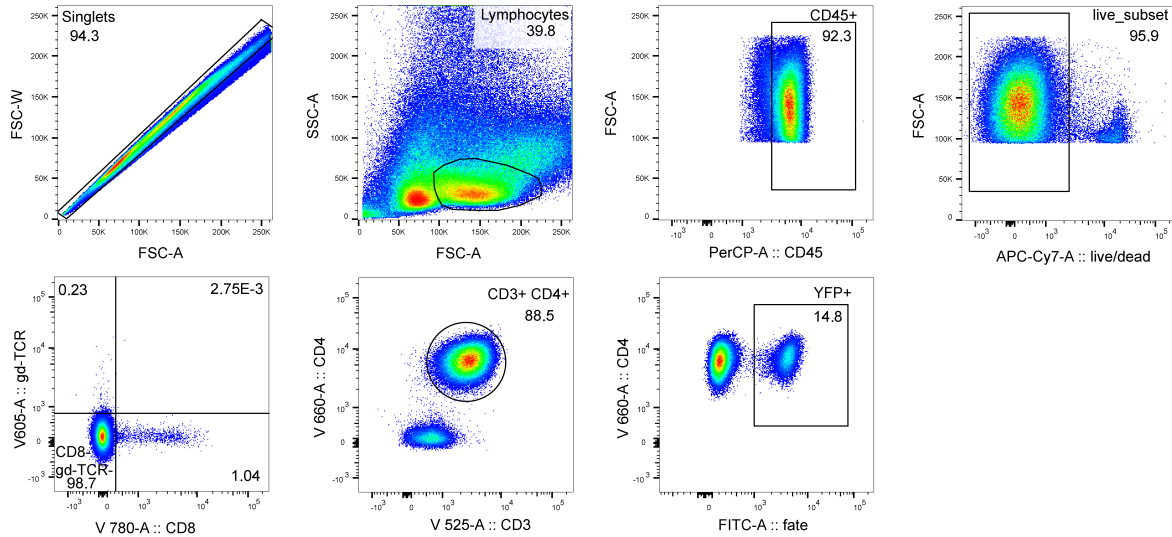


**Figure 36: FACS gating strategy in CD45RB<sup>hi</sup> colitis experiments**

At first singlets, Lymphocytes, CD45<sup>+</sup> and then living cells were selected. CD8<sup>+</sup> and gd-TCR<sup>+</sup> cells were excluded from the analysis and it was then gated on CD3<sup>+</sup>CD4<sup>+</sup> lymphocytes. YFP<sup>+</sup> cells (IL-17a fate<sup>+</sup> cells) were selected for further analysis.

At first possible differences in the amount of YFP<sup>+</sup> cells were assessed. As the T-bet KO in IL17A<sup>CRE</sup> x Tbx21<sup>fllox</sup> CD45RB<sup>hi</sup> receiving animals is only present in cells that are YFP<sup>+</sup>, differences in percentages of YFP<sup>+</sup> cells were not expected. In line with this assumption, no difference in the percentage of YFP<sup>+</sup> cells was observed (see *Figure 37*).

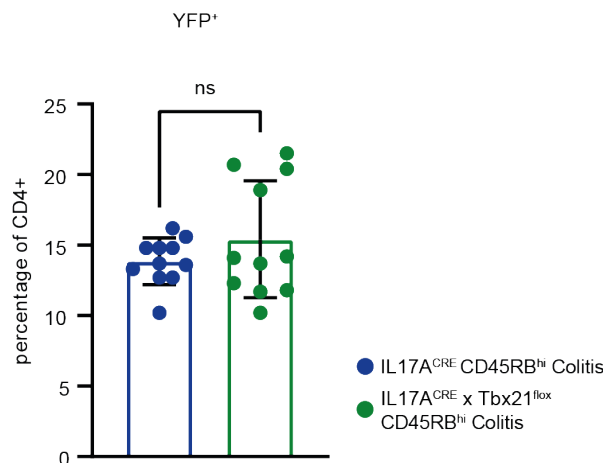


**Figure 37: Percentage of YFP<sup>+</sup> cells in CD45RB<sup>hi</sup> Colitis experiments**

Bar graph of YFP<sup>+</sup> shows mean with SD. Significance was determined with the help of t-tests. Data was acquired from two separate experiments.

As previously in cGN FACS analysis, the T-bet KO in CD45RB<sup>hi</sup> experiments was confirmed to only affect YFP<sup>+</sup> Th17 cells. In comparison to data from cGN experiments, where there was very limited T-bet expression in YFP<sup>+</sup> cells of IL17A<sup>CRE</sup> animals, the baseline T-bet expression in Rag<sup>-</sup> animals receiving CD45RB<sup>hi</sup> cells from IL17A<sup>CRE</sup> animals was considerably higher. In fact, more than half of YFP<sup>+</sup> cells expressed T-bet. T-bet expression was not present in YFP<sup>+</sup> cells from IL17A<sup>CRE</sup> x Tbx21<sup>fllox</sup> animals. YFP<sup>-</sup> cells showed no significant decrease in T-bet production. Hence, it was assured that T-bet was only knocked out in YFP<sup>+</sup> cells.

Further, the master TF of the TH17 lineage ROR $\gamma$ t was assessed. ROR $\gamma$ t expression in YFP<sup>+</sup> positive cells nearly doubled in IL17A<sup>CRE</sup> x Tbx21<sup>fllox</sup> animals (see *Figure 38*).

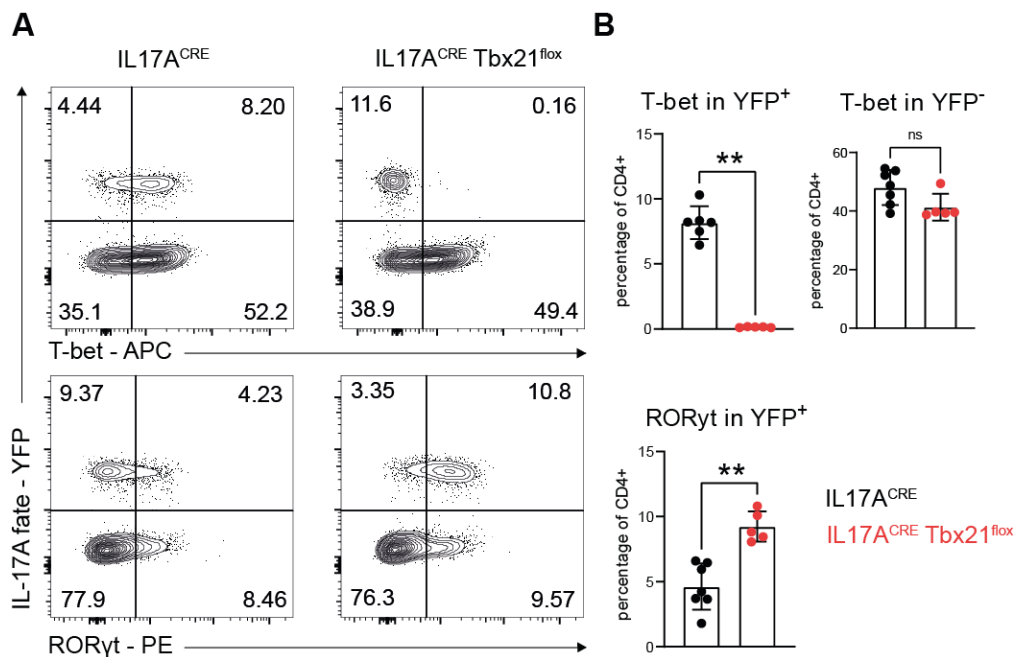


**Figure 38: T-bet and ROR $\gamma$ t expression in YFP<sup>+</sup> and YFP<sup>-</sup> cells**

(A) FACS analysis of T-bet and ROR $\gamma$ t expression in YFP<sup>+</sup> and YFP<sup>-</sup> cells, gated on CD4<sup>+</sup> (B) Bar graphs with SEM showing percentages of T-bet expression in YFP<sup>+</sup> and YFP<sup>-</sup> cells and ROR $\gamma$ t expression in YFP<sup>+</sup> cells of total CD4<sup>+</sup> cells resulting from FACS analysis. Significance was determined with the help of t-tests. Comparable results were obtained in two independent experiments.

After analysis of Th1 and Th17 TFs, the cytokines IFN- $\gamma$ , IL-17A and IL-17F were evaluated. Overall, IFN- $\gamma$  expression in YFP<sup>+</sup> cells of IL17A<sup>CRE</sup> x Tbx21<sup>fllox</sup> mice was halved. IL-17A and IL-17F expression was significantly increased following the T-bet KO. While in the IL17A<sup>CRE</sup> group IFN- $\gamma$  was the dominating cytokine expressed by YFP<sup>+</sup> cells, IL17A<sup>CRE</sup> x Tbx21<sup>fllox</sup> mice expressed IL-17A more frequently. Further, IL-17F expression was very low in IL17A<sup>CRE</sup> animals but was significantly upregulated in T-bet KO mice (see *Figure 39*).

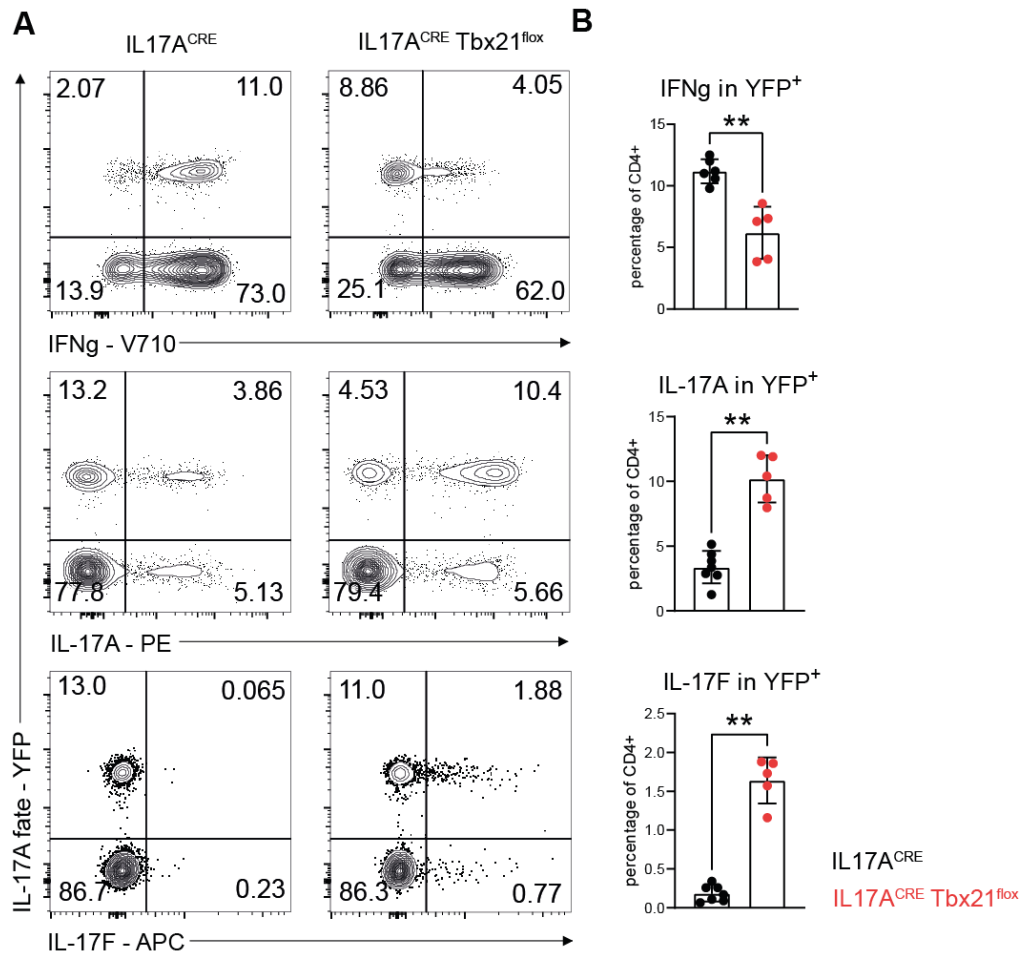


**Figure 39: IFN- $\gamma$  and IL-17A/F expression in YFP<sup>+</sup> cells**

(A) FACS analysis of IFN- $\gamma$ , IL-17A and IL-17F expression in YFP<sup>+</sup> cells, gated on CD4<sup>+</sup> (B) Bar graphs with SEM showing percentages of IFN- $\gamma$ , IL-17A and IL-17F expression in YFP<sup>+</sup> cells of total CD4<sup>+</sup> cells resulting from FACS analysis. Significance was determined with the help of t-tests. Comparable results were obtained in two independent experiments.

Knowing the general changes in IL-17A/F and IFN- $\gamma$  expression, a more detailed analysis of YFP<sup>+</sup> cells allowed to further assess the transdifferentiation of Th17 cells towards the Th1 lineage.

As expected, the plasticity of Th17 cells towards Th1 cells was much higher in colitis than in the model of cGN. In line with other working groups we saw high percentages of IL-17A<sup>+</sup> IFN- $\gamma$ <sup>+</sup> Th1-like and especially IL-17A<sup>-</sup> IFN- $\gamma$ <sup>+</sup> exTh17 cells in the IL-17A<sup>CRE</sup> group (Lee *et al.*, 2009; Harbour *et al.*, 2015). Regarding the IL-17A<sup>CRE</sup> x Tbx21<sup>fllox</sup> group, there was a pronounced shift from exTh17 cells towards IL-17A<sup>+</sup> IFN- $\gamma$ <sup>-</sup> Th17 cells. The amount of IL-17A<sup>+</sup> IFN- $\gamma$ <sup>+</sup> Th1-like cells did not decrease in the KO situation and in fact there was a significant increase within this population (see Figure 40).

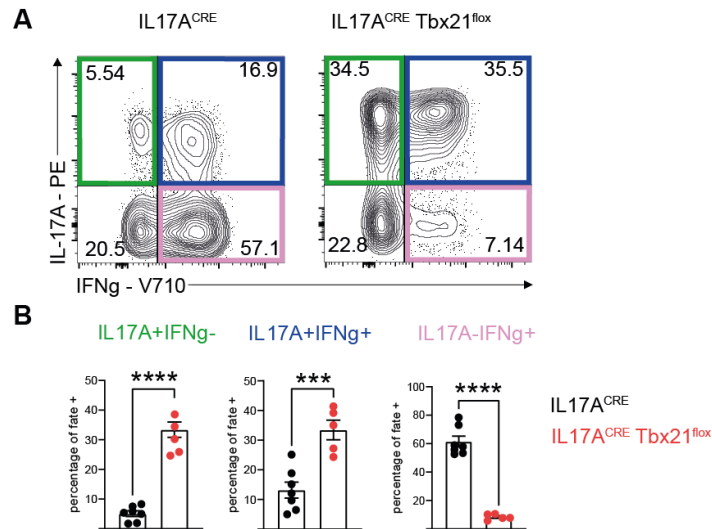


**Figure 40: Th17, Th1-like and exTh17 cells in CD45RB<sup>hi</sup> Colitis**

(A) FACS analysis of IL-17A<sup>+</sup> IFN- $\gamma$ <sup>-</sup> (Th17; green box), IL-17A<sup>+</sup> IFN- $\gamma$ <sup>+</sup> (Th1-like; blue box) and IL-17A<sup>-</sup> IFN- $\gamma$ <sup>+</sup> (exTh17; pink box) cells, pregated on YFP<sup>+</sup> cells. (B) Bar graphs with SEM show percentages of bona fide Th17, Th1-like and exTh17 cells of total YFP<sup>+</sup> cells. Significance was determined with the help of t-tests. Comparable results were obtained in two independent experiments.

Apart from the signature cytokines of the Th17 and Th1 lineage, the expression of the chemokine receptors CCR6 and CXCR3 was affected by the KO.

In line with results from the cGN experiments, we saw decreased expression of CXCR3 in the IL17A<sup>CRE</sup> x Tbx21<sup>flox</sup> group. There was also a pronounced increase in CCR6, which was previously not observed in cGN experiments (see Figure 41).

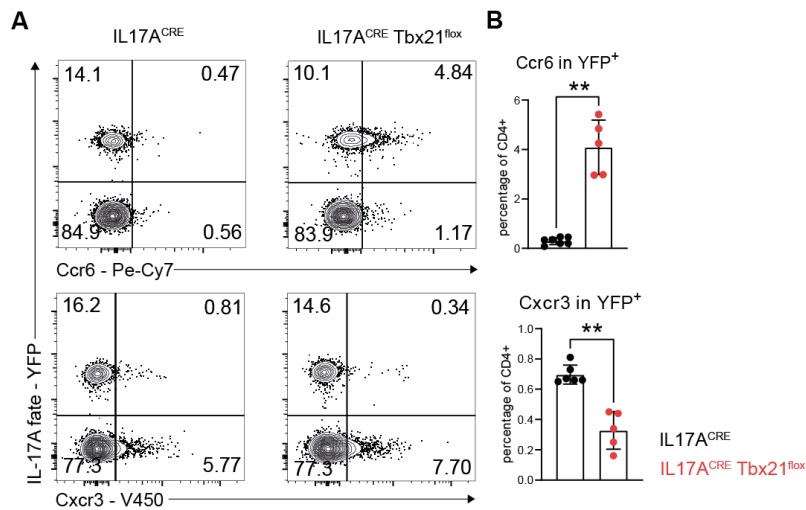


**Figure 41: Chemokine receptors in CD45RB<sup>hi</sup> Colitis**

(A) FACS analysis of CCR6 and CXCR3 expression in YFP<sup>+</sup> cells, gated on CD4<sup>+</sup> cells (B) Bar graphs with SEM showing percentages of CCR6 and CXCR3 expression in YFP<sup>+</sup> cells of total CD4<sup>+</sup> cells resulting from FACS analysis. Significance was determined with the help of t-tests. Comparable results were obtained in two independent experiments.

The cytokines GM-CSF and IL-22 as potential drivers of colonic inflammation were assessed (Pan et al., 2013; Sonderegger et al., 2008). Apart from dictating the development of granulocytes and macrophages as an hematopoietic growth factor, GM-CSF induces proinflammatory monocytes and dendritic cells (Castro-Dopico *et al.*, 2020). IL-22 on the other hand is considered to play a protective role in the context of IBD, at least in certain cytokine milieus. IL-22 increases the production of anti-bacterial peptides, enhances mucus production at the intestinal surface and further via Claudin-2 increases the clearance of intestinal pathogens (Mizoguchi *et al.*, 2018). There was no difference in GM-CSF levels in the conducted experiments. In contrast, IL-22 expression doubled in IL17A<sup>CRE</sup> x Tbx21<sup>fllox</sup> mice (see Figure 42).

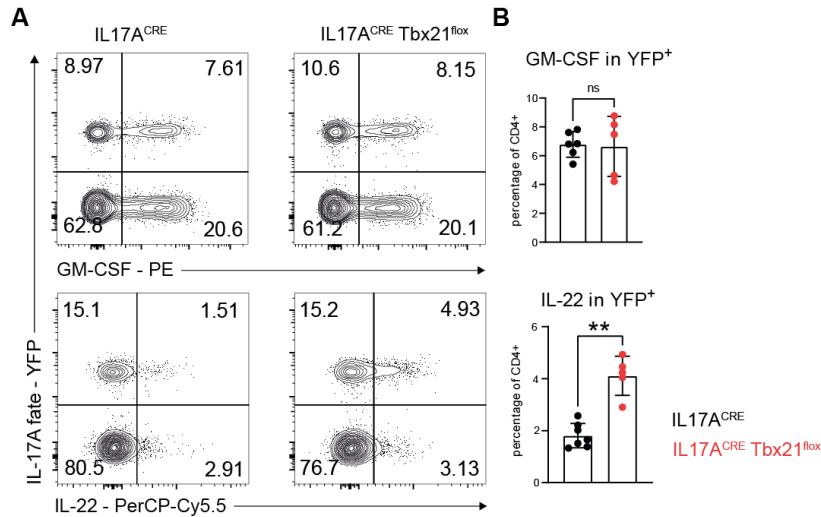


**Figure 42: Effector cytokines in CD45RBhi Colitis**

(A) FACS analysis of GM-CSF and IL-22 expression in YFP<sup>+</sup> cells, gated on CD4<sup>+</sup> cells (B) Bar graphs with SEM showing percentages of GM-CSF and IL-22 expression in YFP<sup>+</sup> cells of total CD4<sup>+</sup> cells resulting from FACS analysis. Significance was determined with the help of t-tests. Comparable results were obtained in two independent experiments.

## 4. Discussion

Over the last decades great advances in immunobiology have been made. Among those were the discoveries of several new CD4<sup>+</sup> T cell subsets. These proved, that the assumption of a dichotomy of only Th1 and Th2 cells was lacking and that the composition of effector T cells is more complex (Huber *et al.*, 2012). Further, several CD4<sup>+</sup> subsets are now believed to not be permanently delimitable from one another but in fact express different amounts of plasticity. This enables them to change their phenotype depending on the current cytokine milieu and thereby execute different effector functions. Especially the introduction of fate-mapping mouse lines, where certain subsets are permanently marked with a fluorochrome, significantly accelerated research in the field of CD4<sup>+</sup> transdifferentiation (Hirota *et al.*, 2011).

Among those plastic subsets are the Th17 cells which can acquire a Th1, Treg or Tfh phenotype in the context of various models of AIDs (Lee *et al.*, 2009; Hirota *et al.*, 2013; Gagliani *et al.*, 2015). Transdifferentiation of Th17 cells towards Th1 cells, including the subpopulations of Th1-like end exTh17 cells, has been linked to pathogenicity in several AIDs (Harbour *et al.*, 2015; Hirota *et al.*, 2011). Two mouse models which led to multiple findings about Th17 plasticity are CD45RB<sup>hi</sup> colitis resembling CD and experimental autoimmune encephalomyelitis (EAE), a model of multiple sclerosis (Lee *et al.*, 2009; Harbour *et al.*, 2015; Brucklacher-Waldert *et al.*, 2016). Th17 cells in these two models possess a high degree of plasticity towards the Th1 population. Earlier experiments in our working group with the NTN model resembling cGN showed, that transdifferentiation of Th17 cells towards Th1 cells plays a minor role in cGN (Krebs and Panzer, 2018).

Both CD and RPGN patients need precise therapeutical targets and therapies still rely on general downregulation of the immune system. Even though beneficial for the patient due to reduced inflammation many side effects can occur. The search for specific therapeutical targets that spare the side effects of immunosuppression is therefore of particular importance. Due to the abundance of Th17 cells at autoimmune inflammation sites and their involvement in tissue damage they represent an attractive target for such a specific therapy. Several cytokines produced by Th17 cells have been linked to pathogenicity in past studies, among those are IL17A/F, GM-CSF and IL-22 (El-Behi *et al.*, 2011; Krebs *et al.*, 2017; Mizoguchi *et al.*, 2018; Paust and Song *et al.*, 2023). Pushing pathogenic Th17 cells towards a more regulatory phenotype might better the clinical situation (Harbour *et al.*, 2015). To do so a better understanding of the pathogenicity of Th17 subsets is needed.

IFN- $\gamma$  produced by Th17 cells was reported to drive inflammation in different mouse models (Hirota *et al.*, 2011; Harbour *et al.*, 2015). Yet, it remains incompletely understood which factors induce IFN- $\gamma$  in Th17 cells and how they affect Th17 pathogenicity. On the one hand, IFN- $\gamma$  production by Th17 cells was shown to be necessary for induction of CD45RB<sup>hi</sup> colitis with the help of a IL17F<sup>Thy1.1</sup> x IFN $\gamma$ <sup>-/-</sup> mouse line (Harbour *et al.*, 2015). On the other hand, it has been reported that T-bet is dispensable in Th17-Th1 driven diseases like EAE and intestinal *Helicobacter hepaticus* inflammation (Duhon *et al.*, 2013; Brucklacher-Waldert *et al.*, 2016).

Our investigation therefore focused on the role of T-bet in driving tissue damage via IFN- $\gamma$  induction in Th17 cells, as well as its implication in Th17 transdifferentiation in two models with different

degrees of plasticity. The NTN model resembling cGN shows very low Th17-Th1 transdifferentiation and the CD model CD45RB<sup>hi</sup> colitis has a strong Th17-Th1 axis. The two models were chosen due to the long experience with the implementation of these models within the laboratory, the contrasting degrees of plasticity and due to earlier publications on Th17-Th1 plasticity applying these models (Harbour *et al.*, 2015; Krebs *et al.*, 2016). Initially, it was planned to further use the EAE model to obtain data from another model with high Th17-Th1 transdifferentiation (Hirota *et al.*, 2011; Krebs and Panzer, 2018). This was ultimately discarded due to time constraints.

The experiments were performed with the previously described IL17A<sup>CRE</sup> x Tbx21<sup>flox</sup> mouse line (see 2.2.3). Further Rag<sup>-/-</sup> mice were used in transfer experiments and IL17A<sup>CRE</sup> animals were used as control. Successful and equivalent disease induction could be shown in all experiments performed and differences in clinical and cellular outcome should consequently result from the Th17 specific Tbx21 KO (see 3.1.1, 3.1.2, 3.2.1 and 3.2.2).

We expected a downregulation of IFN- $\gamma$  as a consequence of the KO and resulting decreased pathogenicity in the colitis model driven by Th17-Th1 transdifferentiation (Harbour *et al.*, 2015). In cGN we did not expect clinical changes due to low Th17 plasticity towards Th1 cells (Krebs *et al.*, 2016).

Our expectations were only partially met, as we only saw decreased weight loss in the IL17A<sup>CRE</sup> x Tbx21<sup>flox</sup> group in the model of CD. In contrast to previous reports with general T-bet KO, we saw no macroscopic (see 3.2.1) or histological (see 3.2.2) amelioration of disease (Harbour *et al.*, 2015).

Apart from lower triglyceride levels in blood analysis of IL17A<sup>CRE</sup> x Tbx21<sup>flox</sup> animals, there were no clinical differences in the model of cGN. Still on the cellular level the T-bet KO in cGN lead to decreased Th1-like and the exTh17 cell populations (see *Figure 24*). However, considering the low initial T-bet expression in cGN it is comprehensible, that this did not result in ameliorated disease (see *Figure 23*).

The transfer of CD45RB<sup>hi</sup> cells does not only trigger inflammation in the colon, but also in the small intestine. Further, induction of tissue damage in stomach, liver and other organ systems might be possible (Ostanin *et al.*, 2006, 2009). Our experiments focused on the murine colon. Studies on the impact of the T-bet KO on small intestinal inflammation and inflammation in other organ systems will be necessary. Amelioration of small intestinal inflammation might contribute to the reduced weight loss in IL17A<sup>CRE</sup> x Tbx21<sup>flox</sup> animals.

The timepoint of the organ extraction heavily affects the downstream analysis. In cGN, kidneys were extracted on day 10 as the Th17 response is the highest between day 6-10 of cGN followed by a more Th1 heavy response with increased IFN- $\gamma$  levels (Krebs and Panzer, 2018). Th17 to Th1 transdifferentiation should therefore be highest around this timepoint. An analysis at a later timepoint of cGN, where IFN- $\gamma$  is more prevalent, may provide further information on the impact of T-bet.

The decision to perform scRNAseq within the model of NTN was based on the low numbers of Th1-like and exTh17 in FACS analysis. The chosen sorting strategy was based on several considerations (see *Figure 26*). First, it aimed at representing the differences between the healthy and the cGN condition. Second, not only Th17 cells but also other CD45<sup>+</sup>CD3<sup>+</sup> were included in the dataset to analyze the similarity of Th17 cells to other CD4<sup>+</sup> subsets. Third, CD45<sup>+</sup>CD3<sup>-</sup> cells were included. This brought the possibility of checking for possible interactions with Th17 cells. Fourth, via the YFP<sup>+</sup>

signal of IL17A<sup>CRE</sup> mice Th17 cells could be permanently separated from YFP<sup>-</sup> cells that never expressed IL17A within the dataset. Using the information of marked YFP<sup>+</sup> cells it was enriched for Th17 and exTh17 cells in the dataset. This provided a cellular basis to analyze the less frequent Th1-like and exTh17 populations in cGN. Finally, through combination of the YFP status and the gene expression the Th17 subclusters could be determined.

## 4.1 The role of T-bet in Th17 IFN- $\gamma$ production

In line with earlier data from IBD experiments with a general T-bet KO in CD4<sup>+</sup> cells (Harbour *et al.*, 2015; Krausgruber *et al.*, 2016) as well as with EAE experiments with a Th17 specific T-bet KO (Brucklacher-Waldert *et al.*, 2016), we saw reduced IFN- $\gamma$  expression in YFP<sup>+</sup> cells of the T-bet KO group in both cGN and CD (see *Figure 24, Figure 39 and Figure 40*). In cGN, the percentages of exTh17 and Th1-like cells in the T-bet KO group were both reduced (see *Figure 24*). In CD, overall reduced IFN- $\gamma$  expression in YFP<sup>+</sup> cells could be attributed to a pronounced decrease in the exTh17 population in the T-bet KO group (see *Figure 40*). The smaller exTh17 population in CD was accompanied by an expanded IL-17A<sup>+</sup> IFN- $\gamma$ <sup>-</sup> bona fide Th17 population. This was in line with previous reports from colitis experiments with a general T-bet KO in CD4<sup>+</sup> cells and a Th17 transfer model with magnetically sorted Th17 cells from T-bet deficient donor animals (Harbour *et al.*, 2015; Krausgruber *et al.*, 2016).

Apart from the bona fide Th17 population, the IL-17A<sup>+</sup> IFN- $\gamma$ <sup>-</sup> Th1-like population expanded in the T-bet KO group in colitis experiments (see *Figure 40*). It has previously been suggested that the colonic microenvironment might be crucial for the generation of Th1-like cells. Brucklacher-Waldert *et al.* showed that while the Th1-like population in EAE is dependent on T-bet, in *H. hepaticus* typhlocolitis T-bet is not required for induction of a Th1-like phenotype (Brucklacher-Waldert *et al.*, 2016). In our experiments Th1-like cells did not only occur T-bet independently, but they were around 3 times more prevalent than in the group with T-bet expression. An increase in Th1-like cells was previously reported in a transfer colitis model with polarized Th17 cells from T-bet KO donor animals (Harbour *et al.*, 2015). Since CD45RB<sup>hi</sup> colitis has a broader spectrum of transferred CD4<sup>+</sup> cells, we claim that it resembles CD more. Further, a general T-bet KO might have already affected Th17 precursors. With the use of the conditional T-bet KO we could assure, that polarization of Th17 cells was not altered.

T-bet dependent IFN- $\gamma$  production by Th1 cells might affect Th17 to Th1 transdifferentiation due to inhibition of IL-17A via IFN- $\gamma$  (Murphy *et al.*, 2003; Langrish *et al.*, 2005). Comparison of our data with data from general T-bet KO in all CD4<sup>+</sup> T cells indicates, that reduced IFN- $\gamma$  production in Th1 cells seems to not further affect Th17-Th1 transdifferentiation as changes with only a Th17 specific KO resulted in comparable percentage changes (Harbour *et al.*, 2015). This highlights the role of T-bet expression in Th17 cells in driving transdifferentiation.

Apart from its role in IFN- $\gamma$  expression, the strong reduction of exTh17 cells in IL17A<sup>CRE</sup> x Tbx21<sup>flox</sup> CD45RB<sup>hi</sup> colitis points at an important role for T-bet in ceasing IL-17A expression. T-bet might act as a checkpoint gene in Th1-like to exTh17 transition which could explain the expansion of Th1-like cells in IL17A<sup>CRE</sup> x Tbx21<sup>flox</sup> CD45RB<sup>hi</sup> colitis. As the majority of Th17 cells in CD is committed to

transdifferentiate towards exTh17 cells, the missing T-bet signal could force the cells to retain a Th1-like phenotype (see *Figure 40*). Previous data showed that inhibition of ROR $\gamma$ t via T-bet ultimately results in reduced IL-17A production (Lazarevic *et al.*, 2011). The possible role in ceasing IL-17A may also explain the increase of bona fide Th17 cells following the T-bet KO. ScRNAseq data from cGN experiments supports a possible checkpoint role for T-bet. Tbx21 expression was highest in the Th1-like Th17 cluster, while it was lower in exTh17 cells (see *Figure 30 (C)*). This may indicate that T-bet might need to be upregulated in Th1-like cells to cease IL-17A expression in transition towards exTh17 cells. However, the remaining exTh17 population in the T-bet KO group points at other TFs with the same ability of ceasing IL-17A production in Th1-like cells.

T-bet may work as an accelerator of Th17-Th1 trans-differentiation. This would explain the expansion of Th1-like cells and further the remaining formation of exTh17 despite the T-bet KO. Interaction of IFN- $\gamma$  with the IFN- $\gamma$  receptor induces STAT1 which is an activator of T-bet expression (Lighvani *et al.*, 2001). The resulting positive feedback loop leads to even more IFN- $\gamma$  expression (Lord *et al.*, 2005). It would be interesting to repeat FACS analysis of the cGN and CD models and analyze, whether at later timepoints plasticity towards Th1 cells is more prevalent in the T-bet KO group. If there happen to be more exTh17 cells in L17A<sup>CRE</sup> x Tbx21<sup>flox</sup> CD45RB<sup>hi</sup> colitis at later timepoints, this may support an accelerating role for T-bet. A limitation of this approach is the severity of disease of the animals, which due to animal welfare reasons makes an extension of test period difficult.

The expansion of IL-17A<sup>+</sup> IFN- $\gamma$ <sup>+</sup> Th1-like cells in IL17A<sup>CRE</sup> x Tbx21<sup>flox</sup> CD45RB<sup>hi</sup> colitis might also result from the lack of inhibition of Th17 master TF ROR $\gamma$ t by T-bet. Inhibition of the Runx1 mediated ROR $\gamma$ t expression by T-bet was previously reported (Lazarevic *et al.*, 2011). It has been shown that retrovirally induced co-expression of T-bet and ROR $\gamma$ t does not induce Th1-like Th17 cells (Wang *et al.*, 2014). In vitro data obtained by Mukasa *et al.* indicates that IL-12 signaling might be more relevant for the generation of exTh17 cells, while Th17 cells under the influence of TGF- $\beta$  do acquire a Th1-like phenotype (Mukasa *et al.*, 2010). Further, it has been shown that IL-12 signaling induces T-bet, while TGF- $\beta$  inhibits IFN- $\gamma$  induced T-bet expression (I.-K. Park *et al.*, 2005; Zhu *et al.*, 2012). This is in line with findings from the Th17 specific T-bet KO and further underlines T-bet's role in the formation of exTh17. TGF- $\beta$  signaling might play an important role in generation of Th1-like cells in IL17A<sup>CRE</sup> x Tbx21<sup>flox</sup> CD45RB<sup>hi</sup> colitis. More research should be done on this topic.

Summarizing the role of T-bet in Th17 IFN- $\gamma$  production we saw a positive correlation of T-bet and IFN- $\gamma$  expression in Th17 cells. Especially IFN- $\gamma$  production by exTh17 was dependent on T-bet. However, in line with earlier reports we could confirm that IFN- $\gamma$  expression in Th1-like Th17 cells is dependent on various TFs and not only on T-bet (Wang *et al.*, 2014; Krausgruber *et al.*, 2016).

## 4.2 Is T-bet necessary for pathogenicity?

There are various studies reporting amelioration of disease in the context of ceased IFN- $\gamma$  or T-bet expression (Wang *et al.*, 2014; Harbour *et al.*, 2015). Multiple studies contrast these results and describe equal to worse disease in IFN- $\gamma$  or T-bet KO situation (Duhon *et al.*, 2013; Brucklacher-Waldert *et al.*, 2016; Krausgruber *et al.*, 2016). Our findings mirror the study situation as T-bet and

IFN- $\gamma$  production seems to be of different importance depending on the disease or used mouse model. As expected in Th17 driven inflammation of cGN, T-bet was not required for induction of inflammation. IL-17A produced by Th17 cells was reported to be the primary driver of tissue damage in cGN during the first 10 days of disease (Krebs and Panzer, 2018).

In the model of CD, Th17 cells showed a high degree of plasticity towards Th1 cells. The KO of T-bet lead to decreased weight loss (see *Figure 32*). Nevertheless, animals were not protected from disease and there were no differences on the macroscopic and histological level (see *Figure 33-35*). On the cellular level we saw the earlier reported increase of bona fide Th17 cells at the expense of exTh17 cells in IL17A<sup>CRE</sup> x Tbx21<sup>fllox</sup> animals. In addition, the Th1-like population significantly expanded. Expression of IL-17A and IL-17F under the control of ROR $\gamma$ t has been linked to pathogenicity in CD45RB<sup>hi</sup> colitis (Leppkes *et al.*, 2009). Despite the elevated ROR $\gamma$ t expression and subsequent increased IL-17A/F expression in T-bet KO animals no aggravated disease was present. This underlines the assumption that pathogenicity in colitis is dependent on both IL-17A and IFN- $\gamma$ .

Apart from the changes in IFN- $\gamma$  and IL-17A expression, there was a significant increase in IL-22 production in IL17A<sup>CRE</sup> x Tbx21<sup>fllox</sup> animals in the CD model (see *Figure 42*). Increased IL-22 production by Th17 following ceased T-bet expression was previously reported (Harbour *et al.*, 2015). IL-22 can be considered a two-edged cytokine. Both protective and proinflammatory effects have been reported (Seiderer and Brand, 2009; Pan *et al.*, 2013). The cytokine environment and also expression of T-bet determines whether IL-22 promotes or reduces inflammation (Mizoguchi *et al.*, 2018). Hence, there are two possibilities. One would be that IL-22 directly contributes to amelioration of the disease and is expressed more frequently due to missing inhibition of ROR $\gamma$ t by T-bet (Lazarevic *et al.*, 2011). Another one would be that increased levels of IL-22 are in fact proinflammatory but are compensated by other anti-inflammatory effects of the KO.

As IL-22 mainly affects respiratory, epidermal and digestive epithelial cells, an interactome analysis of Th17 cells with colonic epithelial cells might reveal, whether IL-22 is in fact anti or proinflammatory in the context of the T-bet KO. (Wolk *et al.*, 2004).

Interestingly we saw partly ameliorated disease as indicated by reduced weight loss following increased production of both IL-22 and IL-17A. This cytokine combination has previously been linked to enhanced inflammation in IBD (Krausgruber *et al.*, 2016; McGeachy and Cua, 2008). However, the previously mentioned T-bet<sup>-/-</sup> Th17 transfer colitis model also reported ameliorated disease in combination with increased IL-22 and IL-17A (Harbour *et al.*, 2015). A possible explanation why this combination was not associated with increased pathogenicity in some experiments might be differences in the composition of the colonic flora.

GM-CSF has been linked to pathogenicity within the EAE model and has been widely studied in Th17 research (Sonderegger *et al.*, 2008; El-Behi *et al.*, 2011; Codarri *et al.*, 2011). We hypothesized that a retained bona fide Th17 phenotype in the T-bet KO group could result in increased GM-CSF expression. Yet, the T-bet KO did not affect GM-CSF expression in CD (see *Figure 42*). Castro-Dopico *et al.* showed that in intestinal inflammation GM-CSF is for the most part ILC3 derived and induces a proinflammatory phenotype in macrophages (Castro-Dopico *et al.*, 2020). GM-CSF produced by Th17 cells therefore seems to play a subordinate role in colonic inflammation which is not affected by T-bet.

Overall, our data indicates that T-bet expression in Th17 cells increases inflammation in CD, most likely via increased production of IFN- $\gamma$  by exTh17 cells. T-bet KO mice did lose significantly less weight, but they were not protected from disease onset. T-bet expression in Th17 cells was therefore not necessary for induction of colitis. T-bet independent formation of Th1-like cells could play an important role in the development of CD. Further research on the TFs that drive the formation of Th1-like Th17 cells in CD is needed.

### 4.3 T-bet's impact on Th17 migration

Chemokine receptors are crucial for CD4<sup>+</sup> T helper subsets to reach sites of inflammation and exert their effector functions. The chemokine receptor CXCR3 is very frequently expressed on Th1 cells, but can also be found on Th17 cells (Lim *et al.*, 2008). CCR6 expression is heavily involved in Th17 migration to sites where the chemokine CCL20 can be found (Wang *et al.*, 2009).

Conditioned by the T-bet KO, CXCR3 expression decreased and CCR6 expression increased in CD (see *Figure 41*). Interestingly, in cGN there was only decreased expression of CXCR3, while CCR6 was not affected by the KO (see *Figure 25*). It was reported earlier that T-bet directly controls CXCR3 expression and that CCR6 expression is upregulated by ROR $\gamma$ t (Wang *et al.*, 2009; Zhu *et al.*, 2012). However, upregulation of CCR6 via ROR $\gamma$ t was reported to be small and ROR $\gamma$ t failed to induce CCR6 in every Th17 cell (Wang *et al.*, 2009).

CCR6 expression can directly be inhibited via binding of T-bet to the CCR6 gene (Zhu *et al.*, 2012). The changes in chemokine expression may therefore largely be conditioned by missing T-bet and not by the accompanying increased expression of ROR $\gamma$ t. The low baseline T-bet expression in cGN may therefore explain the missing upregulation of CCR6 following the KO.

Migration of CCR6<sup>-/-</sup> Th17 cells to PPs and colonic patches is reduced. It has been proposed that CCR6 acts as a homing receptor for Th17 cells. CCR6<sup>-/-</sup> Th17 cells induced more severe intestinal inflammation and higher weight loss than CCR6<sup>+/+</sup> Th17 cells following injection into SCID mice (Wang *et al.*, 2009). The changes in chemokine receptor expression from CXCR3 in T-bet<sup>+/+</sup> to CCR6 in T-bet<sup>-/-</sup> Th17 cells might therefore induce increased homing of Th17 cells to colonic or PPs and thereby lead to reduced pathogenicity. Follow-up experiments investigating the amount of Th17 cells in PPs and colonic patches during CD45RB<sup>hi</sup> may further address this assumption.

Previous research in our institute proved a role for CXCR3 in T cell migration to inflamed kidneys. Less severe nephritis has been observed in CXCR3<sup>-/-</sup> mice during NTN experiments (Panzer *et al.*, 2007). Steinmetz *et al.* followed this up with MRL/lpr mice, a mouse model resembling systemic lupus erythematosus, which among other induces glomerulonephritis. Infiltration of Th1 and Th17 cells into the kidney was reduced in CXCR3<sup>-/-</sup> MRL/lpr mice. This resulted in ameliorated disease (Steinmetz *et al.*, 2009). Even though there was decreased CXCR3 expression in the conducted cGN following the T-bet KO, this was not sufficient to translate to reduced colonic inflammation. T-bet was linked to CXCR3 expression in Th1 cells previous to the discovery of Th17 cells (Szabo *et al.*, 2000; Lord *et al.*, 2005). Our data indicates that T-bet also regulates CXCR3 expression in transdifferentiating Th17 cells. In the scRNAseq analysis we saw high expression of CCR6 in the exTh17 cluster, even though

there were no other markers of bona fide Th17 cells co-expressed (see *Figure 30 (C)*). Additional studies on the implication of Th17-Th1 transdifferentiation on migratory capabilities are needed.

## 4.4 Outlook

In conclusion, IFN- $\gamma$  production by Th17 cells is only partially dependent on T-bet expression. Pathogenicity in CD45RB<sup>hi</sup> colitis was reduced as indicated by less severe weight loss in the KO group. In contrast, there were no differences in disease severity in the cGN experiments.

Due to multiple downstream effects of the T-bet KO in Th17 cells, it is difficult to attribute the reduced weight loss to one specific agent. Overall, a shift from a more Th1 weighed to a Th17 weighed inflammatory response was beneficial. This supports the previous statement that agents inhibiting transdifferentiation of Th17 cells towards Th1 cells or inhibition of IFN- $\gamma$  expressed by Th17 cells should be considered as a treatment in IBD (Harbour *et al.*, 2015). Changes in the migratory capabilities as well as increased IL-22 in T-bet deficient Th17 cells in CD might further contribute to less severe disease and need further research. However, the Th1-like Th17 population was sufficient to induce colonic inflammation. A better understanding of the transcriptional program of Th1-like Th17 cells in CD is needed. Depletion of this population could result in ameliorated disease.

Regarding cGN, it could be an interesting approach to push Th17 cells towards a Th1-like phenotype. This might result in decreased disease severity in cGN. A transfer model of sorted Th1-like and bona fide Th17 cells in mice suffering NTN might answer this question and would be an interesting project to follow up on.

The performed analysis solely focused on the Th17-Th1 axis as T-bet expression in Th17 cells was expected to be particularly important in this context. Yet, T-bet is also part of the transcriptional program of Treg subsets. The KO might also affect regulatory Th17 cells or plasticity on other axes (Levine *et al.*, 2017). Future experiments addressing the effect of a Th17 specific KO on regulatory capacities of Th17 cells are needed.

Analysis of the gene expression via scRNAseq of YFP<sup>+</sup> cells from T-bet KO condition and Th17 with intact T-bet expression might answer the remaining questions regarding the transcriptional program of subsets included in the Th17-Th1 axis. Comparison of exTh17 cells from IL17A<sup>CRE</sup> x Tbx21<sup>flox</sup> animals and IL17A<sup>CRE</sup> animals and especially analysis of cells, which are about to transition from Th1-like towards exTh17 cells might further illuminate the Th17-Th1 axis in IBD.

With the possibility to investigate the gene expression of each individual cell by single cell sequencing, many new possibilities arise. The bioinformatic progress in this field within the last years is astonishing and new possibilities for the analysis of scRNAseq data sets are constantly emerging. In this regard, performing scRNAseq with YFP<sup>+</sup> cells from IL17A<sup>CRE</sup> CD45RB<sup>hi</sup> colitis and IL17A<sup>CRE</sup> x Tbx21<sup>flox</sup> CD45RB<sup>hi</sup> colitis might answer remaining questions regarding Th17-Th1 plasticity. Sorting bona fide Th17, Th1-like and exTh17 and checking for their interactions with colonic or small intestinal epithelial cells might help us to even better understand their roles in pathogenicity.

As the results of this study point at a possible role for T-bet as an important checkpoint in Th1-like to exTh17 transdifferentiation analysis with R packages like “tradeSeq” or “velocity” might lead to a better understanding of this process (La Manno *et al.*, 2018; Van den Berge *et al.*, 2020). Considering

the temporal dynamic of T-bet expression might be crucial to fully understand its role in pathogenicity. This could also reveal other genes involved in the emergence of Th1-like and exTh17 cells. Stat4 and eomesodermin (Eomes) previously have been linked to IFN- $\gamma$  expression in Th17 cells and might be interesting candidates for further research. They could be involved in the generation of Th1-like cells in T-bet deficient animals (Lee *et al.*, 2009; Ichiyama *et al.*, 2011). In EAE, Runx1 and Runx3 was necessary for the induction of Th1-like Th17 cells during EAE (Wang *et al.*, 2014). This could translate to Th1-like Th17 cells in IBD and needs further research.

## 5. Summary

### 5.1 English summary

T cells play an important role in the defense against various pathogens. They are also involved in the development of autoimmune mediated diseases. Th1 and Th17 cells are particularly prevalent in this regard. Th17 cells have been linked to pathogenicity mainly via expression of the name giving cytokines IL-17A and IL-17F. Depending on the cytokine environment, Th17 cells can transdifferentiate towards other T helper subsets. These include Tregs, Tfh and Th1 cells. Plasticity towards Th1 cells involves the Th17 subpopulations Th1-like and exTh17 cells. These subsets have been linked to pathogenicity in experimental autoimmune encephalomyelitis and intestinal bowel disease. In crescentic glomerulonephritis, Th17 cells have been shown to be very stable. Despite an increasing focus, the drivers of pathogenicity of the Th17-Th1 subpopulations remain incompletely understood.

T-bet as the master TF of the Th1 lineage is crucial for the transdifferentiation of Th17 cells towards Th1 cells. Using a Th17 specific knockout of T-bet, we aimed to better understand the role of the Th17-Th1 axis in pathogenicity in crescentic glomerulonephritis and intestinal bowel disease. The experiments conducted show that the expression of T-bet in Th17 cells actively drives pathogenicity in CD45RB<sup>hi</sup> colitis, while it is dispensable for pathogenicity in crescentic glomerulonephritis. Reduced pathogenicity is most likely conditioned by the direct implication of T-bet in the expression of IFN- $\gamma$  in Th17 cells. In line with previous data, we saw a downsized exTh17 and enlarged Th1-like and bona fide Th17 populations following the Th17 specific T-bet knockout. T-bet might act as a checkpoint gene in transition of Th1-like to exTh17 cells via suppression of IL-17A expression in Th1-like cells. IFN- $\gamma$  expression in Th1-like cells was independent of T-bet and could play an important role in the development of Crohn's disease. Further research on the TFs that drive the formation of Th1-like Th17 cells in Crohn's disease is needed. A decreased exTh17 and enlarged Th1-like population in IL17A<sup>CRE</sup> x Tbx21<sup>flox</sup> CD45RB<sup>hi</sup> colitis animals did result in less severe weight loss. ExTh17 cells therefore appear to be more potent inducers of wasting disease than Th1-like cells. In addition, T-bet is involved in regulating the migratory capacity of cells of the Th17-Th1 axis via induction of CXCR3 and inhibition of CCR6.

### 5.2 German summary (Zusammenfassung)

T-Zellen spielen eine wichtige Rolle bei der Abwehr verschiedener Krankheitserreger. Sie sind auch in die Entstehung unterschiedlicher Autoimmunerkrankungen involviert. Vor allem Th1 und Th17 Zellen sind in diesem Kontext relevant. Die Pathogenität von Th17 Zellen wurde vor Allem durch Expression der namensgebenden Zytokine IL-17A and IL-17F erklärt. Abhängig vom Zytokin-Umfeld können Th17 Zellen neben der Expression klassischer Th17-Marker auch in Richtung anderer T-Helfer Populationen transdifferenzieren. Diese sind unter anderem regulatorische, folliculäre oder Typ1-T-Helferzelle. Plastizität hin zu Typ1-T-Helferzellen beinhaltet die Th17 Subpopulationen Th1-like und exTh17 Zellen. Diese Subpopulationen wurden in Modellen der experimentellen

autoimmunen Enzephalomyelitis und der chronisch-entzündlichen Darmerkrankung mit Pathogenität in Verbindung gebracht. Im Modell für rasch progrediente Glomerulonephritis zeigen sich Th17 Zellen jedoch sehr stabil. Trotz der wissenschaftlichen Fokussierung auf die Th17-Th1 Achse sind die Faktoren, die zur Pathogenität der darin enthaltenen Subpopulationen führen, noch nicht vollständig verstanden.

Als Master-Transkriptionsfaktor der Typ1-T-Helferzellen ist T-bet für die Transdifferenzierung der Th17 Zellen hin zu Th1 Zellen entscheidend. Mit Hilfe eines Th17-spezifischen Knockouts von T-bet untersuchten wir die Rolle der Th17-Th1-Achse in Bezug auf die Pathogenität im Rahmen der rasch progrediente Glomerulonephritis und der chronisch-entzündlichen Darmerkrankung. Die durchgeführten Experimente zeigen, dass die Expression von T-bet in Th17 Zellen im Rahmen der CD45RB<sup>hi</sup> Kolitis den Schweregrad der Erkrankung beeinflusst, während sie im Rahmen der rasch progrediente Glomerulonephritis keinen Einfluss auf die Pathogenität hat. Eine abgemilderte Erkrankung im Rahmen der Kolitis Experimente ist sehr wahrscheinlich durch die Rolle von T-bet in der Expression von IFN- $\gamma$  in Th17 Zellen zu erklären. Wie zuvor berichtet, zeigte sich als Folge des T-bet Knockouts eine dezimierte exTh17 Population, sowie vergrößerte Th1-like und bona fide Th17 Populationen. T-bet könnte durch Suppression von IL-17A in Th1-like Zellen als Checkpoint-Gen im Übergang von Th1-like zu exTh17 Zellen fungieren. Die Expression von IFN- $\gamma$  in Th1-like Zellen war unabhängig von T-bet und könnte eine wichtige Rolle in der Entstehung von Morbus Crohn spielen. Weitere Forschung zu den Transkriptionsfaktoren, die die Entstehung von Th1-like Th17 Zellen in Morbus Crohn bedingen, ist nötig. Eine verkleinerte Population von exTh17 in Verbindung mit einer vergrößerten Th1-like Population im Rahmen der IL17A<sup>CRE</sup> x Tbx21<sup>flox</sup> CD45RB<sup>hi</sup> Kolitis resultierte in einer geringeren Gewichtsabnahme der Tiere. ExTh17 Zellen scheinen daher eine höhere Pathogenität als Th1-like Zellen zu besitzen. T-bet beeinflusst außerdem durch Induktion von CXCR3 und Inhibition von CCR6 die Migrationseigenschaften von Zellen der Th17-Th1 Achse.

## 6. List of Abbreviations

AB	Antibodies
ACE	Angiotensin converting enzyme
ACR	Albumin/Creatinine-ratio
AKI	Acute kidney injury
ANA	Antinuclear antibodies
ANCA	Anti-neutrophil cytoplasmatic autoantibodies
aqua dest.	Distilled water
AF	Alexa Fluor
APC	Allophycocyanin
bp	Base pairs
BSA	Bovine serum albumin
BUN	Blood urea nitrogen
BV	Brilliant violet
CCR	C-C chemokine receptor
CD	Crohn's disease
CD“number”	Cluster of differentiation “number”
cGN	Crescentic glomerulonephritis
CKD	Chronic kidney disease
CXCR	CXC-motif chemokine receptor
DAMP	Damage-associated molecular pattern
DC	Dendritic cell
DDT	Dithiothreitol
DNA	Deoxyribonucleic acid
dNTP	Deoxynucleotide triphosphate
DPBS	Dulbecco's phosphate buffered saline
EAE	Experimental autoimmune encephalomyelitis
EDTA	Ethylenediaminetetraacetic acid
EGPA	Eosinophilic granulomatosis with polyangiitis
ELISA	Enzyme-linked immunosorbent assay
EPO	Erythropoietin
ESRD	End-stage renal disease
EtOH	Ethanol
eYFP	Enhanced yellow fluorescent protein
FACS	Fluorescence-activated cell sorting
FCS	Fetal calf serum
FITC	Fluorescein isothiocyanate
FoxP3	Forkhead-box-protein 3
FCS	Forward scattering
GBM	Glomerular basement membrane

gDNA	Genomic DNA
gd-T	gamma delta T cells
GEM	Gel beads in emulsion
GFP	Green fluorescent protein
GFR	Glomerular filtration rate
GN	Glomerulonephritis
GPA	Granulomatosis with polyangiitis
HBSS	Hanks balanced salt solution
HEPES	4-(2-hydroxyethyl)-1-piperazineethanesulfonic acid
Hif1a	Hypoxia-inducible factor 1a
HLA	Human leukocyte antigen
HRP	Horseradish peroxidase
IBD	Intestinal bowel disease
IFN- $\gamma$ (IFNg)	Interferon gamma
Ig	Immunoglobulin
IL	Interleukin
i.p.	Intraperitoneally
KO	Gene knockout
loxP	Locus of X-over P1
mA	Milli Ampere
min	Minutes
MPA	Microscopic polyangiitis
MPO-ANCA	Myeloperoxidase specific anti-neutrophil cytoplasmatic autoantibodies
MHC	Major histocompatibility complex
mM	Milli molar
MOG	Myelin oligodendrocyte glycoprotein
MS	Multiple sclerosis
NIR	Near infrared
NK cell	Natural killer cell
nm	Nanometre
NTN	Nephrotoxic nephritis
PAS (staining)	Periodic acid-Schiff (staining)
PAMP	Pathogen-associated molecular pattern
PCA	Principal component analysis
PCR	Polymerase chain reaction
PD	Peritoneal dialysis
PerCP	Peridinin-chlorophyll-protein
PFA	Paraformaldehyde
PMA	Phorbol 12-myristate 13-acetate
PPs	Peyer's patches

PR3-ANCA	Proteinase 3 specific anti-neutrophil cytoplasmic autoantibodies
PRR	Pattern recognition receptors
RAAS	Renin-angiotensin-aldosterone-system
RNA	Ribonucleic acid
ROSA26 /R26	Reverse oriented splice acceptor, clone 26
RORg	RAR-related orphan receptor gamma
RPGN	Rapid progressive glomerulonephritis
rpm	Revolutions per minutes
RPMI	Roswell Park Memorial Institute
RRT	Renal replacement therapy
RT	Room temperature
RUNX	Runt-related transcription factor
SCID	Severe combined immunodeficiency
scRNAseq	Single cell RNA sequencing
SD	Standard deviation
sec	Seconds
SEM	Standard error of the mean
SI	Small intestine
SLE	Systemic lupus erythematosus
SSC	Side scatter
STAT	Signal transducer and activator of transcription
SPF	Specific-pathogen-free
TB	Trypan blue
T-bet	T-box expressed in T cells
Tbx21	T-box transcription factor 21
Tconv	Conventional T cells
TF	Transcription factor
Tfh	T follicular helper cell
TGF- $\beta$	Transforming growth factor- $\beta$
Th	T helper cell
TLR	Toll-like receptors
TNF-a	Tumor necrosis factor-a
Tr1	Type 1 regulatory T cells
Tris-HCl	Tris(hydroxymethyl)aminomethane hydrochloride
Trm17	Tissue resident Th17 cells
UKE	Universitätsklinikum Hamburg-Eppendorf
v	Volt
vs.	Versus
wt	Wild type
YFP	Yellow fluorescent protein

## 7. Bibliography

### 7.1 Literature

- Ahern**, P.P., Schiering, C., Buonocore, S., McGeachy, M.J., Cua, D.J., Maloy, K.J., Powrie, F., 2010. Interleukin-23 Drives Intestinal Inflammation through Direct Activity on T Cells. *Immunity* 33, 279–288.
- Bartsch**, P., Kilian, C., Hellmig, M., Paust, H.-J., Borchers, A., Sivayoganathan, A., Enk, L., Zhao, Y., Shaikh, N., Büttner, H., Wong, M.N., Puellas, V.G., Wiech, T., Flavell, R., Huber, T.B., Turner, J.-E., Bonn, S., Huber, S., Gagliani, N., Mittrücker, H.-W., Rohde, H., Panzer, U., Krebs, C.F., 2022. Th17 cell plasticity towards a T-bet-dependent Th1 phenotype is required for bacterial control in *Staphylococcus aureus* infection. *PLoS Pathog* 18, e1010430.
- Beaugerie**, L., Seksik, P., Nion-Larmurier, I., Gendre, J.-P., Cosnes, J., 2006. Predictors of Crohn's disease. *Gastroenterology* 130, 650–656.
- Becher**, B., Tugues, S., Greter, M., 2016. GM-CSF: From Growth Factor to Central Mediator of Tissue Inflammation. *Immunity* 45, 963–973.
- Becker**, C., Fantini, M.C., Neurath, M.F., 2006. High resolution colonoscopy in live mice. *Nat Protoc* 1, 2900–2904.
- Berhanu**, D., Mortari, F., De Rosa, S.C., Roederer, M., 2003. Optimized lymphocyte isolation methods for analysis of chemokine receptor expression. *Journal of Immunological Methods* 279, 199–207.
- Bettelli**, E., Carrier, Y., Gao, W., Korn, T., Strom, T.B., Oukka, M., Weiner, H.L., Kuchroo, V.K., 2006. Reciprocal developmental pathways for the generation of pathogenic effector TH17 and regulatory T cells. *Nature* 441, 235–238.
- Böhmer**, F., 1865. Zur pathologischen, Anatomie der Meningitis cerebromedularis epidemia. *Ärztliches Intelligenz-Blatt* 12, 539–550.
- Britton**, G.J., Contijoch, E.J., Mogno, I., Vennaro, O.H., Llewellyn, S.R., Ng, R., Li, Z., Mortha, A., Merad, M., Das, A., Gevers, D., McGovern, D.P.B., Singh, N., Braun, J., Jacobs, J.P., Clemente, J.C., Grinspan, A., Sands, B.E., Colombel, J.-F., Dubinsky, M.C., Faith, J.J., 2019. Microbiotas from Humans with Inflammatory Bowel Disease Alter the Balance of Gut Th17 and ROR $\gamma$ <sup>+</sup> Regulatory T Cells and Exacerbate Colitis in Mice. *Immunity* 50, 212-224.e4.
- Brucklacher-Waldert**, V., Ferreira, C., Innocentin, S., Kamdar, S., Withers, D.R., Kullberg, M.C., Veldhoen, M., 2016. Tbet or Continued ROR $\gamma$ <sup>+</sup> Expression Is Not Required for Th17-Associated Immunopathology. *The Journal of Immunology* 196, 4893–4904.
- Carpenter**, A.C., Bosselut, R., 2010. Decision checkpoints in the thymus. *Nat Immunol* 11, 666–673.
- Castro-Dopico**, T., Fleming, A., Dennison, T.W., Ferdinand, J.R., Harcourt, K., Stewart, B.J., Cader, Z., Tuong, Z.K., Jing, C., Lok, L.S.C., Mathews, R.J., Portet, A., Kaser, A., Clare, S., Clatworthy, M.R., 2020. GM-CSF Calibrates Macrophage Defense and Wound Healing Programs during Intestinal Infection and Inflammation. *Cell Reports* 32, 107857.
- Chung**, Y., Yang, X., Chang, S.H., Ma, L., Tian, Q., Dong, C., 2006. Expression and regulation of IL-22 in the IL-17-producing CD4<sup>+</sup> T lymphocytes. *Cell Res* 16, 902–907.

- Codarri, L., Gyölvézi, G., Tosevski, V., Hesske, L., Fontana, A., Magnenat, L., Suter, T., Becher, B., 2011.** ROR $\gamma$ t drives production of the cytokine GM-CSF in helper T cells, which is essential for the effector phase of autoimmune neuroinflammation. *Nat Immunol* 12, 560–567.
- Couser, W.G., 1988.** Rapidly progressive glomerulonephritis: classification, pathogenetic mechanisms, and therapy. *Am J Kidney Dis* 11, 449–464.
- Couzi, L., Malvezzi, P., Amrouche, L., Anglicheau, D., Blancho, G., Caillard, S., Freist, M., Guidicelli, G. L., Kamar, N., Lefaucheur, C., Mariat, C., Koenig, A., Noble, J., Thaumat, O., Thierry, A., Taupin, J. L., & Bertrand, D., 2023.** Imlifidase for Kidney Transplantation of Highly Sensitized Patients With a Positive Crossmatch: The French Consensus Guidelines. *Transplant international : official journal of the European Society for Organ Transplantation*, 36, 11244.
- Cua, D.J., Sherlock, J., Chen, Y., Murphy, C.A., Joyce, B., Seymour, B., Lucian, L., To, W., Kwan, S., Churakova, T., Zurawski, S., Wiekowski, M., Lira, S.A., Gorman, D., Kastelein, R.A., Sedgwick, J.D., 2003.** Interleukin-23 rather than interleukin-12 is the critical cytokine for autoimmune inflammation of the brain. *Nature* 421, 744–748.
- Diefenbach, A., Colonna, M., Koyasu, S., 2014.** Development, differentiation, and diversity of innate lymphoid cells. *Immunity* 41, 354–365.
- Disteldorf, E.M., Krebs, C.F., Paust, H.-J., Turner, J.-E., Nouailles, G., Tittel, A., Meyer-Schwesinger, C., Stege, G., Brix, S., Velden, J., Wiech, T., Helmchen, U., Steinmetz, O.M., Peters, A., Bannstein, S.B., Kaffke, A., Llanto, C., Lira, S.A., Mittrücker, H.-W., Stahl, R.A.K., Kurts, C., Kaufmann, S.H.E., Panzer, U., 2015.** CXCL5 Drives Neutrophil Recruitment in T<sub>H</sub> 17-Mediated GN. *JASN* 26, 55–66.
- Dobin, A., Davis, C.A., Schlesinger, F., Drenkow, J., Zaleski, C., Jha, S., Batut, P., Chaisson, M., Gingeras, T.R., 2013.** STAR: ultrafast universal RNA-seq aligner. *Bioinformatics* 29, 15–21.
- Du, B., Yu, M., Zheng, J., 2018.** Transport and interactions of nanoparticles in the kidneys. *Nat Rev Mater* 3, 358–374 (Figure "Kidney anatomy" from page 360).
- Duhen, R., Glatigny, S., Arbelaez, C.A., Blair, T.C., Oukka, M., Bettelli, E., 2013.** Cutting Edge: The Pathogenicity of IFN- $\gamma$ -Producing Th17 Cells Is Independent of T-bet. *J.I.* 190, 4478–4482.
- Durant, L., Watford, W.T., Ramos, H.L., Laurence, A., Vahedi, G., Wei, L., Takahashi, H., Sun, H.-W., Kanno, Y., Powrie, F., O’Shea, J.J., 2010.** Diverse targets of the transcription factor STAT3 contribute to T cell pathogenicity and homeostasis. *Immunity* 32, 605–615.
- Ei-Behi, M., Ciric, B., Dai, H., Yan, Y., Cullimore, M., Safavi, F., Zhang, G.-X., Dittel, B.N., Rostami, A., 2011.** The encephalitogenicity of T(H)17 cells is dependent on IL-1- and IL-23-induced production of the cytokine GM-CSF. *Nat Immunol* 12, 568–575.
- EITanbouly, M.A., Noelle, R.J., 2021.** Rethinking peripheral T cell tolerance: checkpoints across a T cell’s journey. *Nat Rev Immunol* 21, 257–267.
- Elyaman, W., Bradshaw, E.M., Uyttenhove, C., Dardalhon, V., Awasthi, A., Imitola, J., Bettelli, E., Oukka, M., van Snick, J., Renault, J.-C., Kuchroo, V.K., Khoury, S.J., 2009.** IL-9 induces differentiation of TH17 cells and enhances function of FoxP3<sup>+</sup> natural regulatory T cells. *Proc Natl Acad Sci U S A* 106, 12885–12890.
- Feagan, B.G., Macdonald, J.K., 2012.** Oral 5-aminosalicylic acid for induction of remission in ulcerative colitis. *Cochrane Database Syst Rev* 10, CD000543.

**Fontenot**, J.D., Gavin, M.A., Rudensky, A.Y., 2003. Foxp3 programs the development and function of CD4+CD25+ regulatory T cells. *Nat Immunol* 4, 330–336.

**Frolkis**, A.D., Dykeman, J., Negrón, M.E., Debruyne, J., Jette, N., Fiest, K.M., Frolkis, T., Barkema, H.W., Rioux, K.P., Panaccione, R., Ghosh, S., Wiebe, S., Kaplan, G.G., 2013. Risk of surgery for inflammatory bowel diseases has decreased over time: a systematic review and meta-analysis of population-based studies. *Gastroenterology* 145, 996–1006.

**Fujino**, S., Andoh, A., Bamba, S., Ogawa, A., Hata, K., Araki, Y., Bamba, T., Fujiyama, Y., 2003. Increased expression of interleukin 17 in inflammatory bowel disease. *Gut* 52, 65–70.

**Fumery**, M., Singh, S., Dulai, P.S., Gower-Rousseau, C., Peyrin-Biroulet, L., Sandborn, W.J., 2018. Natural History of Adult Ulcerative Colitis in Population-based Cohorts: A Systematic Review. *Clin Gastroenterol Hepatol* 16, 343-356.e3.

**Gagliani**, N., Amezcua Vesely, M.C., Iseppon, A., Brockmann, L., Xu, H., Palm, N.W., de Zoete, M.R., Licona-Limón, P., Paiva, R.S., Ching, T., Weaver, C., Zi, X., Pan, X., Fan, R., Garmire, L.X., Cotton, M.J., Drier, Y., Bernstein, B., Geginat, J., Stockinger, B., Esplugues, E., Huber, S., Flavell, R.A., 2015. Th17 cells transdifferentiate into regulatory T cells during resolution of inflammation. *Nature* 523, 221–225.

**Gagliani**, N., Magnani, C.F., Huber, S., Gianolini, M.E., Pala, M., Licona-Limon, P., Guo, B., Herbert, D.R., Bulfone, A., Trentini, F., Di Serio, C., Bacchetta, R., Andreani, M., Brockmann, L., Gregori, S., Flavell, R.A., Roncarolo, M.-G., 2013. Coexpression of CD49b and LAG-3 identifies human and mouse T regulatory type 1 cells. *Nat Med* 19, 739–746.

**Gaitonde**, D.Y., Cook, D.L., Rivera, I.M., 2017. Chronic Kidney Disease: Detection and Evaluation. *Am Fam Physician* 96, 776–783.

**Germain**, R.N., 2002. T-cell development and the CD4–CD8 lineage decision. *Nat Rev Immunol* 2, 309–322.

**Gkouskou**, K.K., Deligianni, C., Tsatsanis, C., Eliopoulos, A.G., 2014. The gut microbiota in mouse models of inflammatory bowel disease. *Front Cell Infect Microbiol* 4, 28.

**Grifka-Walk**, H.M., Giles, D.A., Segal, B.M., 2015. IL-12-polarized Th1 cells produce GM-CSF and induce EAE independent of IL-23: Cellular Immune Response. *Eur. J. Immunol.* 45, 2780–2786.

**Guilherme**, L., Oshiro, S.E., Faé, K.C., Cunha-Neto, E., Renesto, G., Goldberg, A.C., Tanaka, A.C., Pomerantzeff, P.M., Kiss, M.H., Silva, C., Guzman, F., Patarroyo, M.E., Southwood, S., Sette, A., Kalil, J., 2001. T-cell reactivity against streptococcal antigens in the periphery mirrors reactivity of heart-infiltrating T lymphocytes in rheumatic heart disease patients. *Infect Immun* 69, 5345–5351.

**Haas**, M., Verhave, J.C., Liu, Z.-H., Alpers, C.E., Barratt, J., Becker, J.U., Cattran, D., Cook, H.T., Coppo, R., Feehally, J., Pani, A., Perkowska-Ptasinska, A., Roberts, I.S.D., Soares, M.F., Trimarchi, H., Wang, S., Yuzawa, Y., Zhang, H., Troyanov, S., Katafuchi, R., 2017. A Multicenter Study of the Predictive Value of Crescents in IgA Nephropathy. *J Am Soc Nephrol* 28, 691–701.

**Hao**, Y., Hao, S., Andersen-Nissen, E., Mauck, W.M., Zheng, S., Butler, A., Lee, M.J., Wilk, A.J., Darby, C., Zager, M., Hoffman, P., Stoeckius, M., Papalexi, E., Mimitou, E.P., Jain, J., Srivastava, A., Stuart, T., Fleming, L.M., Yeung, B., Rogers, A.J., McElrath, J.M., Blish, C.A., Gottardo, R., Smibert, P., Satija, R., 2021. Integrated analysis of multimodal single-cell data. *Cell* 184, 3573-3587.e29.

- Harbour**, S.N., Maynard, C.L., Zindl, C.L., Schoeb, T.R., Weaver, C.T., 2015. Th17 cells give rise to Th1 cells that are required for the pathogenesis of colitis. *Proc Natl Acad Sci USA* 112, 7061–7066.
- Harrington**, L.E., Hatton, R.D., Mangan, P.R., Turner, H., Murphy, T.L., Murphy, K.M., Weaver, C.T., 2005. Interleukin 17-producing CD4+ effector T cells develop via a lineage distinct from the T helper type 1 and 2 lineages. *Nat Immunol* 6, 1123–1132.
- Helal**, I., Fick-Brosnahan, G.M., Reed-Gitomer, B., Schrier, R.W., 2012. Glomerular hyperfiltration: definitions, mechanisms and clinical implications. *Nat Rev Nephrol* 8, 293–300.
- Heller, F., Fuss, I.J., Nieuwenhuis, E.E., Blumberg, R.S., Strober, W., 2002. Oxazolone Colitis, a Th2 Colitis Model Resembling Ulcerative Colitis, Is Mediated by IL-13-Producing NK-T Cells. *Immunity* 17, 629–638.
- Hirota**, K., Duarte, J.H., Veldhoen, M., Hornsby, E., Li, Y., Cua, D.J., Ahlfors, H., Wilhelm, C., Tolaini, M., Menzel, U., Garefalaki, A., Potocnik, A.J., Stockinger, B., 2011. Fate mapping of IL-17-producing T cells in inflammatory responses. *Nat Immunol* 12, 255–263.
- Hirota**, K., Turner, J.-E., Villa, M., Duarte, J.H., Demengeot, J., Steinmetz, O.M., Stockinger, B., 2013. Plasticity of TH17 cells in Peyer's patches is responsible for the induction of T cell-dependent IgA responses. *Nat Immunol* 14, 372–379.
- Hue**, S., Ahern, P., Buonocore, S., Kullberg, M.C., Cua, D.J., McKenzie, B.S., Powrie, F., Maloy, K.J., 2006. Interleukin-23 drives innate and T cell-mediated intestinal inflammation. *J Exp Med* 203, 2473–2483.
- Hugot**, J.P., Chamaillard, M., Zouali, H., Lesage, S., Cézard, J.P., Belaiche, J., Almer, S., Tysk, C., O'Morain, C.A., Gassull, M., Binder, V., Finkel, Y., Cortot, A., Modigliani, R., Laurent-Puig, P., Gower-Rousseau, C., Macry, J., Colombel, J.F., Sahbatou, M., Thomas, G., 2001. Association of NOD2 leucine-rich repeat variants with susceptibility to Crohn's disease. *Nature* 411, 599–603.
- Hyman**, N.H., Cataldo, P., Osler, T., 2005. Urgent subtotal colectomy for severe inflammatory bowel disease. *Dis Colon Rectum* 48, 70–73.
- Ichiyama**, K., Sekiya, T., Inoue, N., Tamiya, T., Kashiwagi, I., Kimura, A., Morita, R., Muto, G., Shichita, T., Takahashi, R., Yoshimura, A., 2011. Transcription Factor Smad-Independent T Helper 17 Cell Induction by Transforming-Growth Factor- $\beta$  Is Mediated by Suppression of Eomesodermin. *Immunity* 34, 741–754.
- Ivanov**, I.I., McKenzie, B.S., Zhou, L., Tadokoro, C.E., Lepelley, A., Lafaille, J.J., Cua, D.J., Littman, D.R., 2006. The orphan nuclear receptor ROR $\gamma$  directs the differentiation program of proinflammatory IL-17+ T helper cells. *Cell* 126, 1121–1133.
- Jennette**, J.C., 2003. Rapidly progressive crescentic glomerulonephritis. *Kidney International* 63, 1164–1177.
- Jennette**, J.C., Falk, R.J., 1998. Pathogenesis of the vascular and glomerular damage in ANCA-positive vasculitis. *Nephrol Dial Transplant* 13 Suppl 1, 16–20.
- Jennette**, J.C., Falk, R.J., 1997. Small-vessel vasculitis. *The New England journal of medicine* 337.
- Jennette**, J.C., Thomas, D.B., 2001. Crescentic glomerulonephritis. *Nephrology Dialysis Transplantation* 16, 80–82.
- Kalluri**, R., Wilson, C.B., Weber, M., Gunwar, S., Chonko, A.M., Neilson, E.G., Hudson, B.G., 1995.

Identification of the alpha 3 chain of type IV collagen as the common autoantigen in antibasement membrane disease and Goodpasture syndrome. *J Am Soc Nephrol* 6, 1178–1185.

**Kamanaka**, M., Huber, S., Zenewicz, L.A., Gagliani, N., Rathinam, C., O'Connor, W., Wan, Y.Y., Nakae, S., Iwakura, Y., Hao, L., Flavell, R.A., 2011. Memory/effector (CD45RB(Io)) CD4 T cells are controlled directly by IL-10 and cause IL-22-dependent intestinal pathology. *J Exp Med* 208, 1027–1040.

**Kaplan**, M.H., 2013. Th9 cells: differentiation and disease. *Immunol Rev* 252, 104–115.

**Kellum**, J.A., Romagnani, P., Ashuntantang, G., Ronco, C., Zarbock, A., Anders, H.-J., 2021. Acute kidney injury. *Nat Rev Dis Primers* 7, 1–17.

**Kim**, B.-S., Lu, H., Ichiyama, K., Chen, X., Zhang, Y.-B., Mistry, N.A., Tanaka, K., Lee, Y.-H., Nurieva, R., Zhang, L., Yang, X., Chung, Y., Jin, W., Chang, S.H., Dong, C., 2017. Generation of ROR $\gamma$ t+ Antigen-Specific T Regulatory 17 Cells from Foxp3+ Precursors in Autoimmunity. *Cell Rep* 21, 195–207.

**Kim**, J.M., Rasmussen, J.P., Rudensky, A.Y., 2007. Regulatory T cells prevent catastrophic autoimmunity throughout the lifespan of mice. *Nat Immunol* 8, 191–197.

**Kleiner**, J.C., Krebs, C.F., 2022. Persistence, Pathogenicity and Plasticity: The Role of IL-23 in Th17 Fate. *J Cell Immunol.* 4, 121-130.

**Kopf**, M., Le Gros, G., Bachmann, M., Lamers, M.C., Bluethmann, H., Köhler, G., 1993. Disruption of the murine IL-4 gene blocks Th2 cytokine responses. *Nature* 362, 245–248.

**Korsunsky**, I., Millard, N., Fan, J., Slowikowski, K., Zhang, F., Wei, K., Baglaenko, Y., Brenner, M., Loh, P.-R., Raychaudhuri, S., 2019. Fast, sensitive and accurate integration of single-cell data with Harmony. *Nat Methods* 16, 1289–1296.

**Krausgruber**, T., Schiering, C., Adelman, K., Harrison, O.J., Chomka, A., Pearson, C., Ahern, P.P., Shale, M., Oukka, M., Powrie, F., 2016. T-bet is a key modulator of IL-23-driven pathogenic CD4+ T cell responses in the intestine. *Nat Commun* 7, 11627.

**Krebs**, C.F., Kapffer, S., Paust, H.-J., Schmidt, T., Bennisstein, S.B., Peters, A., Stege, G., Brix, S.R., Meyer-Schwesinger, C., Müller, R.-U., Turner, J.-E., Steinmetz, O.M., Wolf, G., Stahl, R.A.K., Panzer, U., 2013. MicroRNA-155 Drives TH17 Immune Response and Tissue Injury in Experimental Crescentic GN. *Journal of the American Society of Nephrology* 24, 1955–1965.

**Krebs**, C.F., **Panzer**, U., 2018. Plasticity and heterogeneity of Th17 in immune-mediated kidney diseases. *Journal of Autoimmunity, Plasticity of Th17 cells in autoimmune disease* 87, 61–68 (Figure " Th17 cell plasticity of kidney-infiltrating T cells" from page 64).

**Krebs**, Christian F., Paust, H.-J., Krohn, S., Koyro, T., Brix, S.R., Riedel, J.-H., Bartsch, P., Wiech, T., Meyer-Schwesinger, C., Huang, J., Fischer, N., Busch, P., Mittrücker, H.-W., Steinhoff, U., Stockinger, B., Perez, L.G., Wenzel, U.O., Janneck, M., Steinmetz, O.M., Gagliani, N., Stahl, R.A.K., Huber, S., Turner, J.-E., Panzer, U., 2016. Autoimmune Renal Disease Is Exacerbated by S1P-Receptor-1-Dependent Intestinal Th17 Cell Migration to the Kidney. *Immunity* 45, 1078–1092.

**Krebs**, C.F., Reimers, D., Zhao, Y., Paust, H.-J., Bartsch, P., Nuñez, S., Roseblatt, M.V., Hellmig, M., Kilian, C., Borchers, A., Enk, L.U.B., Zinke, M., Becker, M., Schmid, J., Klinge, S., Wong, M.N., Puelles, V.G., Schmidt, C., Bertram, T., Stumpf, N., Hoxha, E., Meyer-Schwesinger, C., Lindenmeyer, M.T., Cohen, C.D., Rink, M., Kurts, C., Franzenburg, S., Koch-Nolte, F., Turner, J.-E.,

Riedel, J.-H., Huber, S., Gagliani, N., Huber, T.B., Wiech, T., Rohde, H., Bono, M.R., Bonn, S., Panzer, U., Mittrücker, H.-W., 2020. Pathogen-induced tissue-resident memory T<sub>H</sub> 17 (T<sub>RM</sub> 17) cells amplify autoimmune kidney disease. *Sci. Immunol.* 5, eaba4163.

**Krebs**, C.F., Schmidt, T., Riedel, J.-H., Panzer, U., 2017. T helper type 17 cells in immune-mediated glomerular disease. *Nat Rev Nephrol* 13, 647–659.

**Krebs**, Christian F., Turner, J.-E., Paust, H.-J., Kapffer, S., Koyro, T., Krohn, S., Ufer, F., Friese, M.A., Flavell, R.A., Stockinger, B., Steinmetz, O.M., Stahl, R.A.K., Huber, S., Panzer, U., 2016. Plasticity of Th17 Cells in Autoimmune Kidney Diseases. *J.I.* 197, 449–457.

**Kullberg**, M.C., Jankovic, D., Feng, C.G., Hue, S., Gorelick, P.L., McKenzie, B.S., Cua, D.J., Powrie, F., Cheever, A.W., Maloy, K.J., Sher, A., 2006. IL-23 plays a key role in *Helicobacter hepaticus*-induced T cell-dependent colitis. *Journal of Experimental Medicine* 203, 2485–2494.

**Kurts**, C., Panzer, U., Anders, H.-J., Rees, A.J., 2013. The immune system and kidney disease: basic concepts and clinical implications. *Nat Rev Immunol* 13, 738–753.

**La Manno**, G., Soldatov, R., Zeisel, A., Braun, E., Hochgerner, H., Petukhov, V., Lidschreiber, K., Kastrioti, M.E., Lönnerberg, P., Furlan, A., Fan, J., Borm, L.E., Liu, Z., van Bruggen, D., Guo, J., He, X., Barker, R., Sundström, E., Castelo-Branco, G., Cramer, P., Adameyko, I., Linnarsson, S., Kharchenko, P.V., 2018. RNA velocity of single cells. *Nature* 560, 494–498.

**Lamb**, C.A., Kennedy, N.A., Raine, T., Hendy, P.A., Smith, P.J., Limdi, J.K., Hayee, B., Lomer, M.C.E., Parkes, G.C., Selinger, C., Barrett, K.J., Davies, R.J., Bennett, C., Gittens, S., Dunlop, M.G., Faiz, O., Fraser, A., Garrick, V., Johnston, P.D., Parkes, M., Sanderson, J., Terry, H., Group, I. guidelines eDelphi consensus, Gaya, D.R., Iqbal, T.H., Taylor, S.A., Smith, M., Brookes, M., Hansen, R., Hawthorne, A.B., 2019. British Society of Gastroenterology consensus guidelines on the management of inflammatory bowel disease in adults. *Gut* 68, s1–s106.

**Langrish**, C.L., Chen, Y., Blumenschein, W.M., Mattson, J., Basham, B., Sedgwick, J.D., McClanahan, T., Kastelein, R.A., Cua, D.J., 2005. IL-23 drives a pathogenic T cell population that induces autoimmune inflammation. *Journal of Experimental Medicine* 201, 233–240.

**Lazarevic**, V., Chen, X., Shim, J.-H., Hwang, E.-S., Jang, E., Bolm, A.N., Oukka, M., Kuchroo, V.K., Glimcher, L.H., 2011. T-bet represses TH17 differentiation by preventing Runx1-mediated activation of the gene encoding ROR $\gamma$ t. *Nat Immunol* 12, 96–104.

**Lazarevic**, V., Glimcher, L.H., Lord, G.M., 2013. T-bet: a bridge between innate and adaptive immunity. *Nat Rev Immunol* 13, 777–789.

**Lee**, J.S., Tato, C.M., Joyce-Shaikh, B., Gulen, M.F., Gulan, F., Cayatte, C., Chen, Y., Blumenschein, W.M., Judo, M., Ayanoglu, G., McClanahan, T.K., Li, X., Cua, D.J., 2015. Interleukin-23-Independent IL-17 Production Regulates Intestinal Epithelial Permeability. *Immunity* 43, 727–738.

**Lee**, Y.K., Turner, H., Maynard, C.L., Oliver, J.R., Chen, D., Elson, C.O., Weaver, C.T., 2009. Late Developmental Plasticity in the T Helper 17 Lineage. *Immunity* 30, 92–107.

**Lennard-Jones**, J.E., Longmore, A.J., Newell, A.C., Wilson, C.W., Jones, F.A., 1960. An assessment of prednisone, salazopyrin, and topical hydrocortisone hemisuccinate used as out-patient treatment for ulcerative colitis. *Gut* 1, 217–222.

**Leppkes**, M., Becker, C., Ivanov, I.I., Hirth, S., Wirtz, S., Neufert, C., Pouly, S., Murphy, A.J., Valenzuela, D.M., Yancopoulos, G.D., Becher, B., Littman, D.R., Neurath, M.F., 2009. ROR $\gamma$ -

Expressing Th17 Cells Induce Murine Chronic Intestinal Inflammation via Redundant Effects of IL-17A and IL-17F. *Gastroenterology* 136, 257–267.

**Levey**, A.S., Eckardt, K.-U., Dorman, N.M., Christiansen, S.L., Hoorn, E.J., Ingelfinger, J.R., Inker, L.A., Levin, A., Mehrotra, R., Palevsky, P.M., Perazella, M.A., Tong, A., Allison, S.J., Bockenhauer, D., Briggs, J.P., Bromberg, J.S., Davenport, A., Feldman, H.I., Fouque, D., Gansevoort, R.T., Gill, J.S., Greene, E.L., Hemmelgarn, B.R., Kretzler, M., Lambie, M., Lane, P.H., Laycock, J., Leventhal, S.E., Mittelman, M., Morrissey, P., Ostermann, M., Rees, L., Ronco, P., Schaefer, F., St. Clair Russell, J., Vinck, C., Walsh, S.B., Weiner, D.E., Cheung, M., Jadoul, M., Winkelmayer, W.C., 2020. Nomenclature for kidney function and disease: report of a Kidney Disease: Improving Global Outcomes (KDIGO) Consensus Conference. *Kidney International* 97, 1117–1129.

**Levine**, J.S., Burakoff, R., 2011. Extraintestinal Manifestations of Inflammatory Bowel Disease. *Gastroenterol Hepatol (N Y)* 7, 235–241.

Lighvani, A.A., Frucht, D.M., Jankovic, D., Yamane, H., Aliberti, J., Hissong, B.D., Nguyen, B.V., Gadina, M., Sher, A., Paul, W.E., O’Shea, J.J., 2001. T-bet is rapidly induced by interferon- $\gamma$  in lymphoid and myeloid cells. *Proc Natl Acad Sci U S A* 98, 15137–15142.

**Lim**, H.W., Lee, J., Hillsamer, P., Kim, C.H., 2008. Human Th17 cells share major trafficking receptors with both polarized effector T cells and FOXP3+ regulatory T cells. *J Immunol* 180, 122–129.

**Loly**, C., Belaiche, J., Louis, E., 2008. Predictors of severe Crohn’s disease. *Scand J Gastroenterol* 43, 948–954.

**Lord**, G.M., Rao, R.M., Choe, H., Sullivan, B.M., Lichtman, A.H., Luscinskas, F.W., Glimcher, L.H., 2005. T-bet is required for optimal proinflammatory CD4+ T-cell trafficking. *Blood* 106, 3432–3439.

**Lowin**, B., Peitsch, M.C., Tschopp, J., 1995. Perforin and granzymes: crucial effector molecules in cytolytic T lymphocyte and natural killer cell-mediated cytotoxicity. *Curr Top Microbiol Immunol* 198, 1–24.

**Mathur**, A.N., Chang, H.-C., Zisoulis, D.G., Stritesky, G.L., Yu, Q., O’Malley, J.T., Kapur, R., Levy, D.E., Kansas, G.S., Kaplan, M.H., 2007. Stat3 and Stat4 Direct Development of IL-17-Secreting Th Cells. *The Journal of Immunology* 178, 4901–4907.

**McAdoo**, S.P., **Pusey**, C.D., 2017. Anti-Glomerular Basement Membrane Disease. *CJASN* 12, 1162–1172 (Figure "Renal histopathology in anti-glomerular basement membrane (anti-GBM) GN" from page 1166).

**McGeachy**, M.J., **Cua**, D.J., 2008. Th17 Cell Differentiation: The Long and Winding Road. *Immunity* 28, 445–453.

**Medzhitov**, R., 2007. Recognition of microorganisms and activation of the immune response. *Nature* 449, 819–826 (Figure " Effector TH-cell lineage and pathogen class" from page 823).

**Mizoguchi**, A., Yano, A., Himuro, H., Ezaki, Y., Sadanaga, T., Mizoguchi, E., 2018. Clinical importance of IL-22 cascade in IBD. *J Gastroenterol* 53, 465–474.

**Mosmann**, T.R., Cherwinski, H., Bond, M.W., Giedlin, M.A., Coffman, R.L., 1986. Two types of murine helper T cell clone. I. Definition according to profiles of lymphokine activities and secreted proteins. *J Immunol* 136, 2348–2357.

**Mosmann**, T.R., **Coffman**, R.L., 1989. TH1 and TH2 cells: different patterns of lymphokine secretion

lead to different functional properties. *Annu Rev Immunol* 7, 145–173.

**Mukasa**, R., Balasubramani, A., Lee, Y.K., Whitley, S.K., Weaver, B.T., Shibata, Y., Crawford, G.E., Hatton, R.D., Weaver, C.T., 2010. Epigenetic Instability of Cytokine and Transcription Factor Gene Loci Underlies Plasticity of the T Helper 17 Cell Lineage. *Immunity* 32, 616–627.

**Murphy**, C.A., Langrish, C.L., Chen, Y., Blumenschein, W., McClanahan, T., Kastelein, R.A., Sedgwick, J.D., Cua, D.J., 2003. Divergent Pro- and Antiinflammatory Roles for IL-23 and IL-12 in Joint Autoimmune Inflammation. *Journal of Experimental Medicine* 198, 1951–1957.

**Neurath**, M.F., 2019. Targeting immune cell circuits and trafficking in inflammatory bowel disease. *Nat Immunol* 20, 970–979 (Figure "Clinical features of IBD" from page 971).

**Ng**, W.F., Duggan, P.J., Ponchel, F., Matarese, G., Lombardi, G., Edwards, A.D., Isaacs, J.D., Lechler, R.I., 2001. Human CD4(+)CD25(+) cells: a naturally occurring population of regulatory T cells. *Blood* 98, 2736–2744.

**Niess**, J.H., Leithäuser, F., Adler, G., Reimann, J., 2008. Commensal gut flora drives the expansion of proinflammatory CD4 T cells in the colonic lamina propria under normal and inflammatory conditions. *J Immunol* 180, 559–568.

**Nistala**, K., Adams, S., Cambrook, H., Ursu, S., Olivito, B., de Jager, W., Evans, J.G., Cimaz, R., Bajaj-Elliott, M., Wedderburn, L.R., 2010. Th17 plasticity in human autoimmune arthritis is driven by the inflammatory environment. *Proc Natl Acad Sci U S A* 107, 14751–14756.

**Nylander**, S., Kalies, I., 1999. Brefeldin A, but not monensin, completely blocks CD69 expression on mouse lymphocytes: efficacy of inhibitors of protein secretion in protocols for intracellular cytokine staining by flow cytometry. *J Immunol Methods* 224, 69–76.

**Ostanin**, D.V., Bao, J., Koboziev, I., Gray, L., Robinson-Jackson, S.A., Kosloski-Davidson, M., Price, V.H., Grisham, M.B., 2009. T cell transfer model of chronic colitis: concepts, considerations, and tricks of the trade. *Am J Physiol Gastrointest Liver Physiol* 296, G135–G146.

**Ostanin**, D.V., Pavlick, K.P., Bharwani, S., D'Souza, D., Furr, K.L., Brown, C.M., Grisham, M.B., 2006. T cell-induced inflammation of the small and large intestine in immunodeficient mice. *Am J Physiol Gastrointest Liver Physiol* 290, G109-119.

**Pan**, H.-F., Li, X.-P., Zheng, S.G., Ye, D.-Q., 2013. Emerging role of interleukin-22 in autoimmune diseases. *Cytokine & Growth Factor Reviews* 24, 51–57.

**Panzer**, U., Steinmetz, O.M., Paust, H.-J., Meyer-Schwesinger, C., Peters, A., Turner, J.-E., Zahner, G., Heymann, F., Kurts, C., Hopfer, H., Helmchen, U., Haag, F., Schneider, A., Stahl, R.A.K., 2007. Chemokine receptor CXCR3 mediates T cell recruitment and tissue injury in nephrotoxic nephritis in mice. *J Am Soc Nephrol* 18, 2071–2084.

**Park**, H., Li, Z., Yang, X.O., Chang, S.H., Nurieva, R., Wang, Y.-H., Wang, Y., Hood, L., Zhu, Z., Tian, Q., Dong, C., 2005. A distinct lineage of CD4 T cells regulates tissue inflammation by producing interleukin 17. *Nat Immunol* 6, 1133–1141.

**Park**, I.-K., Shultz, L.D., Letterio, J.J., Gorham, J.D., 2005. TGF- $\beta$ 1 Inhibits T-bet Induction by IFN- $\gamma$  in Murine CD4+ T Cells through the Protein Tyrosine Phosphatase Src Homology Region 2 Domain-Containing Phosphatase-1. *The Journal of Immunology* 175, 5666–5674.

**Paust**, H.-J., Turner, J.-E., Steinmetz, O.M., Peters, A., Heymann, F., Hölscher, C., Wolf, G., Kurts, C., Mittrücker, H.-W., Stahl, R.A.K., Panzer, U., 2009. The IL-23/Th17 Axis Contributes to Renal

Injury in Experimental Glomerulonephritis. *J Am Soc Nephrol* 20, 969–979.

**Paust**, H. J., **Song**, N., De Feo, D., Asada, N., Tuzlak, S., Zhao, Y., Riedel, J. H., Hellmig, M., Sivayoganathan, A., Peters, A., Kaffke, A., Borchers, A., Wenzel, U. O., Steinmetz, O. M., Tiegs, G., Meister, E., Mack, M., Kurts, C., von Vietinghoff, S., Lindenmeyer, M. T., Hoxha E., Stahl R.A.K., Huber T.B., Bonn S., Meyer-Schwesinger C., Wiech T., Turner J.E., Becher B., Krebs C.F., Panzer, U., 2023. CD4<sup>+</sup> T cells produce GM-CSF and drive immune-mediated glomerular disease by licensing monocyte-derived cells to produce MMP12. *Science translational medicine*, 15(687), eadd6137.

**Pedchenko**, V., Bondar, O., Fogo, A.B., Vanacore, R., Voziyan, P., Kitching, A.R., Wieslander, J., Kashtan, C., Borza, D.-B., Neilson, E.G., Wilson, C.B., Hudson, B.G., 2010. Molecular architecture of the Goodpasture autoantigen in anti-GBM nephritis. *N Engl J Med* 363, 343–354.

**Plank**, M.W., Kaiko, G.E., Maltby, S., Weaver, J., Tay, H.L., Shen, W., Wilson, M.S., Durum, S.K., Foster, P.S., 2017. Th22 Cells Form a Distinct Th Lineage from Th17 Cells In Vitro with Unique Transcriptional Properties and Tbet-Dependent Th1 Plasticity. *J Immunol* 198, 2182–2190.

**Ponsioen**, C.Y., de Groof, E.J., Eshuis, E.J., Gardenbroek, T.J., Bossuyt, P.M.M., Hart, A., Warusavitarne, J., Buskens, C.J., van Bodegraven, A.A., Brink, M.A., Consten, E.C.J., van Wagenveld, B.A., Rijk, M.C.M., Crolla, R.M.P.H., Noomen, C.G., Houdijk, A.P.J., Mallant, R.C., Boom, M., Marsman, W.A., Stockmann, H.B., Mol, B., de Groof, A.J., Stokkers, P.C., D'Haens, G.R., Bemelman, W.A., LIR!C study group, 2017. Laparoscopic ileocaecal resection versus infliximab for terminal ileitis in Crohn's disease: a randomised controlled, open-label, multicentre trial. *Lancet Gastroenterol Hepatol* 2, 785–792.

**Quintero-Ronderos**, P., **Montoya-Ortiz**, G., 2012. Epigenetics and autoimmune diseases. *Autoimmune Dis* 2012, 593720.

**Roncarolo**, M.-G., **Battaglia**, M., 2007. Regulatory T-cell immunotherapy for tolerance to self antigens and alloantigens in humans. *Nat Rev Immunol* 7, 585–598.

**Rovin**, B.H., Adler, S.G., Barratt, J., Bridoux, F., Burdge, K.A., Chan, T.M., Cook, H.T., Fervenza, F.C., Gibson, K.L., Glassock, R.J., Jayne, D.R.W., Jha, V., Liew, A., Liu, Z.-H., Mejía-Vilet, J.M., Nester, C.M., Radhakrishnan, J., Rave, E.M., Reich, H.N., Ronco, P., Sanders, J.-S.F., Sethi, S., Suzuki, Y., Tang, S.C.W., Tesar, V., Vivarelli, M., Wetzels, J.F.M., Lytvyn, L., Craig, J.C., Tunnicliffe, D.J., Howell, M., Tonelli, M.A., Cheung, M., Earley, A., Floege, J., 2021. Executive summary of the KDIGO 2021 Guideline for the Management of Glomerular Diseases. *Kidney Int* 100, 753–779.

**Sakaguchi**, S., Sakaguchi, N., Asano, M., Itoh, M., Toda, M., 1995. Immunologic self-tolerance maintained by activated T cells expressing IL-2 receptor alpha-chains (CD25). Breakdown of a single mechanism of self-tolerance causes various autoimmune diseases. *J Immunol* 155, 1151–1164.

**Salinas**, G.F., Braza, F., Brouard, S., Tak, P.-P., Baeten, D., 2013. The role of B lymphocytes in the progression from autoimmunity to autoimmune disease. *Clin Immunol* 146, 34–45.

**Sallusto**, F., Lanzavecchia, A., 2000. Understanding dendritic cell and T-lymphocyte traffic through the analysis of chemokine receptor expression. *Immunol Rev* 177, 134–140.

**Seiderer**, J., Brand, S., 2009. IL-22: A Two-Headed Cytokine in IBD? *Inflammatory Bowel Diseases* 15, 473–474.

**Shevach**, E.M., 2009. Mechanisms of Foxp3<sup>+</sup> T Regulatory Cell-Mediated Suppression. *Immunity*

30, 636–645.

**Shyjan**, A.M., Bertagnolli, M., Kenney, C.J., Briskin, M.J., 1996. Human mucosal addressin cell adhesion molecule-1 (MAdCAM-1) demonstrates structural and functional similarities to the alpha 4 beta 7-integrin binding domains of murine MAdCAM-1, but extreme divergence of mucin-like sequences. *J Immunol* 156, 2851–2857.

**Söderholm**, J.D., Olaison, G., Peterson, K.H., Franzén, L.E., Lindmark, T., Wirén, M., Tagesson, C., Sjö Dahl, R., 2002. Augmented increase in tight junction permeability by luminal stimuli in the non-inflamed ileum of Crohn's disease. *Gut* 50, 307–313.

**Sollid**, L.M., Pos, W., Wucherpfennig, K.W., 2014. Molecular mechanisms for contribution of MHC molecules to autoimmune diseases. *Curr Opin Immunol* 31, 24–30.

**Sonderegger**, I., Iezzi, G., Maier, R., Schmitz, N., Kurrer, M., Kopf, M., 2008. GM-CSF mediates autoimmunity by enhancing IL-6-dependent Th17 cell development and survival. *Journal of Experimental Medicine* 205, 2281–2294.

**Soukou-Wargalla**, S., Kilian, C., Velasquez, L. N., Machicote, A., Letz, P., Tran, H. B., Domanig, S., Bertram, F., Stumme, F., Bedke, T., Giannou, A., Kempski, J., Sabihi, M., Song, N., Paust, H. J., Borchers, A., Garcia Perez, L., Pelczar, P., Liu, B., Ergen, C., Steglich B., Muscate F., Huber T.B., Panzer U., Gagliani N., Krebs C.F., Huber, S., 2023. Tr1 Cells Emerge and Suppress Effector Th17 Cells in Glomerulonephritis. *Journal of immunology (Baltimore, Md. : 1950)*, 211(11), 1669–1679.

**Steinmetz**, O.M., Summers, S.A., Gan, P.-Y., Semple, T., Holdsworth, S.R., Kitching, A.R., 2011. The Th17-Defining Transcription Factor ROR $\gamma$ t Promotes Glomerulonephritis. *JASN* 22, 472–483.

**Steinmetz**, O.M., Turner, J.-E., Paust, H.-J., Lindner, M., Peters, A., Heiss, K., Velden, J., Hopfer, H., Fehr, S., Krieger, T., Meyer-Schwesinger, C., Meyer, T.N., Helmchen, U., Mittrücker, H.-W., Stahl, R.A.K., Panzer, U., 2009. CXCR3 mediates renal Th1 and Th17 immune response in murine lupus nephritis. *J Immunol* 183, 4693–4704.

**Sternberg**, N., Hamilton, D., 1981. Bacteriophage P1 site-specific recombination. I. Recombination between loxP sites. *J Mol Biol* 150, 467–486.

**Stevens**, P.E., Levin, A., Kidney Disease: Improving Global Outcomes Chronic Kidney Disease Guideline Development Work Group Members, 2013. Evaluation and management of chronic kidney disease: synopsis of the kidney disease: improving global outcomes 2012 clinical practice guideline. *Ann Intern Med* 158, 825–830.

**Stritesky**, G.L., Yeh, N., Kaplan, M.H., 2008. IL-23 promotes maintenance but not commitment to the Th17 lineage. *J Immunol* 181, 5948–5955.

**Szabo**, S.J., Kim, S.T., Costa, G.L., Zhang, X., Fathman, C.G., Glimcher, L.H., 2000. A Novel Transcription Factor, T-bet, Directs Th1 Lineage Commitment. *Cell* 100, 655–669.

**Takahashi**, T., Tagami, T., Yamazaki, S., Uede, T., Shimizu, J., Sakaguchi, N., Mak, T.W., Sakaguchi, S., 2000. Immunologic Self-Tolerance Maintained by Cd25+Cd4+Regulatory T Cells Constitutively Expressing Cytotoxic T Lymphocyte-Associated Antigen 4. *Journal of Experimental Medicine* 192, 303–310.

**Tysk**, C., Lindberg, E., Järnerot, G., Flodérus-Myrhed, B., 1988. Ulcerative colitis and Crohn's disease in an unselected population of monozygotic and dizygotic twins. A study of heritability and the influence of smoking. *Gut* 29, 990–996.

- Vagianos, K., Bector, S., McConnell, J., Bernstein, C.N., 2007.** Nutrition assessment of patients with inflammatory bowel disease. *JPEN J Parenter Enteral Nutr* 31, 311–319.
- Van den Berge, K., Roux de Bézieux, H., Street, K., Saelens, W., Cannoodt, R., Saeys, Y., Dudoit, S., Clement, L., 2020.** Trajectory-based differential expression analysis for single-cell sequencing data. *Nat Commun* 11, 1201.
- Van Dyken, S.J., Locksley, R.M., 2013.** Interleukin-4- and interleukin-13-mediated alternatively activated macrophages: roles in homeostasis and disease. *Annu Rev Immunol* 31, 317–343.
- van Langenberg, D.R., Gibson, P.R., 2010.** Systematic review: fatigue in inflammatory bowel disease. *Aliment Pharmacol Ther* 32, 131–143.
- Veldhoen, M., Uyttenhove, C., van Snick, J., Helmbj, H., Westendorf, A., Buer, J., Martin, B., Wilhelm, C., Stockinger, B., 2008.** Transforming growth factor-beta “reprograms” the differentiation of T helper 2 cells and promotes an interleukin 9-producing subset. *Nat Immunol* 9, 1341–1346.
- Wang, C., Kang, S.G., Lee, J., Sun, Z., Kim, C.H., 2009.** The roles of CCR6 in migration of Th17 cells and regulation of effector T cell balance in the gut. *Mucosal Immunol* 2, 173–183.
- Wang, L., Wang, F.-S., Gershwin, M.E., 2015.** Human autoimmune diseases: a comprehensive update. *Journal of Internal Medicine* 278, 369–395.
- Wang, Y., Godec, J., Ben-Aissa, K., Cui, K., Zhao, K., Pucsek, A.B., Lee, Y.K., Weaver, C.T., Yagi, R., Lazarevic, V., 2014.** The transcription factors T-bet and Runx are required for the ontogeny of pathogenic interferon- $\gamma$ -producing T helper 17 cells. *Immunity* 40, 355–366.
- Wehkamp, J., Harder, J., Weichenthal, M., Schwab, M., Schäffeler, E., Schlee, M., Herrlinger, K.R., Stallmach, A., Noack, F., Fritz, P., Schröder, J.M., Bevins, C.L., Fellermann, K., Stange, E.F., 2004.** NOD2 (CARD15) mutations in Crohn’s disease are associated with diminished mucosal alpha-defensin expression. *Gut* 53, 1658–1664.
- Wolk, K., Kunz, S., Witte, E., Friedrich, M., Asadullah, K., Sabat, R., 2004.** IL-22 increases the innate immunity of tissues. *Immunity* 21, 241–254.
- Xavier, R.J., Podolsky, D.K., 2007.** Unravelling the pathogenesis of inflammatory bowel disease. *Nature* 448, 427–434 (Figure " Histologic hallmarks of IBD: clues to immunopathogenesis" from page 427).
- Yamaguchi, Y., Suda, T., Suda, J., Eguchi, M., Miura, Y., Harada, N., Tominaga, A., Takatsu, K., 1988.** Purified interleukin 5 supports the terminal differentiation and proliferation of murine eosinophilic precursors. *J Exp Med* 167, 43–56.
- Yang, X.O., Pappu, B.P., Nurieva, R., Akimzhanov, A., Kang, H.S., Chung, Y., Ma, L., Shah, B., Panopoulos, A.D., Schluns, K.S., Watowich, S.S., Tian, Q., Jetten, A.M., Dong, C., 2008.** T helper 17 lineage differentiation is programmed by orphan nuclear receptors ROR alpha and ROR gamma. *Immunity* 28, 29–39.
- Zheng, W., Flavell, R.A., 1997.** The transcription factor GATA-3 is necessary and sufficient for Th2 cytokine gene expression in CD4 T cells. *Cell* 89, 587–596.
- Zhu, J., 2015.** T helper 2 (Th2) cell differentiation, type 2 innate lymphoid cell (ILC2) development and regulation of interleukin-4 (IL-4) and IL-13 production. *Cytokine* 75, 14–24.
- Zhu, J., Jankovic, D., Oler, A.J., Wei, G., Sharma, S., Hu, G., Guo, L., Yagi, R., Yamane, H., Punkosdy, G., Feigenbaum, L., Zhao, K., Paul, W.E., 2012.** The Transcription Factor T-bet Is Induced

by Multiple Pathways and Prevents an Endogenous Th2 Cell Program during Th1 Cell Responses. *Immunity* 37, 660–673.

## 7.2 Online

Smart Servier <https://smart.servier.com> (last request 15 of March 2023, 15:15)

User Guide Chromium Next GEM Single Cell 5' Reagent Kits v2 (Dual Index)

[https://assets.ctfassets.net/an68im79xiti/57JaTECQNBPSpyDz8oucdi/ced6aa8eaf73d6ee18dea8fdb945faa/CG000331\\_Chromium\\_Next\\_GEM\\_Single\\_Cell\\_5-v2\\_UserGuide\\_RevD.pdf](https://assets.ctfassets.net/an68im79xiti/57JaTECQNBPSpyDz8oucdi/ced6aa8eaf73d6ee18dea8fdb945faa/CG000331_Chromium_Next_GEM_Single_Cell_5-v2_UserGuide_RevD.pdf)(Figure “Step 1 GEM Generation & Barcoding” adopted from page 16, figure “Inside individual GEMs” adopted from page 16, figure “Step 5 5' Gene Expression (GEX) Library Construction” adopted from page 18, last request 16 of March 2023, 14:30)

<https://www.carlroth.com/com/en/counting-cells/counting-chamber-neubauer-improved-bright-lines/p/t735.1> (last request 19 of January 2023, 15:30)

PubMed Gene <https://www.ncbi.nlm.nih.gov/gene/> (last request 15 of March 2023, 16:15)

OMIM <https://www.omim.org> (last request 15 of March 2023, 16:30)

Satija Lab <https://satijalab.org> (last request 15 of March 2023, 16:30)

Gene Cards <https://www.genecards.org> (last request 16 of March 2023, 17:30)

## 8. List of Tables

Table 1: Stages of CKD based on GFR	16
Table 2: Interpretation of Albumin/Creatinine-ratios (ACR)	16
Table 3: PCR mix for genotyping	33
Table 4: Programs for genotyping (Thermal cycler)	34
Table 5: Sample dilutions for ELISA	40
Table 6: Standard dilutions for ELISA	40
Table 7: Readout of albuminuria quantification with Multistix	40
Table 8: Plate design for ELISA	40
Table 9: Standard dilutions for Jaffee creatinine quantification	41
Table 10: Plate design for Jaffee creatinine quantification	41
Table 11: Histological Colitis Score	49
Table 12: Number of sorted cells for scRNAseq	61

## 9. List of Figures

Figure 1: Effector TH cell lineage and pathogen class	7
Figure 2: Kidney anatomy	13
Figure 3: Histological correlates of crescentic glomerulonephritis	14
Figure 4: Histological correlates of CD and UC	19
Figure 5: Clinical features of IBD	21
Figure 6: IL-17A fate reporter mice	36
Figure 7: IL-17A fate Tbx21 flox reporter mice	36
Figure 8: Generation of sheep-anti-mouse GMB ABs	37
Figure 9: Experimental outline of cGN experiments	37
Figure 10: Murine urine collection in metabolic cage	38
Figure 11: Proteinuria quantification with Siemens Multistix	38
Figure 12: Counting areas of a Neubauer cell chamber	43
Figure 13: Experimental outline of CD45RBhi Colitis	44
Figure 14: Endoscopic evaluation of disease in CD45RBhi Colitis	45
Figure 15: Generation of GEM'S (scRNAseq)	50
Figure 16: Reverse transcription inside GEM (cDNA generation)	51
Figure 17: Generation of 5' Gene Expression Library	52
Figure 18: Albumin/Creatinine-ratios in cGN	55
Figure 19: Blood analysis of cholesterol, triglycerides and BUN in cGN	56
Figure 20: Histological analysis of renal sections in cGN	56
Figure 21: FACS gating strategy in cGN experiments	57
Figure 22: Percentage of YFP+ cells in IL-17ACRE Tbx21flox cGN mice	57
Figure 23: T-bet expression in IL-17ACRE Tbx21flox cGN mice	58
Figure 24: Th17-Th1 axis in IL-17ACRE Tbx21flox cGN mice	59
Figure 25: Chemokine receptor expression in IL17ACRE Tbx21flox cGN mice	60
Figure 26: Sorting strategy cGN scRNAseq	61
Figure 27: QC metrics and cell cycle scoring (scRNAseq)	62
Figure 28: Identification of T cell clusters (scRNAseq)	63
Figure 29: Subclustering of CD4+ T cells (scRNAseq)	65
Figure 30: Th17-Th1 axis in cGN (scRNAseq)	67
	104

Figure 31: Supplementary Figure 1 (scRNAseq)	68
Figure 32: Change in weight during CD45RBhi	70
Figure 33: Endoscopic scoring of CD45RBhi Colitis mice	71
Figure 34: Spleen size and colon length in CD45RBhi Colitis	72
Figure 35: Histological analysis of colon sections in CD45RBhi colitis	72
Figure 36: FACS gating strategy in CD45RBhi colitis experiments	73
Figure 37: Percentage of YFP+ cells in CD45RBhi Colitis experiments	73
Figure 38: T-bet and ROR $\gamma$ t expression in YFP+ and YFP- cells	74
Figure 39: IFN- $\gamma$ and IL-17A/F expression in YFP+ cells	75
Figure 40: Th17, Th1-like and exTh17 cells in CD45RBhi Colitis	76
Figure 41: Chemokine receptors in CD45RBhi Colitis	76
Figure 42: Effector cytokines in CD45RBhi Colitis	77

## 10. Acknowledgements

I would like to express my sincere gratitude to Prof. Dr. Christian Krebs for granting me the opportunity to work on this highly interesting topic and for his exceptional supervision throughout my doctoral thesis. His support, receptiveness and assistance in planning have been instrumental in the successful progression of my research. I am grateful to have chosen him as my doctoral supervisor.

I would like to convey my appreciation to Prof. Dr. Samuel Huber for the regular constructive meetings, provision of materials, and assistance in designing the colitis experiments. I extend my thanks to Liz for sharing her knowledge in the execution of the colitis experiments. Additionally, I acknowledge Penelope Pelczar for coloscopic grading of the mice and Jenny Krause for histological scoring of the colonic slices.

I appreciate the research fellowship “Mechanisms of Immune-Mediated Tissue Injury” within the framework of the Sonderforschungsbereich 1192 (Special research project 1192) led by Prof. Dr. Ulf Panzer for the financial support for my research endeavors.

I would like to express thanks for the practical assistance provided by the UKE FACS Core Facility and Dr. Hans-Joachim Paust during FACS panel design. Additionally, I extend thanks to Varshi for her contribution in the NTN experiments, Alina for her work on 10x scRNAseq library construction and genotyping support, Liz for her contribution in CD45RB<sup>hi</sup> colitis experiment, Malte for his role in RNA sequencing data alignment, AG Panzer and for the provision of various reagents, kits, and consumables and to AG Huber for providing the flora for CD45RB<sup>hi</sup> colitis experiments.

The conducive working environment within the entire SFB1192, particularly within my working group alongside my dear colleagues Christian, Alina, Malte, Leon, and Varshi, contributed to an exceptional research period.

Special recognition goes to my partner Marlene and all my friends for their mental support and the necessary distraction during challenging times. Lastly, I express my gratitude to my entire family for enabling my academic pursuit as well as their unwavering support throughout my studies.

## **11. Curriculum Vitae**

Entfällt aus Datenschutzrechtlichen Gründen

## 12. Affidavit

### Eidesstattliche Versicherung:

Ich, Jens Christian Kleiner, versichere ausdrücklich, dass ich die Arbeit selbständig und ohne fremde Hilfe verfasst, andere als die von mir angegebenen Quellen und Hilfsmittel nicht benutzt und die aus den benutzten Werken wörtlich oder inhaltlich entnommenen Stellen einzeln nach Ausgabe (Auflage und Jahr des Erscheinens), Band und Seite des benutzten Werkes kenntlich gemacht habe.

Ferner versichere ich, dass ich die Dissertation bisher nicht einem Fachvertreter an einer anderen Hochschule zur Überprüfung vorgelegt oder mich anderweitig um Zulassung zur Promotion beworben habe.

Ich erkläre mich einverstanden, dass meine Dissertation vom Dekanat der Medizinischen Fakultät mit einer gängigen Software zur Erkennung von Plagiaten überprüft werden kann.

### Declaration on oath

I, Jens Christian Kleiner, hereby declare that I have written the thesis independently and without outside help, that I have not used sources and aids other than those I have specified and that I have identified the passages taken verbatim or in terms of content from the works used individually by edition (edition and year of publication), volume and page of the work used.

Furthermore, I confirm that I have not yet submitted the dissertation to a subject representative at another university for review or applied for admission to doctorate in any other way.

I agree that my dissertation may be checked by the Dean's Office of the Faculty of Medicine using standard plagiarism detection software.

Berlin, 19.01.2024

City and Date



Signature